HYDROLOGICAL RESPONSE UNIT-BASED BLOWING SNOW MODELLING OVER MOUNTAINOUS TERRAIN

A Thesis Submitted to the College of

Graduate Studies and Research

In Partial Fulfillment of the Requirements

For the Degree of Master of Science

In the Department of Geography and Planning

(Centre for Hydrology)

University of Saskatchewan

Saskatoon

By

MATTHEW KENNETH MACDONALD

Permission to Use

In presenting this thesis in partial fulfilment of the requirements for a Postgraduate degree from the University of Saskatchewan, I agree that the Libraries of this University may make it freely available for inspection. I further agree that permission for copying of this thesis in any manner, in whole or in part, for scholarly purposes may be granted by the professor or professors who supervised my thesis work or, in their absence, by the Head of the Department or the Dean of the College in which my thesis work was done. It is understood that any copying or publication or use of this thesis or parts thereof for financial gain shall not be allowed without my written permission. It is also understood that due recognition shall be given to me and to the University of Saskatchewan in any scholarly use which may be made of any material in my thesis.

Requests for permission to copy or to make other use of material in this thesis in whole or part should be addressed to:

Head of the Department of Geography and Planning

University of Saskatchewan

Saskatoon, Saskatchewan S7N 5C8

ABSTRACT

Wind transport and sublimation of snow particles are common phenomena across high altitude and latitude cold regions and play important roles in hydrological and atmospheric water and energy budgets. In spite of this, blowing snow processes have not been incorporated in many mesoscale hydrological models and land surface schemes.

A physically based blowing snow model, the Prairie Blowing Snow Model (PBSM), initially developed for prairie environments was used to model snow redistribution and sublimation by wind over two sites representative of mountainous regions in Canada: Fisera Ridge in the Rocky Mountain Front Ranges in Alberta, and Granger Basin in the Yukon Territory. Two models were used to run PBSM: the object-oriented hydrological model, Cold Regions Hydrological Modelling Platform (CRHM) and Environment Canada's hydrological-land surface scheme, Modélisation Environmentale Communautaire – Surface and Hydrology (MESH). PBSM was coupled with the snowcover energy and mass-balance model (SNOBAL) within CRHM. Blowing snow algorithms were also incorporated into MESH to create MESH-PBSM. CRHM, MESH and MESH-PBSM were used to simulate the evolution of snowcover in hydrological response units (HRUs) over both Fisera Ridge and Granger Basin.

To test the models of blowing snow redistribution and ablation over a relatively simple sequence of mountain topography, simulations were run from north to south over a linear ridge in the Canadian Rocky Mountains. Fisera Ridge snowcover simulations with CRHM were performed over two winters using two sets of wind speed forcing: (1) station observed wind speed, and (2) modelled wind speed from a widely applied empirical, terrain-based windflow model. Best results were obtained when using the site meteorological station wind speed data. The windflow model performed poorly when comparing the magnitude of modelled and observed wind speeds. Blowing snow sublimation, snowmelt and snowpack sublimation

quantities were considerably overestimated when using the modelled wind speeds. As a result, end-of-winter snow accumulation was considerably underestimated on windswept HRUs. MESH and MESH-PBSM were also used to simulate snow accumulation and redistribution over these same HRUs. MESH-PBSM adequately simulated snow accumulation in the HRUs up until the spring snowmelt period. MESH without PBSM performed less well and overestimated accumulation on windward slopes and the ridge top whilst underestimating accumulation on lee slopes. Simulations in spring were degraded by a large overestimation of melt by MESH. The early and overestimated melt warrants a detailed examination that is outside the scope of this thesis.

To parameterize snow redistribution in a mountain alpine basin, snow redistribution and sublimation by wind were calculated for three winters over Granger Basin using CRHM. Snow transport fluxes were distributed amongst HRUs using inter-HRU snow redistribution allocation factors. Three snow redistribution schemes of varying complexity were evaluated. CRHM model results showed that end-of-winter snow accumulation can be most accurately simulated when the inter-HRU snow redistribution schemes take into account wind direction and speed and HRU aerodynamic characteristics, along with the spatial arrangement of HRUs in the catchment. As snow transport scales approximately with the fourth power of wind speed (u^4), inter-HRU snow redistribution allocation factors can be established according to the predominant u^4 direction over a simulation period or can change at each time step according to an input measured wind direction. MESH and MESH-PBSM were used to simulate snow accumulation and ablation over these same HRUs. MESH-PBSM provided markedly better results than MESH without blowing snow algorithms.

That snow redistribution by wind can be adequately simulated in computationally efficient HRUs over mountainous terrain has important implications for representing snow transport in large-scale hydrology models and land surface schemes. Snow redistribution by wind caused mountain snow accumulation to vary from 10% to 161% of seasonal snowfall within a headwater catchment in the Canadian Rocky Mountains, and blowing snow sublimation losses ranged from 10 to 37% of seasonal snowfall.

ACKNOWLEDGMENTS

First and foremost I acknowledge my supervisors Dr. John Pomeroy and Dr. Alain Pietroniro for scientific guidance and mentoring. I also gratefully acknowledge my committee members Dr. Philip Marsh, Dr. Charles Maule, and my external examiner Dr. Amin Elshorbagy for insightful comments and advice.

I must thank a number of colleagues from various institutions for thought-provoking discussions, programming assistance and data acquisition that made this thesis possible: Chad Ellis, Chris DeBeer, Jimmy MacDonald, Chris Marsh, Tom Brown, Joni Onclin, Dr. Muluneh Mekonnen (University of Saskatchewan), Dr. Pablo Dornes (University of La Pampa), Michael Solohub (RESCAN), Rick Janowicz, Glenn Carpenter (Yukon Environment), Dr. Diana Verseghy, Brenda Toth, Dell Bayne, Newell Hedstrom, Dr. Frank Seglenieks, Bruce Davison, Dr. Paul Bartlett, Dr. Raoul Granger (Environment Canada), Dr. Bryan Tolson (University of Waterloo), Dr. Richard Essery (University of Edinburgh), Susanne Hanson (Danish National Space Centre), Dr. Dan Bewley (University of British Columbia), Dr. Tim Link (University of Idaho) and Dr. Jean Emmanuel Sicart (Université Montpellier).

Logistical help from the Nakiska Ski Resort and the University of Calgary Biogeoscience Institute is gratefully acknowledged.

I gratefully acknowledge the financial support provided by the IP3 Network (funded by Canadian Foundation for Climate and Atmospheric Sciences), IPY Project (Government of Canada), the Department of Geography and Planning, the National Science and Engineering Research Council and the Canada Research Chair Program.

Finally, this thesis is dedicated to my parents Stephanie Thomson and Ken MacDonald. I would not have reached this point in my career if it were not for their years of support.

TABLE OF CONTENTS

page

LIST OF TABLES

LIST OF FIGURES

LIST OF SYMBOLS

Acronyms

ASL	above sea level
CLASS	Canadian Land Surface Scheme
CLASS-PBSM	PBSM coupled to CLASS
CRHM	Cold Regions Hydrological Model
DEM	digital elevation model
DDS	Dynamically Dimensioned Search Algorithm
FR	Fisera Ridge
Forest	Forest [FR HRU]
GB	Granger Basin
GPS	global positioning system
GRU	grouped response unit
HRU	hydrological response unit
km	kilometres
LAI	leaf area index
LAI'	effective leaf area index
LiDAR	light detection and ranging
LSS	land surface scheme
LST	local standard time
m	metres
MESH	Modélisation Environmentale Communautaire – Surface and Hydrology
MCRB	Marmot Creek Basin
NF	North-facing Slope [both FR and GB HRUs]
PBSM	Prairie Blowing Snow Model
PILPS	Project for the Intercomparison of Land-surface Parameterization Schemes
PLT	Plateau [GB HRU]
RMM	Ryan/MicroMet distributed windflow algorithm
SF	South-facing Slope [GB HRU]
SF-lower	Lower South-facing Slope [FR HRU]
SF-upper	Upper South-facing Slope [FR HRU]
SHE	Système Hydrologique Européen
SnowMIP	Snow Model Intercomparison Project
SWE	snow water equivalent (kg m^{-2} = mm)
TIN	triangulated irregular network
UB	Upper Basin [GB HRU]
VB	Valley Bottom [GH HRU]
WCRB	Wolf Creek Research Basin
WIA	Whitehorse International Airport

Roman

a_c	radiation absorbed by ozone (2%)
a_w	radiation absorbed by water vapour (7%)
ALIC	near-infrared albedo of vegetation [CLASS parameter]
ALVC	visible albedo of vegetation [CLASS parameter]
A_S	vegetation width (m)
B	thermal quality of snow or the fraction of ice in a unit mass of wet snow (0.95-0.97)
c_1	dimensionless ratio of saltation velocity to friction velocity (2.8)
c_2	square root of the ratio of the initial vertical saltating particle velocity to u^*
c_3	ratio of z_0 to saltation height (0.07519)
c_4	drag coefficient (0.5)
C_1	dimensionless canopy-leaf contact per ground
d	interface lengths between source and sink HRUs perpendicular to the wind direction
d_v	vegetation stalk diameter (m)
e	dimensionless efficiency of saltation ($1/4.2u^*$)
E	sublimation from the snowpack (kg m^{-2} s^{-1})
E_B	blowing snow sublimation rate (kg m^{-2} s^{-1})
$f(r)$	relative frequency of suspended snow particles with radius *r*
F	total snow transport rate (kg m^{-1} s^{-1})
F_{salt}	snow transport rate in the saltation layer (kg m^{-1} s^{-1})
F_{susp}	snow transport rate in the suspension layer (kg m^{-1} s^{-1})
g	acceleration due to gravity (m s^{-2})
h_f	latent heat of fusion (333.5 kJ kg^{-1})
h_v	height of vegetation (m)
h^*	reference height near the top of the saltation layer (m)
H	hour angle measured from solar noon measured positively towards west
Ht	vegetation height (m)
I	intensity of extraterrestrial radiation
I	natural logarithm of the hours since the last snowfall
I_s^*	maximum intercepted snow load in canopy (kg m^{-2})
k	von Kármán constant (0.41)
k	shortwave irradiance extinction coefficient
L_C	fractional term that accounts for the "snow trapping efficiency" of a leeward slope
L_S	latent heat of sublimation ($2.838 \cdot 10^6$ J kg^{-1})
m	optical air mass
m	coefficient to account for the difference in average and maximum surface

	shear stress to initiate erosion
m	mean mass of a single ice particle at height z
M	molecular weight of water (18.01 kg mol^{-1})
M	snowmelt (kg m^{-2} s^{-1})
L	distance downwind from an aerodynamic barrier to snow transport (m)
LAMN	minimum leaf area index [CLASS parameter]
LAMX	maximum leaf area index [CLASS parameter]
MB	model bias
MNS	modified Nash-Sutcliffe efficiency coefficient
N	number of simulated-observed pairs
N	vegetation number density (number m^{-2})
NRMSE	normalized root mean squared error
Nu	Nusselt number
N_S	vegetation density (number m^{-2})
p	probability of blowing snow occurrence
p	mean zenith path transmissivity of the atmosphere
P	precipitation rate (kg m^{-2} s^{-1})
Q_A	small-scale advective heat from bare ground (W m^{-2})
Q_e	convective latent heat flux (W m^{-2})
Q_{ext}	extraterrestrial radiation on a horizontal surface at the outer limit of the earth's atmosphere
Q_{dif}	diffuse clear-sky radiation
Q_{dir}	theoretical direct beam component of solar radiation
Q_g	conductive ground heat flux (W m^{-2})
Q_h	convective sensible heat flux (W m^{-2})
Q_m	energy available for snowmelt (W m^{-2})
Q_n	net radiation (W m^{-2})
Q_p	advective heat from rainfall (W m^{-2})
Q_r	radiation absorbed by the particle (J s^{-1} m^{-2})
r	radius of a snow particle with mass m (μm)
R	universal gas constant (8313 J mol^{-1} K^{-1})
R^2	coefficient of determination (goodness of fit)
RMSE	root mean squared error
S	snow accumulation on ground (kg m^{-2})
Sh	Sherwood number
S_R	Snow redistribution allocation factor
t	time (s)
T	ambient atmospheric temperature (ºC, K)
u^4	fourth power of wind speed
u^*	friction velocity (m s^{-1})

u^*_n	portion of friction velocity applied to nonerodible roughness elements (m s^{-1})
u^*_t	threshold friction velocity for snow erosion (m s^{-1})
u_{mean}	mean wind speed (location parameter)
u_z	wind speed at height z above ground or snow surface (m s^{-1})
U	internal energy of a snow mass (J m^{-2} K^{-1})
W	reference wind speed
W_W	wind weight
x	fetch distance (m)
z	height above ground or snow surface (m)
z_b	top of the blowing snow boundary layer (m)
z_0	aerodynamic roughness length (m)
$z_{sim,OBS}$	observed snow depth (m)
$z_{snow,SIM}$	simulated snow depth (m)
Z	slope angle
ZPLG	maximum ponding depth for frozen water (m) [MESH parameter]
ZPLS	maximum ponding depth for liquid water (m) [MESH parameter]
ZSNL	limiting snow depth for areal snow-covered area calculations (m) [MESH parameter]

Greek

α	dimensionless shape parameter
α_s	snow albedo
β	ratio of element to surface drag
β	scale parameter (m)
γ_c	weight assigned to the curvature function
γ_s	weight assigned to the slope function
δ	declination of the sun
δ	standard deviation (scale parameter) of wind speed u (m s^{-1})
η	mass concentration of blowing snow at height z (kg m^{-3})
η	curvature length scale (m)
θ	latitude
Γ	gamma function
ℓ	transmission path-length
λ	dimensionless roughness element density
λ_T	thermal conductivity of the atmosphere (J s^{-1} K^{-1})
ρ	atmospheric density (kg m^{-3})
ρ_s	snow density (kg m^{-3})
ρ_s	saturation density of water vapour at T (kg m^{-3})
ρ_w	density of water (kg m^{-3})

σ	ambient atmospheric undersaturation with respect to ice
τ_C	shortwave radiation transmissivity through a forest canopy
Ω_C	grid cell curvature
Ω_S	slope in the direction of wind (º)

CHAPTER 1
INTRODUCTION

1.1 Background

Mountains are commonly referred to as ``water towers`` in reference to their importance to lowland water supplies. The water supply from mountains is important for agricultural, domestic and industrial water supplies. Spring snowmelt runoff from the mountains provides a significant portion of the water supply to Western Canada. Approximately 70% of the annual discharge occurs during the primary snowmelt runoff season (April through July) for snowmelt dominated streams located in southeastern Alberta (Stewart *et al*., 2004). The Prairie Provinces Master Agreement on Apportionment allows Alberta to take up to 50% of the natural water flows originating from within its boundaries and up to 50% of the flow entering its boundaries and the remainder flows to Saskatchewan and Manitoba (Prairie Provinces Water Board, 2003). Snowcover also plays an important biological and ecological role (Jones *et al*., 2001). Snow insulates the ground surface, allowing certain types of vegetation and small animals to survive through winter. Snowmelt runoff affects river and stream temperatures (Webb *et al*., 2008).

The hydrology of mountainous cold regions can be remarkably complex as interactions between climate systems, vegetation and water stores produce dynamic hydrological and hydrometeorological regimes. These water stores are predominantly in the form of snowcover. Snowcover has a strong control on a number of other hydrological fluxes, such as the magnitude, timing and duration of snowmelt, runoff, lake levels, soil moisture, the infiltration of meltwater and glacier mass balances. Snowcover increases the surface albedo and provides a colder surface to interact with the atmosphere compared to snow-free zones. Thus, there are marked differences in energy and moisture fluxes over snow-covered and snow-free surfaces, which have implications for evapotranspiration, permafrost, and glaciers. The wind transport of snow is an

important process that can significantly affect snowcover distribution patterns both during accumulation- and ablation-dominated periods. The sublimation of wind transported snow is a loss to the atmosphere of important surface water stores.

A number of single column models of blowing snow transport and sublimation have been developed (Pomeroy *et al*., 1993; Shao and Li, 1999; Déry and Yau, 1999, 2001; Bintanja, 2000; Gauer, 2001; Nemoto and Nishimura, 2004), and advances have been made in recent years towards understanding and quantifying the spatial distribution of blowing snow transport fluxes over complex terrain (Liston and Sturm, 1998; Purves *et al*., 1998; Essery *et al*., 1999; Winstral *et al*., 2002). Good modelling results have been achieved over moderately complex terrain, such as arctic tundra (Pomeroy *et al*., 1997; Essery *et al*., 1999; Liston and Sturm, 2002) and prairie landscapes (Fang and Pomeroy, 2009), though the same level of success has not generally been achieved over mountainous terrain. This is mainly due to challenges in adequately predicting wind fields at a scale appropriate for blowing snow modeling (Wood, 2000).

Macroscale and mesoscale hydrological models have been developed for large-scale discharge prediction and land surface schemes have been developed to provide the lower boundary for global and regional climate models. Hydrological models vary widely in the complexity of their mathematical descriptions (Grayson and Blöschl, 2001), and model development and application should be based on a combination of top-down (i.e. an emphasis on dominant physical processes and appropriate spatial discretizations) and bottom-up (i.e. mechanistic, physically based equations) approaches (Savenije, 2009). The increasing prominence of complex physically based models is accompanied by a reliance on more model parameters. Subgrid variability in large-scale hydrological models and land surface schemes is

often achieved by dividing the model grids into landscape units based on terrain and landcover characteristics.

With the exception of the work presented by Bowling *et al*. (2004) and Gordon *et al*. (2006), blowing snow processes have yet to receive widespread parameterization in mesoscale hydrological models and land surface schemes, though they play important roles in land surface and atmospheric water and energy budgets.

1.2 Objectives

The foundations for the objectives of this research are the importance of mountain water supplies, the importance of blowing snow to other hydrological fluxes and the lack of landscape-based parameterizations of snow redistribution by wind. The purpose of this research is to improve mesoscale snowcover simulations over mountainous terrain. The objectives of this research are to:

i) Evaluate the ability of a prairie-derived blowing snow model to estimate snow transport and sublimation in mountain environments when coupled to a hydrological model and a hydrological land-surface scheme;

ii) Develop and test an approach to derive hydrological response unit scale wind speed forcing over alpine topography;

iii) Identify hydrological response unit parameterizations that are suitable for modelling snow accumulation and redistribution over mountainous terrain; and

iv) Simulate snow transport, sublimation and accumulation over these environments using a physically based mesoscale hydrological model and a hydrological land-surface model.

CHAPTER 2
LITERATURE REVIEW

2.1 Introduction

Blowing snow involves the horizontal redistribution and sublimation of snow mass. The accuracy of hydrological predictions with physically based models depends on model representations of the distribution, storage and transfer of water. Model representations of water in the form of snow are particularly important for hydrological predictions in cold regions.

The snow mass balance over a uniform element of a landscape (Figure 2.1) is the result of snowfall accumulation, the distribution and divergence of blowing snow fluxes both within and surrounding the element, sublimation and melt from the snowpack given by Equation [2.1].

$$\frac{dS}{dt}(x) = P - p\left[\nabla \cdot F(x) + \frac{\int E_B(x)dx}{x}\right] - E - M \qquad [2.1]$$

where dS/dt is the surface snow accumulation (kg m^{-2} s^{-1}), P is snowfall (kg m^{-2} s^{-1}), p is the probability of blowing snow occurrence within the landscape element, F is the blowing snow transport out of the element (kg m^{-1} s^{-1}) which is the sum of snow transport in the saltation and suspension layers, F_{salt} and F_{susp}, $\int E_B(x)dx$ is the vertically integrated blowing snow sublimation rate (kg m^{-1} s^{-1}) over fetch distance x (m), E is the snowpack sublimation (kg m^{-2} s^{-1}) and M is snowmelt (kg m^{-2} s^{-1}).

Snowmelt energetics are controlled by the energy budget for a snow mass (Figure 2.1), given by Equation [2.2]

$$Q_m = Q_n + Q_h + Q_e + Q_g + Q_p + Q_A + \Delta U/\Delta t \qquad [2.2]$$

where Q_m is the energy available for melt, Q_n is the net radiation (incoming and outgoing shortwave and longwave radiation), Q_h is the convective sensible heat flux, Q_e is the convective

latent heat flux, Q_g is the conductive ground heat flux, Q_p is the advective heat from rainfall, Q_A is the small-scale advective heat from bare ground and $\Delta U/\Delta t$ is the change in internal energy of the snow mass (all components in W m^{-2}).

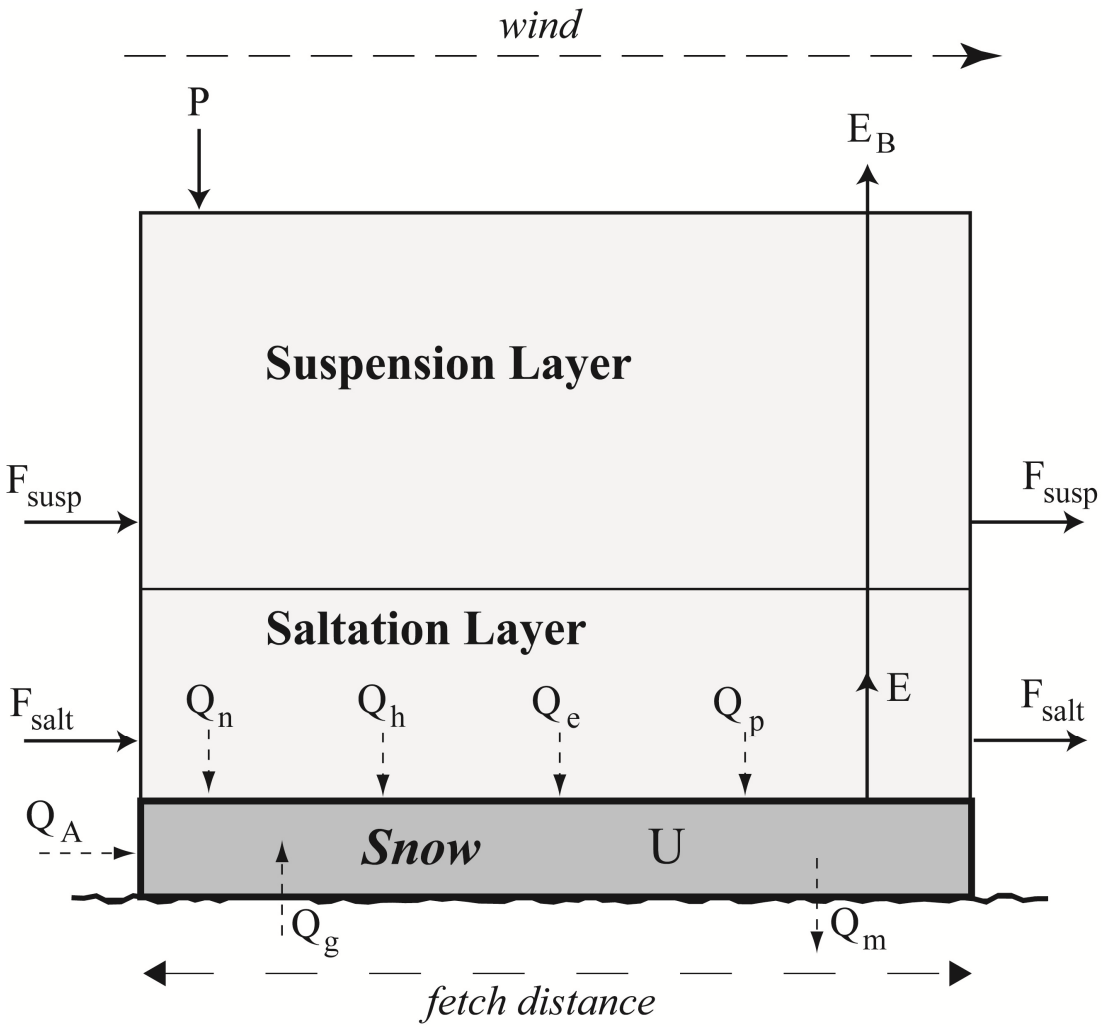

Figure 2.1 Control volume for blowing snow mass fluxes and snowmelt energy

What follows in this chapter is a discussion of the hydrological and meteorological importance of blowing snow, followed by a description of the relevant blowing snow processes (namely saltation, suspension and sublimation) along with a discussion of the primary studies that have improved both the understanding of these processes and model development. A

challenge related to blowing snow modelling over complex terrain is the availability of good wind data or an adequate windflow model. Finally, because this is a modelling study, spatially distributed hydrological models and land surfaces schemes are discussed.

2.2 Blowing Snow in High Altitude Regions

The wind transport of snow particles is a common phenomenon across high altitude and latitude cold regions. Surface snow is eroded and transported via saltation (Schmidt, 1986; Pomeroy and Gray, 1990) and suspension (Budd *et al*., 1966; Pomeroy and Male, 1992) from flat surfaces, hilltops, windward slopes and sparsely vegetated surfaces to topographic depressions, leeward slopes and more densely vegetated surfaces (Pomeroy *et al*., 1993; Liston and Sturm, 1998). Blowing snow can proceed when the surface wind speed exceeds a threshold wind speed dictated by the snow cohesive bond forces, which depend on the time and temperature histories of the snowpack (Schmidt, 1986; Li and Pomeroy, 1997a). There are three recognized modes of snow transport: creep, saltation and suspension. Creep is the rolling of snow particles along the snow surface. It comprises an extremely small portion of the total snow transport that affects the spatial distribution of snowcover and surface-atmosphere moisture fluxes; as such it is not typically explicitly represented in snow transport models. Snow particles transported by wind are well ventilated and undergo sublimation in the presence of an unsaturated atmosphere (Dyunin, 1959, Schmidt, 1972; 1986). Sublimation of blowing snow particles is very rapid relative to that of stationary snow on the ground.

Blowing snow plays an important hydrological role. Snow transport involves the redistribution of snow reserves between locations. Surface snow is eroded and transported from flat surfaces, hilltops, windward slopes and sparsely vegetated surfaces to topographic depressions, leeward slopes and more densely vegetated surfaces. Different maximum snow

accumulations have been observed over different landcover types within the same catchment, presuming a uniform spatial distribution of precipitation through the catchment. Pomeroy *et al*. (1997) found maximum snow accumulations of 68, 252 and 617 mm SWE on tundra, shrub tundra and steep slopes, respectively, on a low Arctic catchment (total winter snowfall of 190 mm SWE). McCartney *et al*. (2006) measured maximum seasonal snow accumulations of 102, 229, 164 and 201 mm SWE in short shrub, tall shrub, windward slopes and leeward slopes on a sub-Arctic alpine tundra catchment (total winter snowfall of approximately 130 mm SWE). Woo and Marsh (1978) measured maximum snow accumulations of approximately 49, 121, 109, 250, 524 and 139 mm SWE on hilltops, high flats, low flats, gullies, valleys and slopes, respectively, in a high Arctic basin (total winter snowfall of approximately 65 mm). Gray *et al*. (1979) present relative maximum snow accumulation for a number of different landscapes in open grassland environments.

The spatial distribution of seasonal snowcover caused by blowing snow redistribution governs the magnitude, timing and duration of snow ablation. Snowmelt for a given snow mass is controlled by the energy balance (Equation [2.2]). Observations show a negative covariance between snow accumulation and melt rates (Pomeroy *et al*., 2004). This is because the change in the internal energy of a snowpack largely depends on its volumetric heat capacity, which is a function of snowpack depth and density. Snow erosion and deposition regimes control snowpack depth and snowpack density is generally greater for deeper snowpacks (Pomeroy and Gray, 1995). Vegetation cover associated with shallow, windswept snowpacks often differs from that of deeper snowpacks, resulting in differences in incoming shortwave and longwave radiation and latent and sensible heat fluxes (Pomeroy *et al*., 2006). A discontinuous snowcover is produced as melt progresses. Advected energy from bare ground often increases melt (Shook and Gray, 1997;

Neumann and Marsh, 1998). It is apparent that since blowing snow redistribution so strongly affects snowmelt that it also affects the infiltration of meltwater and runoff. Blowing snow can also affect glacier mass balances (Hasholt *et al*., 2003; Jaedicke and Gauer, 2004).

Sublimation of blowing snow is a loss of snow reserves. Blowing snow sublimation losses of 15 to 41% of annual snowfall have been estimated for the Canadian Prairies (Pomeroy and Gray, 1995), 28% of annual snowfall over the western Canadian Arctic tundra (Pomeroy *et al*., 1997), 18-25% of winter precipitation over the Alaskan arctic (Liston and Sturm, 2002) and up to 20% of the annual precipitation over certain areas of the Antarctic ice sheet (Bintanja, 1998). Blowing snow sublimation impacts atmospheric moisture budgets.

2.3 Blowing Snow Processes and Models

2.3.1 Saltation

Saltation is the horizontal movement of snow particles "skipping" along the snow surface induced by wind shear at the snow surface. Saltating particles follow ballistic trajectories and their maximum height is generally restricted to a few centimetres above the snow surface. The saltation of a snow particle can be initialized in three ways: aerodynamic entrainment, rebound or ejection. Aerodynamic entrainment refers to the direct mobilization of stationary snow particles on the snow surface by windflow (Anderson and Haff, 1991). Aerodynamic entrainment has traditionally been considered unimportant to steady state snow saltation relative to rebound and ejection though recent modelling evidence suggests otherwise (Doorschot and Lehning, 2002). As saltating particles return to the surface, kinetic energy is transferred to the snow surface. A portion of this energy causes the impacting particles to bounce off the snow surface and become re-entrained, the process known as rebound. Another portion of this energy destroys surface particle bonds and causes the ejection of snow surface particles. The framework for

models of saltating snow are Bagnold's (1941, 1966) theoretical analyses of the wind transport of sand. Dyunin (1954, 1959, 1974) applied Bagnold's theory to calculate the mass flux of saltating snow as a function of wind speed. Owen (1964) developed steady state theory for saltating particles using a balance of the kinetic energy of saltating particles and the excess energy at the surface. Owen proposed that the drifting mass density and the mean initial vertical velocity of saltating particles is governed by the shear stress imparted by the atmosphere on the surface, which Owen treated as constant. Radok (1968) applied Owen's work to saltating snow particles and identified the significance of using the saltating drift density as a reference for the calculation of the turbulent diffusion of suspended blowing snow which had been examined by Budd (1966). Schmidt (1986) compared elements of Bagnold's theory with vertical measurements of blowing snow mass fluxes over a frozen lake located in southeastern Wyoming high prairies. Schmidt's analysis demonstrated the importance of snowpack surface hardness and roughness (as characterized by threshold wind speeds, the friction between snow particles and the snow surface, aerodynamic roughness height and friction velocity) to snow transport rates. Schmidt introduced a coefficient to characterize the efficiency of saltation. Pomeroy (1988) and Pomeroy and Gray (1990) used field measurements of blowing snow at a flat, semi-arid, windswept agricultural plot in the Canadian Prairies to estimate coefficients for saltation height, saltation efficiency and saltation velocity. More analytically complex saltation models have been developed that account for microscale snow properties, such as grain size, and include a more detailed description of microscale processes, such as particle-snowpack collisions, particle trajectories and windflow modification by particles (Shao and Li, 1999; Nemoto and Nishimura, 2004; Doorschot and Lehning, 2002). Doorschot and Lehning's model accounts for the effect of

slope on saltation calculations with the saltation height and length being larger over uphill and downhill slopes than over flat surfaces.

2.3.2 Suspension

Suspension is the transport of snow particles by turbulent diffusion whereby the particles do not regularly come into contact with the snow surface. Saltating particles can become suspended if their response to fluctuations in the vertical component of wind speed creates a drag sufficient for particles to accelerate upwards. Falling snow can also contribute to the mass flux in suspension as turbulent fluctuations reduce particle fall velocities. Suspended blowing snow has been observed to extend upwards of 300 m from the snow surface over essentially limitless snowcover and fetch during high wind speeds (Budd *et al*., 1966), though this is unlikely in most areas of the world with limited fetch or during the presence of temperature inversion layers. Turbulent snow transport theory was developed independently by Shiotani and Arai (1953) and Loewe (1956). From this theory, Dingle and Radok (1961) developed relationships for snow drift density as functions of height and wind speed that approximate a power law. Budd (1966) showed that suspended snow particle size can be approximated by a two-parameter gamma distribution over height and extended existing turbulent snow transport theory to account for non-uniform particle size effects on fall velocities. The two-parameter gamma distribution has been used in a number of blowing snow models (Pomeroy *et al*., 1993; Déry *et al*., 1998; Liston and Sturm, 1998; Déry and Yau, 1999; Déry and Yau, 2001; Nemoto and Nishimura, 2004; Yang and Yau, 2008). Using extensive field measurements, Pomeroy (1988) and Pomeroy and Male (1992) developed relationships to estimate the vertical diffusion velocity and the height and concentration of the reference drift near the lower bound of suspended snow. These relationships facilitated the calculation of the suspended snow transport rate using a vertical integration of the

mass flux from the reference height located at the saltation/suspension interface. Déry *et al*. (1998) estimated the gamma-distribution using spectra of suspended snow particle sizes (typically 64 particle size bins) and later developed a more computationally efficient, bulk version of the spectral model by representing the mass of suspended blowing snow with a mixing ratio (Déry and Yau, 1999). A double-moment model was then developed; in that both the blowing snow mixing ratio and total number of suspended snow particles is calculated (Déry and Yau, 2001). More recent models of suspended blowing snow have used modified Navier-Stokes equations to describe the motion of the air-snow mixture and have approximated turbulent transport using turbulent closure schemes (e.g. Bintanja, 2000; Gauer, 2001). Nemoto and Nishimura (2004) used Lagrangian stochastic theory to account for turbulent effects on the motion of suspended snow particles.

2.3.3 Sublimation

Saltating and suspended snow particles undergo sublimation. The blowing snow particle sublimation rate is controlled by atmospheric turbulence, temperature, humidity, incoming radiation and particle size. Blowing snow sublimation rate calculations are based on Thorpe and Mason's (1966) relationships for the sublimation rate of an ice sphere based on a balance of atmosphere-particle heat transfer and latent heat due to sublimation at the particle surface. Schmidt (1972) applied Thorpe and Mason's expressions to blowing snow particles assuming the particle ventilation velocity to be equal to the particle terminal fall velocity. Lee (1975) improved upon by Schmidt's work by developing a drag coefficient that accounts for turbulent fluctuations in particle vertical velocity. From this work, Pomeroy (1988) developed an expression for the ventilation velocity as a function of only the friction velocity and threshold friction velocity. An expression was also developed for the vertical gradient in under-saturation

during blowing snow events using several measurements of vertical humidity profiles (Pomeroy, 1988; Pomeroy *et al*., 1993). This facilitated the calculation of sublimation rates over both the saltation and suspension layers. Pomeroy's formulation for the sublimation of blowing snow particles has been used in other models (e.g. Liston and Sturm, 1998). Other models calculate a thermodynamic feedback (i.e. a negative feedback in the form of decreased water vapour deficit and temperature) during the sublimation of blowing snow (Bintanja, 1998; Bintanja, 2001; Bintanja and Reijmer, 2001; Déry *et al*., 1998; Déry and Yau, 1999; Déry and Yau, 2001). This negative feedback in turn reduces calculated sublimation rates. There is still debate over this model component as some argue that atmospheric mixing during blowing snow events entrains sufficient dry air so as to diminish the effect of the negative feedback (Pomeroy and Li, 2000). The snow transport models presented by Doorschot *et al*. (2001) and Lehning *et al*. (2008) neglect the sublimation of blowing snow particles.

2.3.4 Distributed Blowing Snow Models

Much of the spatiotemporal variability in snowcover over aerodynamically complex terrain can be attributed to snow redistribution by wind. Landscape snow accumulation patterns are strongly related to topography and vegetation cover. A number of studies have examined the relation between snowcover and landscape characteristics and have developed statistical models to predict snowcover based on attributes such as aspect, canopy characteristics, elevation, radiation input, slope and wind exposure (e.g. Elder *et al*., 1991; Stähli *et al*., 2001; Anderton *et al*., 2004; Molotch *et al*., 2005).

Since these snow accumulation patterns are extremely important for estimating other hydrological fluxes, much research has focused on accurately simulating the spatial redistribution of snow by wind. Spatially distributed models of snow accumulation and

redistribution can be categorized according to their: 1) spatial representation of mass and energy calculations (fully distributed or spatially aggregated), and 2) process description (empirical or physically based). A distributed spatial representation refers to a landscape being represented by a grid of uniformly-sized cells. A spatially aggregated representation refers to a landscape being represented by a number of elements that share common biophysical properties (e.g. soil, topography, vegetation) and are presumed to have the same hydrological response. These landscape elements are referred to by a variety of terms including hydrological response units (HRUs), land classes and landscape units.

Empirical or "rule-based" models of snow redistribution redistribute snow mass based on a range of topographic and vegetation parameters, but do not calculate snow transport fluxes using physically based algorithms. Purves *et al*. (1998) developed a rule-based fully distributed model of snow redistribution based on meteorology and terrain characteristics. An empirical, distributed wind flow model was used to drive empirical calculations of snow transport fluxes. Winstral *et al*. (2002) developed terrain-based parameters that quantify the effects of complex wind fields on snow distribution patterns. A regression tree model consisting of the terrain-based parameters as well as elevation, solar radiation and slope was used to predict snow depth distribution over alpine terrain using 10 m and 30 m grids. Neither the Purves nor the Winstral models calculate blowing snow sublimation. Prasad *et al*. (2001) used a distributed physically based snow transport model (SnowTran-3D; Liston and Sturm, 1998) to derive ``drift factors``. The drift factors were meant to be used in larger scale hydrological models to simulate the spatial redistribution of snow by wind without the use of a physically based snow transport model.

Physically based fully distributed snow redistribution models have been developed. Essery *et al*. (1999) and Essery and Pomeroy (2004) applied a fully distributed simplified version of

PBSM over a low-Arctic tundra catchment using an 80 m grid, where snow transport fluxes out of a cell were directed to an adjacent cell in one of four directions. Another physically based fully distributed model with similar physics to PBSM, SnowTran-3D (Liston and Sturm, 1998), has been widely applied using grid sizes ranging from 5 to 100 m. For instance, SnowTran-3D has been applied over Arctic tundra characterized by gently rolling ridges and valleys (Liston and Sturm, 1998), over mountainous terrain above the treeline (Greene *et al*., 1999), over arctic rolling uplands and flat coastal plains (Liston and Sturm, 2002), over gently arching ridges in the treeline zone (Hiemstra *et al*., 2002) and over glaciated arctic terrain with alpine relief (Hasholt *et al*., 2003). Physically based spatially aggregated models, wherein snow is relocated from bare and sparsely vegetated surfaces to more densely vegetated and leeward surfaces, have been applied (Pomeroy *et al*., 1991, 1997; Pomeroy and Li, 2000; Essery and Pomeroy, 2004). Essery and Pomeroy (2004) showed that a spatially aggregated, landscape-based version of PBSM was able to match snow accumulation predicted by a fully distributed version of PBSM reasonably well for a low-Arctic tundra catchment with moderate topography at the catchment scale. Similarly, Fang and Pomeroy (2009) found that fully distributed (6 m grid cells; ~264 000 cells) and spatial aggregated (seven HRUs) blowing snow models provided similar snow accumulations in a prairie wetland region.

2.4 Windflow Over Complex Terrain

Wind has a strong control on snow mass and energy fluxes over complex terrain. Windflow over complex terrain, such as mountains, can be highly spatially and temporally variable and occurs at multiple scales. Local windflow is a manifestation of synoptic scale and mesoscale flow interactions with smaller scale features and processes, such as the acceleration, diversion and sheltering by topography, diurnal variations in thermally driven cross-valley circulations,

horizontal pressure gradients causes by differential solar radiation heating and longwave radiation cooling, flow separation and heterogeneous surface friction.

Estimating windflow over mountainous terrain is extremely difficult because of complex turbulence structures and divergent and convergent flow directions. This is compounded by the sparse distribution of alpine wind measurements. Distributed windflow simulations over complex terrain have been made using both physically based atmospheric models, and empirical models using reference station measurements of wind speed. Physically based atmospheric models can be very computationally expensive compared to the hydrological models to which they may be coupled (Utnes and Eidsvik, 1996). Bernhardt *et al*. (2009) applied a computationally inexpensive approach to use wind fields generated from the MM5 atmospheric model to drive a snow transport model. First, a library of 220 wind fields were generated using MM5 and were subsequently used for 200 m distributed snow transport simulations over a montane region in Germany. Empirical models based on terrain and vegetation parameters are much more computationally efficient than the physically based atmospheric models, can be developed for a wide range of scales, and have been successful for hydrological modelling purposes. Ryan (1977) developed a windflow model for mountainous terrain that accounts for the sheltering and diverting effects of topography. Ryan's parameterization was incorporated in Liston and Elder's (2006) meteorological distribution system MicroMet. MicroMet generates distributed wind fields from reference wind speed and direction using digital elevation (DEM) model information. Winstral *et al*. (2009) developed an empirical method to distribute wind fields from reference wind speed and direction from a DEM-based upwind slope parameterization and vegetation information.

2.5 Hydrological Models and Land Surface Schemes

A hydrological model provides a mathematical description of a landscape's hydrological transport and storage processes given precipitation and energy inputs. Hydrological models vary widely in their governing assumptions, data input requirements, the complexity of their mathematical descriptions, spatial discretization and in the array of hydrological responses simulated. Hydrological models can be classified based on three model characteristics according to Grayson and Blöschl (2001): 1) the type of algorithms (empirical, conceptual or physically based), 2) the input and parameter method (deterministic or stochastic), and 3) the spatial representation (distributed or lumped).

Empirical models are mathematically simple input-output relationships that do not explicitly describe hydrological processes (e.g. streamflow calculated simply as a function of precipitation and some calibrated coefficient). Conceptual models are composed of a suite of mathematical representations of the most basic and important hydrological processes, but the individual processes are described by calibrated input-output relationships (e.g. the Stanford Watershed Model [Crawford and Linsley, 1966]; UBC model [Quick and Pipes, 1977]). Physically based models use fundamental physics to mathematically describe the vast majority of actual hydrological processes. Physically based models are the most mathematically complex and computationally expensive. The rationale behind the use of physically based models it that it is believed that most reliable hydrological prediction can be achieved when simulating all hydrological processes. In reality, most physically based hydrological models contain some conceptual components (e.g. streamflow routing).

Most models use the more simple deterministic approach to parameter specification and input. This is where a single set of parameters and input data are used to generate a single set of output. This contrasts the stochastic approach where statistical distributions of input data and parameters

are used to generate multiple sets of outputs calculated using combinations of the input data and parameters.

Model spatial representation refers to how the modelled landscape is segregated into its computational elements. A lumped spatial representation is one in which the modelled landscape is represented as a single computational element (e.g. the STANFORD watershed model [Crawford and Linsley, 1966]; the original version of SLURP [Kite, 1975]). This differs from the distributed representation where the modelled landscape is divided into a number of spatially explicit computational elements. Spatially explicit distributed model elements can take one of four forms: gridded, contour based, Triangulated Irregular Networks (TINs) or conceptual elements. The gridded representation is the most commonly used and in it the model elements are spatially explicit rectangles, most often equally spaced squares (e.g. SHE – *Système Hydrologique Européen* [Abbott *et al*., 1986]). Contour based models` computational elements are divided by topographic contour lines (e.g. TOPOG [Vertessy *et al*., 1993]; UBC watershed model [Quick and Pipes, 1977]). The computational elements of TINs are irregularly shaped triangular facets (e.g. Palacios-Vélez *et al*., 1998; Vivoni *et al*., 2004). Conceptual elements are subjective computational elements selected with the goals of reducing the number of computational elements compared to the other spatially explicit representations while also reducing sub-element variability of flow path and slope (e.g. KINEROS [Smith *et al*., 1995]; finite element polygon schematization of Kuchment *et al*., 2000). There are also non-spatially explicit distributed spatial representations, known as distribution spatial representations. These model elements are not spatially contiguous, but rather have conceptual locations, and are selected based on common biophysical (e.g. soil and vegetation) and topographic properties (e.g. the wetness index used in TOPMODEL [Beven and Kirkby, 1979]). Yet another approach uses

spatially aggregated elements that share common biophysical properties (e.g. soil, topography, vegetation) and are presumed to have the same hydrological response. These landscape elements are referred to by a variety of terms including hydrological response units (HRUs), land classes and landscape units. HRUs do not have an explicit spatial representation but do often have a hydrological sequence. HRU-based models include PRMS (Leavesley and Stannard, 1995) and CRHM (Pomeroy *et al*., 2007). The WATFLOOD model (Kouwen, 1988) uses grouped response units (GRUs), which are grouped HRUs that do not have a hydrological sequence.

Land surface schemes (LSS) provide the lower boundary for atmospheric models and calculate land-atmosphere exchanges of energy, mass and momentum. Most LSSs are physically based though they do range in complexity from the bucket model (Manabe, 1969), to having more physically detailed descriptions of soil-vegetation-atmosphere interactions (e.g. Verseghy, 1991; Verseghy *et al*., 1993), to having even more detailed biophysical descriptions of photosynthesis, respiration and decay (e.g. Zhang *et al*., 2001). LSSs generally have gridded spatial representations to match their atmospheric model, though some account for sub-grid variability in the landscape using a stochastic approach to parameter input (Avissar, 1992), or non-spatially explicit land class-based spatial representations within grid squares (e.g. Verseghy, 1991; Verseghy *et al*., 1993).

All hydrological models and land surface schemes require careful parameter estimation in order to obtain reliable predictions. One of the perceived advantages to using physically based models as opposed to more rudimentary ones is that certain parameters can be estimated from field measurements, thereby reducing the need for calibration. However, in practice, some physically based parameters are difficult to measure or are rarely measured in the field (e.g. stomatal resistance). This difficulty is exacerbated if the model domain is large or highly

heterogeneous. For these reasons Beven (1989) suggested that physically based models be best considered complex conceptual models. An approach to this problem is the use of "effective" parameter values that represent the behaviour of a finite model area. Effective parameters are scale-dependent and parameter values may not be transferable between different spatial and temporal scales (Grayson and Blöschl, 2001). Parameter selection for physically based modelling involves selecting physically realistic parameter values that provide an "acceptable fit" to some observed behaviour. The acceptable fit can be qualitatively judged by visual comparison, though quantitative measures of acceptable fit are most commonly cited. These quantitative measures are usually given by objective function values that quantify the error between observations and model output. Objective functions commonly used in hydrology include the correlation coefficient, deviation of volumes, model bias, Nash-Sutcliffe coefficient (Nash and Sutcliffe, 1970) and root-mean squared error. Parameter values can be calibrated manually by trial and error, though this can be highly subjective and time consuming. Automatic calibration (optimization) algorithms are commonly used, preferably after some initial manual calibration. Given the complexity and potentially large number of parameters, global automatic optimization algorithms (e.g dynamically dimensioned search [Tolson and Shoemaker, 2007], genetic algorithms [Wang, 1991], particle swarm optimization [Gill *et al*., 2006], shuffled complex evolution [Duan *et al*., 1992] and simulated annealing [Thyer *et al*., 1999]) are typically used rather than local optimization algorithms. There are a number of difficulties inherent in automatic calibration procedures. Random or systematic errors in observed data will cause algorithm solutions to deviate from optimum sets. The nonlinear interaction of model parameters often produces multiple local optima that cause solutions to deviate from the global optimum. Beven and Binley (1992) proposed the concept of equifinality in hydrological modelling, where

different parameter sets produce quite similar objective function values. There are approaches to alleviate these difficulties: reducing the number of parameters calibrated (degrees of freedom), reducing the range of parameter values and using multiple objective functions (e.g. combining multiple objective function equations and/or objective functions for different observations). Model parameter sets should be validated before being accepted. Validation of a parameter sets involves analyzing the error between model output and observations that were not used in the calibration process. For instance, calibration can be performed using a particular time series of data and validation can be performed using another time series, or calibration and validation can be performed using observations of different variables during the same time series. Though a model parameter set may provide an adequate prediction of a particular variable (e.g. discharge), it may not provide adequate predictions of variables (e.g. soil moisture, water table depth, snow depth) for which there no observations available for validation (Refsgaard, 2001)

Hydrological and atmospheric models require some description of blowing snow redistribution and sublimation that is suitable for complex terrain for application to cold regions (Dornes *et al*., 2008). The large scale application of these models in mountain and polar environments precludes a finely distributed approach such as employed for small basins (e.g. Liston and Sturm, 1998; Essery *et al*., 1999) and some form of landscape aggregation is necessary and has been successfully demonstrated for mountain topography in northern Canada (Dornes et. al, 2008a and 2008b).

CHAPTER 3
STUDY SITES AND OBSERVATIONS

3.1 Introduction

Two mountainous sites in Canada were selected for this study (Figure 3.1): Fisera Ridge (FR) in the Marmot Creek Research Basin (MCRB), Alberta, and Granger Basin (GB) in the Wolf Creek Research Basin (WCRB), Yukon Territory. These two sites were selected for two reasons: 1) they are climatologically and physiographically different, and are representative of different mountainous regions in Canada, and 2) an abundance of field data is available for both sites. Furthermore, prediction at these sites does not require the application of complex windflow models because of the abundance of field data and that they are mountainous terrain of only moderate complexity and roughness. The MCRB was re-established as a research basin in 2004 and part of the intensive 2007-2009 field campaign involved detailed meteorological and snow survey measurements over FR for blowing snow studies. Meteorological and snow survey measurements have been made regularly at WCRB since 1993.

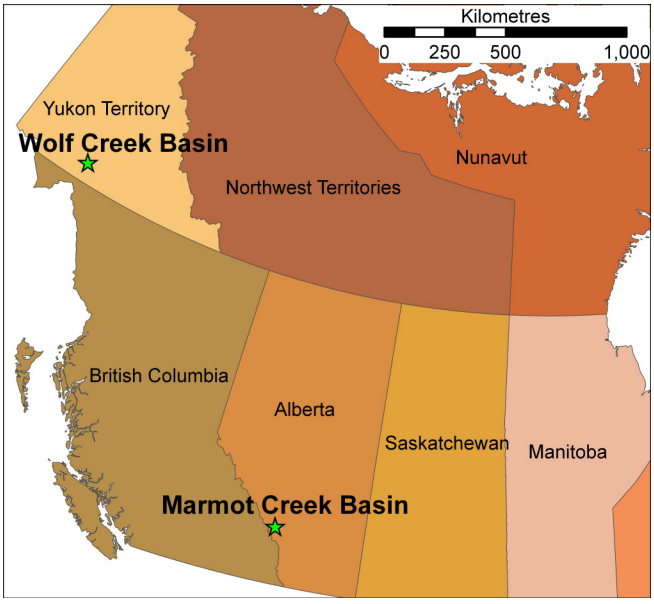

Figure 3.1 Site locations (Coordinate system is NAD1983/UTM Zone 14N. Projection is Transverse Mercator.)

3.2 Fisera Ridge (Marmot Creek Research Basin)

3.2.1 Description

Marmot Creek Research Basin (MCRB) is a 9.4 km^2 watershed located in the Rocky Mountain Front Ranges in Alberta, Canada. The general aspect of MCRB is easterly. The basin is primarily montane with subalpine forest and alpine tundra ridgetops. The basin landcover consists of dense lodgepole pine, mature spruce and subalpine fir forest at lower elevations, larch, shrubs and grasses at and just below the treeline, and talus and bare rocks in the high alpine. MCRB is underlain by glacial and post-glacial deposits ranging from 10 to 30 m depth above bedrock, except at high elevations and along portions of the creek channels (Stevenson, 1967). Seasonally frozen soils are present at higher elevations. Annual precipitation is typically around 900 kg m^{-2} with 60-75% being snow. Climate normals as recorded at the Kananaskis Pocaterra station (ID 3053604; 1610 m ASL) range from a low of -11.1 °C in January to a high of 11.4 °C in August. Temperatures are typically colder at MCRB since it is at a higher elevation. Marmot Creek itself is a tributary of the Kananaskis River and is part of the Bow River system. FR (hereafter FR ; 50°57'N; 115°12'W) is an alpine ridge located within the MCRB. FR is located just above treeline, where subalpine fir and larch give away to sparse shrubs, exposed soils and grass. FR decreases in elevation from approximately 2617 m ASL to approximately 2317 m ASL along its east-northeast axis. The predominant windflow is generally normal to FR and is northwesterly. The north-facing slope and the ridge-top are generally windswept and the southeast-facing slope and further downwind forested area are snow deposition zones.

3.2.2 Field Methods and Observations

Observations from October through April or May 2007/2008 and 2008/2009 were used. Instrumentation was set up and maintained, and data were collected by staff and students of the University of Saskatchewan Centre for Hydrology. Meteorological observations from three stations located at FR (RT, NF, SF), from a mid-elevation forest clearing station (UC: upper clearing) at 1845 m ASL 2 km away and from a meadow station (HM: hay meadow) 4.8 km away at 1437 m ASL were used (Figure 3.2). The RT station is located at the top of FR and measures air temperature, relative humidity, incoming shortwave radiation, incoming longwave radiation, snow depth, wind speed and direction. The NF and SF stations are located on the northern and southern faces of FR, respectively, and measure snow depth, wind speed and direction. A Geonor T200B accumulating precipitation gauge was installed in a sheltered area near the ridge-top FR station during the fall of 2008. Thus, for 2008/2009, precipitation data from the FR Geonor gauge were used. There are elevation-induced differences in precipitation between the FR and UC sites. 2008/2009 FR precipitation data were correlated with precipitation data from the FC Geonor T200B accumulating precipitation gauge to develop a multiplier (1.86) to extrapolate 2007/2008 UC precipitation data to the FR site. The Geonor precipitation gauge data were corrected for undercatch according to the equation presented by MacDonald and Pomeroy (2007). Atmospheric pressure is measured at the HM station. The barometric formula and known site elevations were used to estimate FR atmospheric pressure from the HM observations.

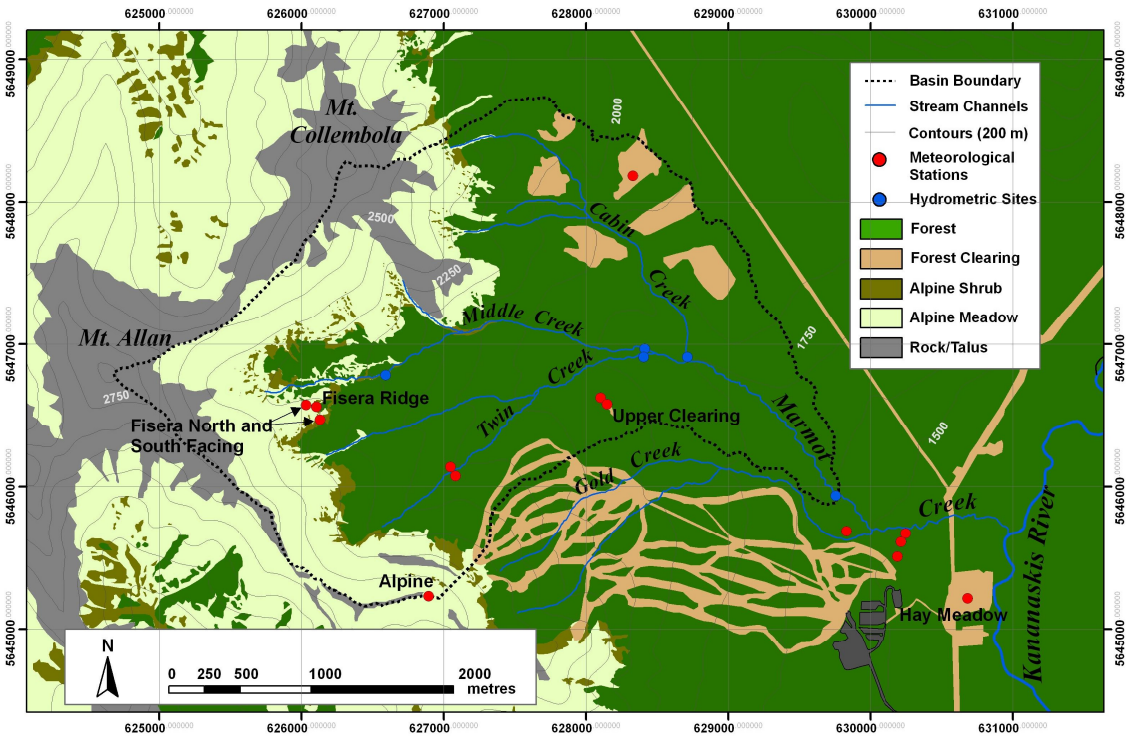

Figure 3.2 Marmot Creek Research Basin landcover and station locations

Manual snow surveys of depth and density were performed over FR during 2007/2008 and 2008/2009. The snow survey transect extended 201 m from the NF station over FR, beyond the SF station and into the forested area (Figure 3.3a). This snow survey followed the modelled transect. Snow depth was measured every 1-3 m and snow density was measured every fifth depth measurement using an ESC30 snow tube when possible. The snowpack was often too shallow to measure on the windswept north-facing slope and too deep (> 120 cm) to measure on the south-facing slope with the ESC30 tube. Snow pits were dug when possible at the locations shown on Figure 3.3a. Snow density was measured in the snow pit to depth by weighing samples obtained using a fixed triangular cutting device (Perla "Swedish Sampler"). To calculate mean SWE for an HRU, the mean measured snow density for a particular HRU was applied to each depth measurement in that HRU. FR HRUs are presented in section 5.3.2.

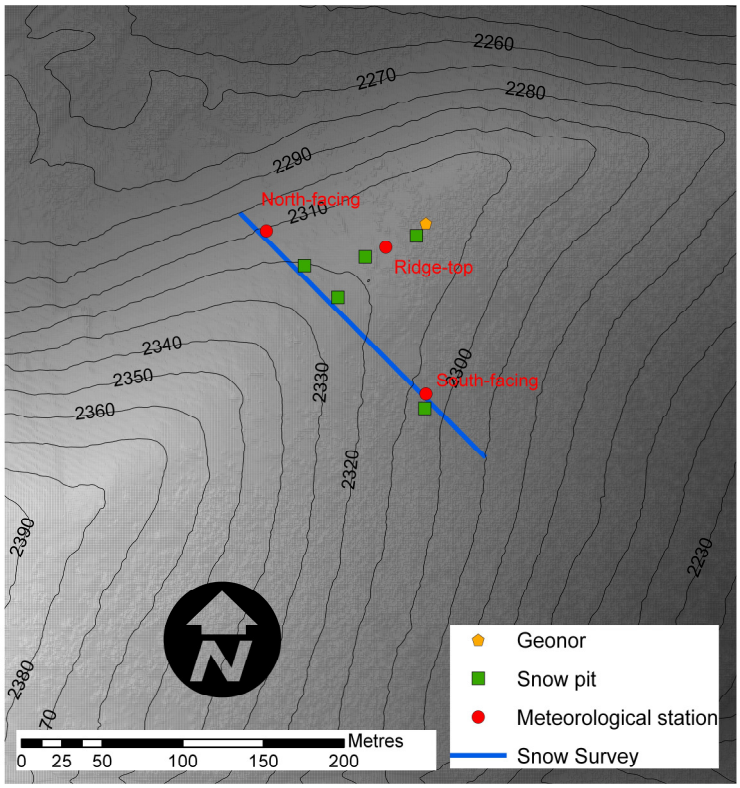

Figure 3.3 Fisera Ridge (a) meteorological station, snow survey, snow pit and Geonor locations, and (b) Site photograph taken 16 April 2010 (credit: Logan Fang)

A vegetation survey was conducted along the FR snow survey on 3 July 2008. A shrub count was performed within two 9 m × 9 m grids (on the north-facing slope and one on the south-facing slope). Twenty-three shrub height and width measurements were made with a ruler along the snow survey. Table 3.1 presents a summary of shrub measurements. The shrub width measurements included the aggregation of several clumps of shrubs. Photographs taken with a camera equipped with a hemispherical lens were analyzed with GLA software (Frazer *et al*., 1999) to determine leaf area index (LAI) for the spruce forest downslope from the SF station. An average LAI of 0.91 and an average canopy height of 2.3 m was determined.

Table 3.1 Fisera Ridge shrub survey summary

	North-facing	**South-facing**
Shrub density (number m^{-2})	0.1	0.6
Height (m)	0.51	0.82
Width (m)	1.07	1.11

An airborne light detection and ranging (LiDAR) data collection campaign was deployed over MCRB research during August 2007 (Hopkinson and Fox, 2007). High-resolution digital elevation data was obtained. A 1 m DEM of MCRB was created using this high-resolution LiDAR data using Golden Software Surfer 8.00.

Appendix A includes a summary of field work at Marmot Creek performed by Matthew MacDonald.

3.3 Granger Basin (Wolf Creek Research Basin)

3.3.1 Description

WCRB is part of the headwater region of the Yukon River Basin. Climate normals (1971-2000) for the Whitehorse International Airport (WIA; 60°42'N, 135°04'W; 706 m ASL) specify an annual daily average temperature of -0.7°C, with January (coldest month) and July (warmest month) having daily average temperatures of -17.7°C and 14.1°C, respectively. The mean annual precipitation at the WIA is 267 kg m^{-2} with approximately half as snowfall, though Pomeroy *et al*. (1999) showed that precipitation is 25 to 35% greater over WCRB and that the fraction that is snowfall is higher, mainly due to the elevation difference. There are 71 days per annum with snowfall at WIA, though likely more over WCRB. The snowfall regime of WCRB is typical of the northern boreal cordillera of Western Canada (Pomeroy *et al*., 1999). The annual average relative humidity at 0600 and 1500 LST is 74% and 55%, respectively. GB (60°31'N, 135°07'W; 1310-2100 m ASL), is an 8 km^2 sub-basin in the northwest region of WCRB, located approximately 15 km south of Whitehorse, Yukon Territory, Canada (Figure 3.4b). The aspect is generally northeasterly. GB is drained by a 3 km creek in a generally northeast direction.

GB landcover at high elevations consists of exposed mineral soils and very sparse grasses, lichens and mosses. At intermediate elevations, mineral soils are overlain by a thin organic layer and the ground is more densely covered by short shrubs. Continuous permafrost is present on the north facing slope and discontinuous permafrost is present on the south facing slope. At low elevations, tall shrubs cover a relatively wetter organic layer. A surficial organic layer up to 0.4 m thick is present in permafrost and low elevations areas (Carey and Quinton, 2004).

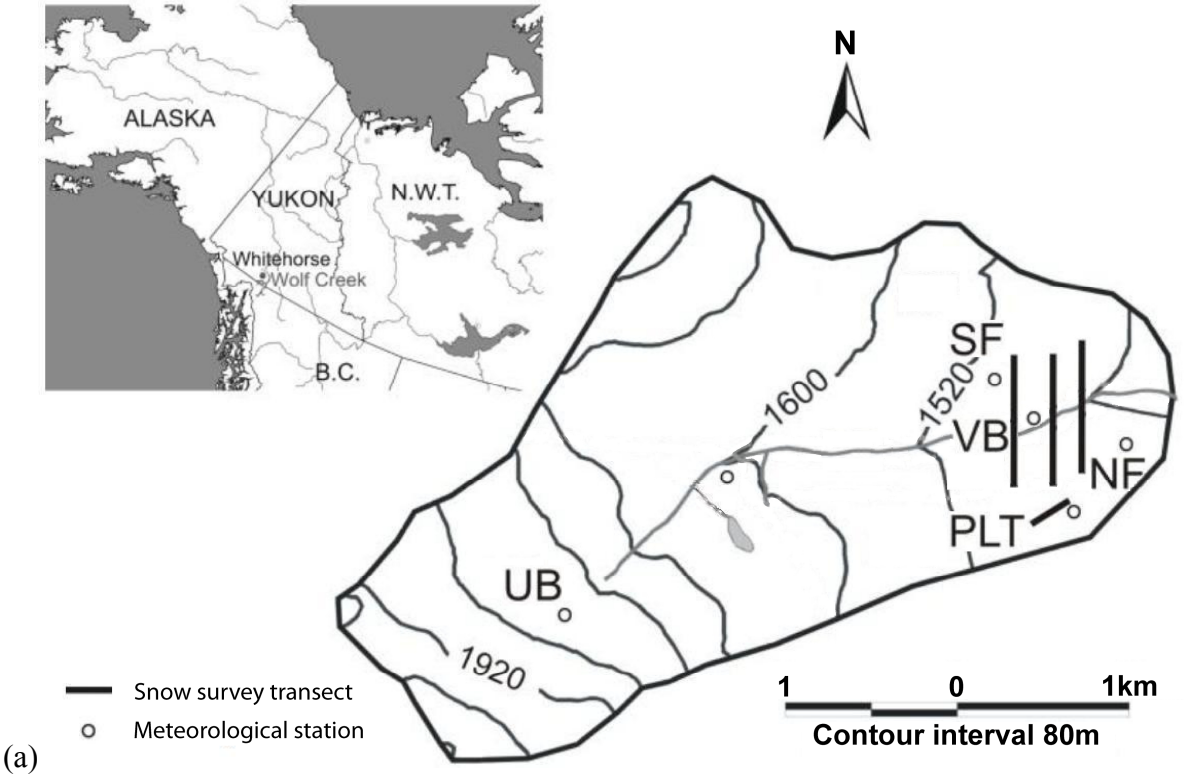

(a)

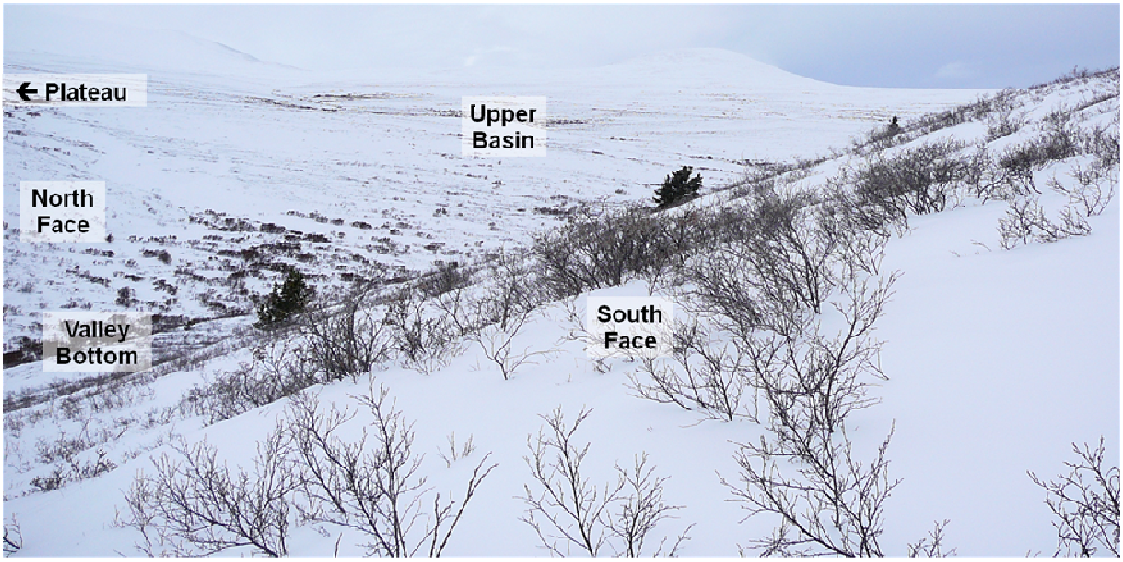

(b)

Figure 3.4 Granger Basin (a) Locations of meteorological stations and snow survey transects, and (b) Site photograph taken 15 February 2008.

3.3.2 Field Methods and Observations

Observations from October through May 1998/1999, 2000/2001 and 2003/2004 were used. Meteorological observations from five stations located at GB (Upper Basin [UB], Plateau [PLT], North-facing Slope [NF], South-facing Slope [SF] and Valley Bottom [VB]; Figure 3.4a) and from one nearby high-elevation windswept site [ALP] were used. Meteorological measurements used include air temperature, relative humidity, incoming shortwave radiation, incoming longwave radiation, atmospheric pressure, wind speed and direction. Atmospheric pressure from the ALP station was used for GB. The PLT meteorological station data are only available for 2003/2004. PLT simulations were driven by UB meteorological measurements for 1998/1999 and 2000/2001. Since the UB meteorological station was not installed until April 1999, linear regression relationships of UB meteorological observations to SF meteorological observations from other years were used to create synthetic data for UB from October 1998 to March 1999. The correlation coefficients for these linear regression relationships ranged in value from a low of 0.54 for wind speed to a high of 0.91 for temperature. Daily precipitation was not measured at WCRB over the study periods; therefore precipitation data from the WIA Nipher-shielded snow gauge was used. Precipitation measurements were corrected for wind effects, wetting losses and unrecorded trace events using the correction procedure recommended by Goodison *et al*. (1998). WIA precipitation measurements had to be increased for application over GB, due to the elevation difference-induced greater precipitation over WCRB than over WIA (Pomeroy *et al*., 1999). Cumulative snowfall observations from nipher-shielded snow gauges at various elevations of WCRB during winters 1993/1994, 1994/1995 and 1996/1997 were used to generate multipliers which ranged from 1.09 to 1.70 to extrapolate precipitation from the WIA to various elevations at GB. The mean of the precipitation multipliers generated for all three winters (1.31 to 1.41 depending on HRU elevation) was applied to the WIA precipitation measurements to

extrapolate WIA precipitation measurements to each GB HRU (refer to section 5.4 GB HRUs). This mean precipitation multiplier proved to be adequate for simulating GB snow redistribution for 1998/1999 and 2000/2001 when compared to GB snow surveys. For 2003/2004, however, GB snow accumulation was severely overestimated over each HRU suggesting that the mean multiplier was unrealistic in that season. For that reason the lowest measured seasonal precipitation multiplier (1.09 to 1.12 depending on HRU elevation) was applied to WIA precipitation measurements for 2003/2004 simulations. Pomeroy *et al*. (1999) showed that the seasonal precipitation multiplier for WCRB can change year-to-year and that there is not a consistent relationship between elevation and precipitation. The multipliers generated are consistent with an analysis of WCRB corrected snowfall by Pomeroy *et al*. (1999) and an observed increase in snow accumulation over mountains in Southern British Columbia (Auld, 1995). Total precipitation was greatest over 1998/1999 and lowest over 2000/2001.

Manual snow surveys over part of GB (Figure 3.4a) were performed from April through May of 1999, 2001 and 2004, and in January, February and March 1999. The 1999 and 2001 surveys spanned a distance of approximately 615 m (centre snow survey transect in Figure 3.4a). Approximately 160, 400 and 50 depth measurements were taken on the NF, SF and VB, respectively. Snow depth was measured every 1-2 m, while snow density was measured every 20-25th depth measurement using an ESC30 snow tube. The 2004 snow survey spanned all three transects shown in Figure 3.4a but did not go as far north as the 1999 and 2001 surveys. Depth measurements were taken approximately every 5-10 m. Approximately 50, 50 and 10 depth measurements were taken on the NF, SF and VB, respectively. A snow survey was also performed around the PLT station during April and May 2004. The PLT snow survey spanned 120 m and consisted of 25 depth measurements and 4 density measurements. To calculate mean

SWE for an HRU, the mean measured snow density for a particular HRU was applied to each depth measurement in that HRU. GB HRUs are discussed in section 5.4.2.

Canopy structure measurements were taken around the GB snow surveys locations during spring 2004 (Bewley, 2006). Aerial photographs showed the fraction of land covered by shrubs in a 30 m x 30 m grid in the valley bottom of GB was 71.4% during the late snowmelt period. A LAI-2000 Canopy Analyzer was used to determine LAI of the shrubs located at 5 m intervals along the snow survey transects. An average LAI of 0.43 was measured for shrubs along the GB snow surveys. Photographs taken with camera equipped with a hemispherical lens were analyzed with GLA software (Frazer *et al*., 1999) to determine LAI for short shrubs located near the PLT meteorological station. An average LAI of 0.31 was determined for photographs taken at the end of April 2004. LAI measurements of 2 were measured during the summer at various locations in WCRB. Shrub height and width measurements were taken along the snow survey transects on the north-facing and south-facing slopes of GB during February 2008. The mean shrub height on the north-facing and south-facing slopes were both 87 cm.

A 30 m DEM of Granger Basin was created from topographic maps and handheld global positioning system (GPS) measurements (personal communication with Dr. Sean Carey, Carleton University).

Appendix A includes a summary of field work at Marmot Creek performed by Matthew MacDonald.

CHAPTER 4
MODEL DEVELOPMENT AND SINGLE COLUMN APPLICATION

4.1 Introduction

Two models were used to simulate snow accumulation, redistribution and ablation. The Cold Regions Hydrological Modelling Platform (CRHM), which includes the Prairie Blowing Snow Model (PBSM), the snowcover energy and mass-balance model (SNOBAL), radiation balance and forest water and energy balances modules, was used. PBSM was coupled with the Modélisation Environmentale Communautaire – Surface and Hydrology (MESH). MESH is a combination of the hydrological model WATFLOOD and the land surface scheme CLASS. Algorithms developed by Ryan (1977) and implemented in MicroMet (Liston and Sturm, 2006) were tested as a means to estimate distributed wind fields. Parameter calibration was performed using the Dynamically Dimensioned Search Algorithm (DDS). This chapter includes point simulation tests of CRHM and PBSM coupled to MESH using field data collected at FR.

4.2 Model Descriptions

4.2.1 Cold Regions Hydrological Model

CRHM is an object-oriented hydrological modelling platform developed for Canadian environments (e.g. boreal forest, mountain forests, muskeg, arctic tundra and prairies). The spatial discretization is in the form of HRUs as a conceptual landscape sequence or water flow cascade. As such the spatial representation is flexible in that point, distributed and lumped simulations can be performed. CRHM has a modular structure in that the modeller creates a model by selecting from a library of process modules. Model parameters are dependent on the modules selected. CRHM is not coupled to any automatic calibration programs. The process modules are algorithms of varying levels of complexity and are selected based on data

availability, purpose and scale. Modules are available for: meteorological data interpolation using adiabatic relationships and saturation vapour pressure calculations, snow transport, rainfall interception, snowfall interception and sublimation, snow albedo decay, canopy transmissivity, shortwave direct and diffuse radiation, slope corrections to solar radiation, evaporation, snowmelt, snow cover depletion, infiltration into frozen and unfrozen soils, soil moisture, balance, organic layer flow, mineral flow, groundwater flow, overland flow and storage, and streamflow routing. The following CRHM modules were used in this study: Global and Slope_Qsi (radiation calculations with adjustments for aspect, elevation and slope), PBSM (snow transport and sublimation), SNOBAL (snowmelt), Canopy (adjusts shortwave and longwave radiation exchanges beneath needleleaf forest canopies and accounts for canopy effects on water mass balance at the ground surface). Figure 4.1 depicts the CRHM model and modules used in this study.

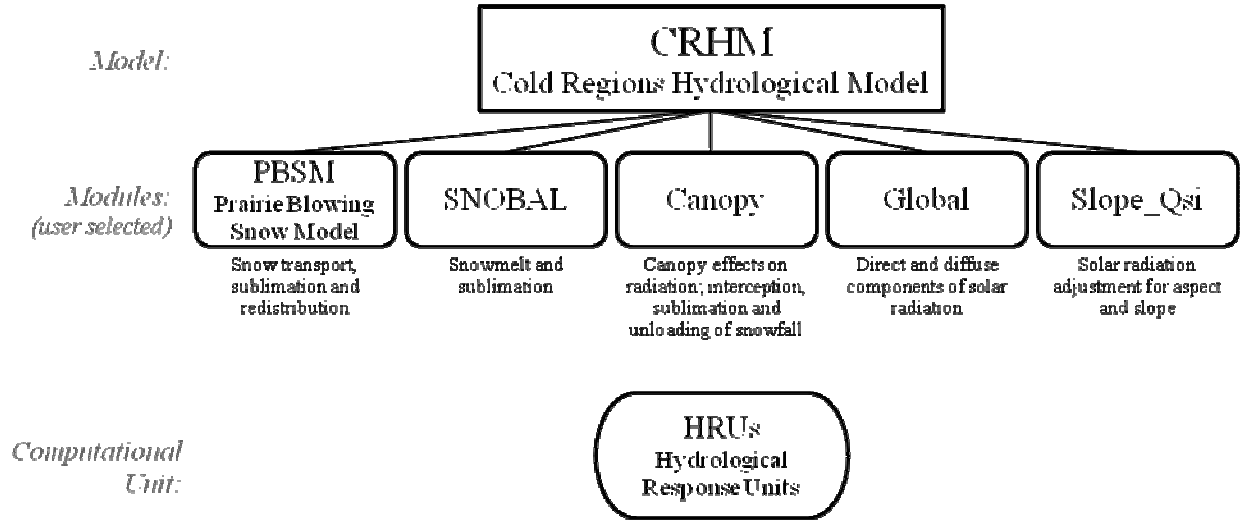

Figure 4.1 CRHM Model Structure for this study.

4.2.2 Global and Slope_Qsi

The CRHM Global module calculates theoretical clear-sky direct and diffuse solar radiation. Global calculates the theoretical direct beam component of solar radiation, Q_{dir}, according to Garnier and Ohmura (1970) and the diffuse clear-sky radiation component, Q_{dif}, according to List (1968) as

$$Q_{dir} = I \cdot p^{m}\left[(\sin\theta\cos H)(-\cos A\sin Z) - \sin H(\sin A\cos Z)\right. \\ \left. + (\cos\theta\cos H)\cos Z\right]\cos\delta + \left[\cos\theta(\cos A\sin Z) + (\sin\theta\cos Z)\right]\sin\delta \text{ `} \quad [4.1]$$

$$Q_{dif} = 0.5\left((1 - a_w - a_c)Q_{ext} - Q_{dir}\right) \quad [4.2]$$

where I is the intensity of extraterrestrial radiation, p is the mean zenith path transmissivity of the atmosphere, m is the optical air mass, δ is the declination of the sun, θ is the latitude, H is the hour angle measured from solar noon positively towards west, A is the slope azimuth measured from the north through east, Z is the slope angle, a_w is the radiation absorbed by water vapour (7%), a_c is the radiation absorbed by ozone (2%) and Q_{ext} is the extraterrestrial radiation on a horizontal surface at the outer limit of the earth's atmosphere. m is calculated from Kasten and Young (1989) as

$$m = \frac{1.0}{\cos Z + 0.50572(96.07995 - Z)^{-1.6364}} \quad [4.3]$$

The Slope_Qsi module calculates incident solar radiation on slopes based on the ratio of measured incident shortwave radiation on a level plane and the calculated clear-sky direct and diffuse shortwave radiation on a level plane (from Global).

4.2.3 Prairie Blowing Snow Model

PBSM calculates two-dimensional blowing snow transport and sublimation rates for steady-state conditions over a landscape element using mass and energy balances. PBSM was initially

developed for application over the Canadian Prairies, characterized by relatively flat terrain and homogeneous crop cover (e.g. Pomeroy, 1989; Pomeroy *et al*., 1993). Certain assumptions and parameterizations in PBSM were derived from field observations in the Canadian Prairies and therefore should be applied outside this environment with caution. However, versions have been applied to variable vegetation height (Pomeroy *et al*., 1991), over alpine tundra (Pomeroy, 1991) and arctic tundra (Pomeroy and Li, 2000) and show an ability to simulate winter snowpack evolution. Only key equations are presented here. Refer to Pomeroy (1988), Pomeroy and Gray (1990), Pomeroy and Male (1992), Pomeroy *et al*. (1993) and Pomeroy and Li (2000) for details on algorithm development.

The snow mass balance over a uniform element of a landscape (e.g. a HRU) is a result of snowfall accumulation and the distribution and divergence of blowing snow fluxes both within and surrounding the element given by Equation [2.1]. Since PBSM is for fully-developed blowing snow conditions, PBSM is restricted to minimum fetch distances of 300 m following measurements by Takeuchi (1980). Blowing snow transport fluxes are the sum of snow transport in the saltation and suspension layers, F_{salt} and F_{susp} (kg m^{-1} s^{-1}), respectively. Saltation of snow must be initiated before snow transport can occur in the suspension layer and blowing snow sublimation can occur.

F_{salt} is calculated by partitioning the atmospheric shear stress into that required to free particles from the snow surface, to that applied to nonerodible roughness elements and to that applied to transport snow particles (Pomeroy and Gray, 1990)

$$F_{salt} = \frac{c_1 e \rho u*_t}{g}\left(u*^2 - u*_n^2 - u*_t^2\right) \qquad [4.4]$$

where c_1 is the dimensionless ratio of saltation velocity to friction velocity ($u_p/u* = 2.8$), e is the dimensionless efficiency of saltation ($1/4.2u*$), ρ is atmospheric density (kg m^{-3}), g is

acceleration due to gravity (m s^{-2}), u^* is the atmospheric friction velocity (m s^{-1}), and u^*_n and u^*_t refer to the portions of the u^* applied to nonerodible roughness elements such as vegetation (nonerodible friction velocity) and the open snow surface itself (threshold friction velocity), respectively. Mechanical turbulence controls atmospheric exchange during blowing snow, thus u^* is calculated using the Prandtl logarithm wind profile as

$$u^* = \frac{u_z k}{\ln\left[\frac{z}{z_o}\right]} \quad [4.5]$$

where k is the von Kármán constant (0.41), u_z is the wind speed (m s^{-1}) at height z (m) above the snow surface and z_0 is the aerodynamic roughness length (m). z_0 is controlled by the saltation height and is given by

$$z_0 = \frac{c_2 c_3 u^{*2}}{2g} + c_4 \lambda \quad [4.6]$$

where c_2 is the square root of the ratio of the initial vertical saltating particle velocity to u^*, c_3 is ratio of z_0 to saltation height (0.07519; Pomeroy and Gray, 1990), c_4 is a drag coefficient (0.5; Lettau, 1969) and λ is the dimensionless roughness element density. Recent work has raised uncertainty in the turbulent exchange processes during blowing snow. Doorschot *et al*. (2004) showed that the aerodynamic roughness length in alpine terrain is more influenced by surrounding topography than by the saltation height. According to their findings, z_0 in this environment may be underestimated by the Pomeroy and Gray (1990) formulation. According to Helgason (2010) and Helgason and Pomeroy (2005), the advected turbulence associated with surrounding topography primarily enhances shear stress via horizontal turbulence and considerably less so via vertical turbulence. So the effects on particle lift and vertical fluxes such as sublimation may be muted. For this reason, it is assumed that snow-atmosphere exchange in

alpine environments can be adequately simulated using roughness length calculations derived from measurements over saltation and vegetation roughness in open and flat terrain.

u^*_n is calculated using an algorithm developed by Raupach *et al*. (1993) for wind erosion of soil calculations that relates the partitioning of the shear stress to the geometry and density roughness elements given by

$$\frac{u^*_n}{u^*} = \frac{(m\beta\lambda)^{0.5}}{(1+m\beta\lambda)^{0.5}} \qquad [4.7]$$

where β is the ratio of element to surface drag and λ is the dimensionless roughness element density. Raupach *et al*. (1993) found $\beta \approx 170$, which is used for shortgrass and crop stalks. m is an empirical coefficient to account for the difference in average and maximum surface shear stress to initiate erosion. The default value for m in PBSM is 1.0 for grass and cereal grain stalks. Wyatt and Nickling (1997) determined a mean $\beta = 202$ and mean $m = 0.16$ for desert creosote shrubs (*Larrea tridentata*) in a Nevada desert. Wyatt and Nickling's β and m are presumed to be more suitable for shrubs found in northwestern Canada than the grass and cereal grain default values in PBSM. λ is calculated as per Pomeroy and Li's (2000) modification of an original equation by Lettau (1969)

$$\lambda = Nd_v\left(h_v - \frac{S}{\rho_s}\right) \qquad [4.8]$$

where N is the vegetation number density (number m^{-2}), d_v is the vegetation stalk diameter (m), h_v is the height of vegetation (m) and the snow depth is snow accumulation, S, divided by snow density (ρ_s; kg m^{-3}).

u^*_t is calculated from the meteorological history of the snowpack using an algorithm developed by Li and Pomeroy (1997a) from observations at low vegetation sites in the Canadian prairies. Assuming an aerodynamic roughness height $z_o = 0.2$ mm, u^*_t is given by

$$u*_t = 0.35 + \frac{T}{150} + \frac{T^2}{8200} \quad [4.9]$$

where T is the ambient atmospheric temperature at 2 m (ºC).

F_{susp} is calculated as a vertical integration from a reference height near the top of the saltation layer, $h*$, to the top of blowing snow boundary layer (z_b), given by Pomeroy and Male (1992)

$$F_{susp} = \frac{u*}{k}\int_{h*}^{z_b} \eta(z) \ln\left(\frac{z}{z_0}\right) dz \quad [4.10]$$

where k is von Kármán's constant (0.41), η is the mass concentration of blowing snow (kg m^{-3}) at height z (m) and z_0 is the aerodynamic roughness height. z_b is governed by the time available for the vertical diffusion of snow particles from $h*$, calculated using turbulent diffusion theory and the logarithmic wind profile. $h*$ increases with friction velocity and is estimated as given by Pomeroy and Male (1992)

$$h* = 0.08436u*^{1.27} \quad [4.11]$$

For fully-developed flow it is constrained at z_b = 5 m. At z_b shear stress is constant ($d\tau/dt = 0$) and suspension occurs under steady-state conditions ($d\eta/dt = 0$). Note that as suspension diffuses from the saltation layer, saltation must be active for suspension to proceed.

E_B is calculated as a vertical integration of the sublimation rate of a single ice particle. Assuming particles to be in thermodynamic equilibrium, the sublimation rate of a single ice sphere is controlled by radiative energy exchange convective heat transfer to the particle, turbulent transfer of water vapour from the particle to the atmosphere and latent heat associated by sublimation, and is given by (Schmidt, 1972) as

$$\frac{dm}{dt} = \frac{2\pi r \sigma - \frac{Q_r}{\lambda_T T Nu}\left(\frac{L_S M}{RT} - 1\right)}{\frac{L_S}{\lambda_T T Nu}\left(\frac{L_S M}{RT} - 1\right) + \frac{1}{D\rho_S Sh}} \quad [4.12]$$

where r is the radius of a snow particle with mass m (μm), σ is the atmospheric undersaturation with respect to ice (dimensionless), Q_r is the radiation absorbed by the particle (J s^{-1} m^{-2}), L_S is the latent heat of sublimation ($2.838 \cdot 10^6$ J kg^{-1}), M is the molecular weight of water (18.01 kg mol^{-1}), λ_T is the thermal conductivity of the atmosphere ($0.00063T + 0.0673$; J s^{-1} K^{-1}), Nu is the Nusselt number (dimensionless), R is the universal gas constant (8313 J mol^{-1} K^{-1}), T is the ambient atmospheric temperature (K), ρ_s is the saturation density of water vapour at T (kg m^{-3}) and Sh is the Sherwood number (dimensionless).

The mean particle mass is characterized by a two-parameter gamma distribution of particle size that varies with height. The relative frequency, $f(r)$, of particles with radius r is given by

$$f_r = \frac{r^{(\alpha-1)} \exp\left(-\frac{r}{\beta}\right)}{\beta^{\alpha}\Gamma(\alpha)} \qquad [4.13]$$

where Γ is the gamma function, β is a scale parameter (m) and α is a dimensionless shape parameter.

The vertically integrated sublimation rate is given by

$$E_B = \int_0^{z_b} \frac{1}{m(z)} \frac{dm}{dt}(z)\eta(z)dz \qquad [4.14]$$

where m is the mean mass of a single ice particle at height z. The rate that water vapour can be removed from the ice particle's surface layer, dm/dt, is calculated using Equation [4.12]. E_B calculations are highly sensitive to ambient relative humidity, temperature and wind speed (Pomeroy *et al*., 1993; Pomeroy and Li, 2000).

Field observations show that blowing snow is a phenomenon that is unsteady over both space and time. Small scale spatial variability in snowcover properties produce sub-element (e.g. grid cell or HRU) variability in snow transport. These small scale features make it difficult to justify

assumptions of uniform fetch and time step-constant wind speed in modelling efforts. Li and Pomeroy (1997b) developed an algorithm to estimate the temporal probability of blowing snow occurrence. Pomeroy and Li (2000) applied the algorithm in order to upscale blowing snow fluxes from point to area, under the assumption that the model area (e.g. grid cell or HRU) is uniform in its mean attributes. The probability of blowing snow occurrence, p, can be approximated by a cumulative normal distribution as

$$p = \frac{1}{\delta\sqrt{2\pi}} \int_0^u e^{-\frac{(u_{mean}-u)^2}{2\delta^2}} du \qquad [4.15]$$

where u_{mean} is the mean wind speed (location parameter), δ is the standard deviation (scale parameter) of wind speed u (m s^{-1}). Empirical equations for u_{mean} and δ were developed from six years of data collected at 15 locations in the Canadian prairies. For dry snow

$$u_{mean} = 0.3665T + 0.00706T^2 + 0.9I + 11.2 \qquad [4.16]$$

$$\delta = 0.145T + 0.00196T^2 + 4.3 \qquad [4.17]$$

where I is the natural logarithm of the hours since the last snowfall and T is the ambient atmospheric temperature (ºC). For wet snow, u_{mean} = 21 m s^{-1} and δ = 7 m s^{-1}.

Since Equations [4.15], [4.16] and [4.17] were developed from prairie observations, a discussion of its applicability in mountain environments is warranted. It is unclear if the temporal probability of blowing snow occurrence in mountain environments is sufficiently similar to prairies environments to justify applying Equations [4.15], [4.16] and [4.17]. Winds in mountains environments are certainly more turbulent than in the prairies. However, Pomeroy and Li's (2000) assumption of applying the time series-derived probability algorithm to a uniform is appropriate for mountain environments if HRUs or grid cells sizes are selected carefully. A study of the probability of blowing snow occurrence is warranted for mountain environments.

4.2.4 SNOBAL

SNOBAL (Marks *et al*., 1998, 1999) calculates the amount of snowmelt using the energy equation and was developed for deep mountain snowcover. SNOBAL approximates the snowcover as two layers: a surface active layer of fixed depth and a lower layer that represents the remaining snowpack. SNOBAL was previously applied at MCRB by DeBeer and Pomeroy (2009).

Snowmelt in either layer occurs when the available energy exceeds that required to bring the snow layer temperature above 0 °C. The amount of snowmelt is calculated using

$$M = \frac{Q_m}{\rho_w h_f B} \qquad [4.18]$$

where Q_m is the energy available for melt, ρ_w is the density of water, h_f is the latent heat of fusion (333.5 kJ kg^{-1}) and B is the fraction of ice in a unit mass of wet snow (0.97). Q_m is calculated from the energy equation (Equation [2.2]).

Snow albedo, α_s, during winter was estimated using the method outlined by Gray and Landine (1987). The albedo depletion was approximated by three lines of different slope representing three periods: pre-melt, melt and post-melt.

Sublimation (and condensation) at the snow-atmosphere interface is diagnosed from the latent heat flux, and sublimation (and condensation) at the snow-soil interface is calculated from the specific humidities of the snow and soil layers and a diffusion coefficient (Marks *et al*., 1998). Liquid water in the snowpack is first evaporated using the ratio of latent heat of vaporization to sublimation at 0°C (0.882). The remaining diagnosed evaporative loss is calculated as ice sublimation. Half of the sublimated ice decreases snowpack depth but does not alter its density.

All of the evaporated liquid water and the other half of sublimated ice decrease the snowpack density and specific mass.

4.2.5 Canopy

The CRHM Canopy module calculates energy and water input to the snow surface beneath a needleleaf forest canopy and is more fully described by Ellis *et al*. (2010).

Shortwave transmissivity through the forest canopy is given by a Beer-Bouger type formulation given by a variation of Pomeroy and Dion's (1996) formulation (Pomeroy *et al*., 2009)

$$\tau_C = \exp\left(-\frac{1.081\cos(\theta)PAI'}{\sin(\theta)}\right) \quad [4.19]$$

where θ is the solar angle above the horizon (radians). Multiple reflections within the canopy are not explicitly account for and there are not separate calculations for canopy foliage, trunks and gaps.

Enhanced longwave irradiance to the surface from the forest canopy. The incoming longwave radiation to the snowpack beneath the forest canopy, $L{\downarrow}_f$, is given by

$$L{\downarrow}_f = vL{\downarrow} + (1-v)\varepsilon_f \sigma T_f^4 \quad [4.20]$$

where v is the sky view factor, ε_f is the forest thermal emissivity (unitless), σ is the Stefan-Boltzmann constant (W m^{-2} K^{-4}) and T_f is the forest temperature (K).

Canopy also estimates the canopy throughfall of rain and snow, the canopy interception and evaporation of rain, the canopy interception and sublimation of snow, the unloading of intercepted snow and the drip of intercepted rain.

Canopy interception of snowfall and sublimation of intercepted snow is calculated using relationships presented by Pomeroy *et al*. (1998). The amount of intercepted snow is calculated as

$$I_S = I_S^* \left(1 - e^{-C_1 P / I_S^*}\right) \quad [4.21]$$

where C_1 is the dimensionless canopy-leaf contact per ground, P is snowfall and I_s^* is the maximum intercepted snow load, which is estimated as a function of the maximum snow load per unit area of branch, the density of falling snow and LAI`. The sublimation of intercepted snow is calculated by adjusting the sublimation rate of an ice sphere by an intercepted snow exposure coefficient (Pomeroy and Schmidt, 1993; Pomeroy *et al*., 1998).

4.2.6 Modélisation Environmentale Communautaire – Surface and Hydrology

MESH is the land-surface hydrology configuration of Environment Canada's community environmental modelling system, MEC (Modélisation Environmentale Communautaire; Pietroniro *et al*., 2007)). The objective of MEC is complete coupling of land surface hydrology and atmospheric models to produce operational weather and hydrological forecasts. In this study MESH was used in offline mode, meaning atmospheric forcings were read from files rather than in coupled online mode with an atmospheric model providing the forcings and receiving the output. MESH 1.2.1 was used in this study. The version of MESH used is essentially WATCLASS (Soulis *et al*., 2000), a coupling of CLASS (Verseghy, 1991, 2000; Verseghy *et al*., 1993) and components of the hydrological model WATFLOOD (Kouwen, 1988, 2001; Kouwen and Mousavi, 2002). CLASS was developed at the Meteorological Service of Canada for use in the Canadian General Circulation Model. In MESH, CLASS calculates vertical water and energy balances, WATDRAIN (Soulis *et al*., 2000) calculates interflow between landscape units and

WATROUTE routes channel flow between grid cells. MESH 1.2.1 contains CLASS 3.4 (Verseghy, 2008). WATROUTE and WATDRAIN were not used in this study and are thus not discussed. CLASS is designed to run at time steps of 30 minutes or less. Figure 4.2 depicts the CRHM model and modules used in this study.

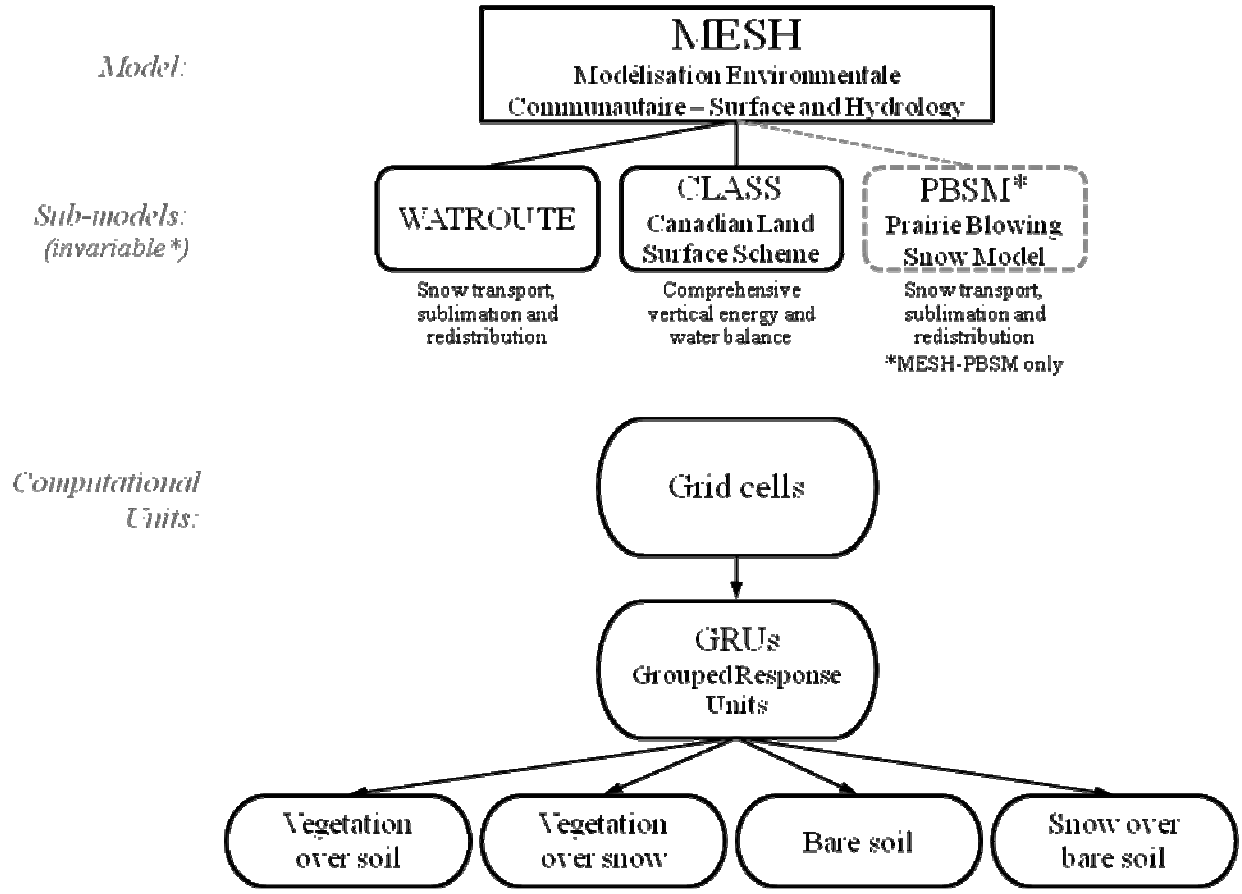

Figure 4.2 MESH/MESH-PBSM Model Structure.

CLASS calculates the vertical energy and water balances separately for four subareas: canopy over snow, canopy over bare ground, bare ground and snow. A number of prognostic variables are calculated: temperature of the soil layers, liquid and frozen water contents of the soil layers; temperature, depth and density of the snowpack; temperature and mass of intercepted liquid and frozen water; temperature and depth of ponded water on the ground surface. CLASS uses

physically based algorithms to calculate: evaporation and sublimation from vegetation canopy; interception, throughfall and drip of rainfall and snowfall; freezing and thawing of liquid and frozen water on the canopy and in soil layers; surface ponding and freezing of ponded water; sublimation from the snowpack; snowmelt; infiltration of rain into the snowpack; infiltration into soil; soil water movement between soil layers in response to gravity and suction forces; temporal variation of snow albedo and density.

Surface energy fluxes are evaluated using a balance of the net shortwave radiation, net longwave radiation, latent heat flux, sensible heat flux and surface flux (Equation [2.2]). The components of the energy balance are solved iteratively as functions of a single unknown, the surface temperature, using either a combination of secant and bisection methods or the Newton-Raphson method.

Multiple soil layers depths can be used, with the default parameterization being three soil layers with depths of 0.10, 0.35 and 4.10 m below the ground surface. The depths of 0.10 and 4.10 m were selected to approximate the lower boundaries affected by diurnal and annual temperature waves, respectively (Verseghy, 1991). The percent clay, sand and organic matter is explicitly stated for each soil layer. Bedrock layers are allowed at any depth.

Four main vegetation types are included in CLASS algorithms: needleleaf trees, broadleaf trees, crops and grass. Each vegetation type is assigned a background value for physiological parameters such as albedo, roughness, maximum and minimum leaf area index (LAI), etc. The physiological parameters vary throughout a simulation using annual or diurnal functions.

The snowpack is modelled as a single layer using a coupled mass and energy balance. Snowmelt occurs if energy available for melt is calculated as part of the surface energy balance solution or if the snowpack temperature is projected to rise above 0ºC. A residual water content

is allowed in the snowpack. Snow surface near-infrared and visible albedo vary temporally according to decay curves from background albedo values for fresh, old dry and melting snow. The snowpack density increases temporally from a background fresh snow value to a maximum value according to empirical exponential functions. The snowpack transmissivity is calculated from the snow depth using Beer's law. Areal snowcover depletion is parameterized via a limiting snow depth parameter and snow depletion curves. Snowcover is complete until the snow depth falls below a limiting snow depth value; then the snow depth is reset to this value and snowcovered area is calculated according to depletion curves (Donald *et al*., 1995). CLASS 3.4 does not include blowing snow calculations, though Gordon *et al*. (2006) did incorporate a parameterization of blowing snow sublimation in CLASS 3.0.

The spatial discretization used in MESH is a combination of the approaches used in WATFLOOD and CLASS. CLASS performs calculations over a mosaic of five subareas: needleaf trees, broadleaf trees, crops, grass, bare ground and urban. WATFLOOD grid cells are typically 1-15 km in dimension with subgrid variability accounted for using GRUs. GRUs are similar to HRUs in that they are model elements that share common biophysical properties, however their model representation is simpler in that GRUs do not follow a landscape sequence or a water cascade. Runoff from each GRU within a grid cell is routed directly into the grid channel, not at all through the GRUs. In MESH, model elements are GRUs that are composed of one or more CLASS subareas.

4.2.7 Ryan/MicroMet Windflow Model

The Ryan/MicroMet distributed windflow algorithm (hereafter RMM) is part of the MicroMet meteorological model (Liston and Sturm, 2006). A wind direction diverting parameterization developed by Ryan (1977) is critical to its distributed application. RMM takes a reference wind

speed and direction and calculates distributed wind speed direction over a DEM. In this study RMM was implemented using MATLAB.

Wind speed and direction are converted to zonal and meridional components to avoid problems with interpolating over 0º/360º. From a DEM, RMM calculates topographic slope, azimuth and curvature at each grid cell. Grid cell curvature, Ω_C, is calculated from the elevation of opposing grid cells in four directions and the average of these four curvature values is the curvature of the grid cell of interest. Ω_C is given by

$$\Omega_C = \frac{1}{4}\left[\frac{z - 1/2\left(z_W + z_E\right)}{2\eta} + \frac{z - 1/2\left(z_S + z_N\right)}{2\eta} + \frac{z - 1/2\left(z_{SW} + z_{NE}\right)}{2\sqrt{2}\eta} + \frac{z - 1/2\left(z_{NW} + z_{SE}\right)}{2\sqrt{2}\eta}\right] \quad [4.22]$$

where z_N, z_{SW}, etc. are the elevation of cells in directions north, southwest, etc. of the cell of interest at the curvature length scale η (m) from the cell of interest. The curvature length scale is approximately equal to a half wavelength of a topographic feature with the DEM (e.g. distance from a ridge to a valley bottom).

The slope in the direction of the wind, Ω_S, is given by

$$\Omega_S = \beta\cos\left(\theta - \xi\right) \quad [4.23]$$

where β is the terrain slope, θ is the wind direction and ξ is the terrain slope azimuth.

The modified wind speed at the cell of interest is given by

$$W_T = W_W W \quad [4.24]$$

where W is the reference wind speed and W_W is the wind weight calculated using

$$W_W = 1 + \gamma_S\Omega_S + \gamma_C\Omega_C \quad [4.25]$$

where γ_s and γ_c are the weights assigned to the slope and curvature functions, respectively.

The wind direction at the cell of interest is modified according to Ryan (1977) as

$$\theta_d = -0.5\Omega_S \sin[2(\xi - \theta)] \quad [4.26]$$

and the modified wind direction at the cell of interest is given by

$$\theta_t = \theta + \theta_d \quad [4.27]$$

4.2.8 Dynamically Dimensioned Search Algorithm

DDS is an automatic heuristic stochastic single-solution based global search algorithm presented by Tolson and Shoemaker (2007). DDS has been used to calibrate SWAT (Tolson and Shoemaker, 2007), CLASS (Dornes *et al*., 2008b and 2008c) and MESH (Dornes *et al*., 2008c). Algorithm input includes the maximum number of evaluations and the range of values for each parameter. The algorithm was designed to find "good" global solutions, as opposed to globally optimal solutions, within a specified number of model evaluations. The algorithm is scaled such that it initially searches globally and searches more locally as the number of iterations approaches the specified number of model evaluations. The transition from global to more local search occurs as the number of parameters being calibrated at each iteration is reduced. The parameters perturbed at each iteration are randomly selected at a magnitude randomly sampled from a normal distribution of parameter values. The only algorithm parameter to be set is the scalar neighbourhood size perturbation parameter that defines the magnitude of the random perturbation as a fraction of the input parameter ranges. All calibrated parameters have the same perturbation parameter value, thus have the same random perturbation relative to their respective parameter value range. The default perturbation parameter value of 0.2 was used in this study.

4.3 CLASS-PBSM Development

PBSM code in C++ from the CRHM source code was converted to Fortran 90 to be compatible with CLASS and MESH. The single column PBSM snow transport and sublimation calculations were coded into the CLASS part of the MESH code. The inter-GRU redistribution of wind-transported snow mass was coded into MESH, outside of the CLASS section (refer to Section 5.2). For single column applications of PBSM coupled to MESH (i.e. no inter-GRU snow redistribution) the model is herein referred to as CLASS-PBSM. For distributed applications of PBSM coupled to MESH (i.e. including inter-GRU snow redistribution) the model is herein referred to as MESH-PBSM.

PBSM routines were coded into the CLASS water budget calculation routine (CLASSW). PBSM calculations are made at the GRU-level, therefore snow transport calculations are not performed separately for the subareas. The PBSM calculations are made following all the subarea water balance calculations as described in Verseghy (2008). Following the PBSM calculations, the subarea snow depths and heat capacities are recalculated by subtracting an equal amount of SWE from each subarea that had snow on the ground prior to the snow transport and sublimation calculations. If a subarea does not have sufficient snow on the ground for its complete equal amount to be removed, then all of that subarea snow is removed (i.e. contributes to total GRU snow transport), and this difference between the original equal amount calculated to be removed and the actual amount removed is equally subtracted from subsequent subareas. The subareas snow removal calculations are performed in the following sequence: canopy over bare ground > bare ground > canopy over snow > snow-cover ground. The logic behind this sequence is that the least amounts of snow will be found in the canopy over bare ground and bare ground subareas.

No changes were made to the CLASS surface energy budget calculations (CLASST). The calculated blowing snow sublimation loss is removed from the mass balance and thermodynamic feedback is not included as it is in other blowing snow models (Bintanja, 1998, 2000, 2001; Déry *et al*., 1998; Déry and Yau, 1999 and 2001). Any thermodynamic feedback is reflected in the driving meteorology (i.e. humidity and temperature). The negative feedback included in other models (i.e. decreased water vapour deficit and temperature) due to blowing snow sublimation significantly reduces calculated sublimation rates and does not always agree with field measurements (Pomeroy and Li, 2000) due to the entrainment and mixing of dry air during blowing snow events. Further advancement of theory supported by field measurements is required to close this research gap.

The addition of PBSM to CLASS required four additional parameters per GRU: fetch distance (Equation [2.1]), vegetation height, width and number density (Equation [4.8]). In addition the specification of an additional initial state, the snowpack age (Equation [4.16]), is required. The term $m\beta$ (Equation [4.7]) was hardcoded into CLASS as 1.0×170 for the crop and grass vegetation categories, and as 0.16×202 for the needleleaf and broadleaf tree vegetation categories.

4.4 Fisera Ridge Point Simulations

4.4.1 Parameterization

Point simulations at the RT station were performed in order to evaluate CRHM (PBSM and SNOBAL), CLASS and CLASS-PBSM in this environment. Simulations were performed using RT observations from 22 October 2007 – 8 April 2008 and 14 October 2008 – 22 May 2009. These periods were selected because of good, continuous point snow depth measurements. Simulated snow depth was compared to automatic SR50 sonic snow depth gauge measurements.

Simulations were performed using a 15-minute time step with CRHM and a 30-minute time step with CLASS and CLASS-PBSM.

CRHM model parameters for the RT point simulations are presented in Table 4.1. The vegetation density and silhouette area parameter values were set based on observations over the north-facing slope which is also windswept (refer to Table 3.1). The vegetation height was set to a nominal value of 0.05 m to represent the area surrounding the RT station. The SR50 measures snow depth over an area sparsely covered with short grass; however, there are shrubs in the surrounding area that increase the effective roughness length around the SR50. A blowing snow fetch distance of 300 m was specified as this is the minimum value required for the fully-developed flow calculations performed by PBSM.

Table 4.1 Fisera Ridge RT CRHM model parameters

Vegetation height (m)	0.05
Vegetation density (shrubs·m^{-2})	0.1
Vegetation silhouette area(m^2)	0.5

Calibration of CLASS and CLASS-PBSM parameters was performed using DDS on the 2008/2009 data because it is a longer period of data than 2007/2008. Root mean squared error (*RMSE*) of snow depth was used as the objective function.

$$RMSE = \sqrt{\frac{\sum \left(z_{snow,SIM} - z_{snow,OBS} \right)^2}{n}} \qquad [4.28]$$

where n is the number of simulated-observed pairs, and $z_{snow,SIM}$ and $z_{sim,OBS}$ are the simulated and observed snow depth in metres, respectively. Four optimization trials of 2000 objective functions evaluations were performed for both CLASS and CLASS-PBSM. The optimal parameter sets had an *RMSE* of 33.7 cm and 19.0 cm for CLASS and CLASS-PBSM, respectively.

Table 4.2 shows the optimum parameter values and parameter ranges for the calibrations for (a) CLASS and (b) CLASS-PBSM. CLASS parameters definitions and recommended values are included in Appendix B. The optimum parameter sets (MESH_parameters_CLASS.ini and MESH_parameters_hydrology.ini) for both CLASS and CLASS-PBSM are included in Appendix C.

Table 4.2 Optimized parameter values for Fisera Ridge RT point simulation for (a) CLASS and (b) CLASS-PBSM. Values in parentheses indicate parameter bounds.

(a)

Parameter	Shrubs	Grass
Veg. roughness length [m]	0.049 (0.025, 0.1)	0.026 (0.01, 0.04)
Veg. visible albedo ALVC []	0.025 (0.02, 0.1)	0.044 (0.02, 0.08)
Veg. near-IR albedo ALIC []	0.188 (0.15, 0.3)	0.202 (0.2, 0.4)
Maximum LAI LAMX []	0.307 (0.1, 0.5)	0.902 (0.2, 1)
Minimum LAI LAMN []	0.188 (0.05, 0.2)	0.584 (0.1, 0.6)
Limiting snow depth ZSNL (m)	0.02 (0.01, 1.00)	

(b)

Parameter	Shrubs	Grass
Veg. roughness length [m]	0.083 (0.025, 0.1)	0.021 (0.01, 0.04)
Veg. visible albedo ALVC []	0.094 (0.02, 0.1)	0.070 (0.02, 0.08)
Veg. near-IR albedo ALIC []	0.232 (0.15, 0.3)	0.284 (0.2, 0. 4)
Maximum LAI LAMX []	0.426 (0.1, 0.5)	0.965 (0.2, 1)
Minimum LAI LAMN []	0.149 (0.05, 0.2)	0.236 (0.1, 0.6)
Vegetation height Ht [m]	0.088 (0.05, 0.2)	
Limiting snow depth ZSNL (m)	0.17 (0.01, 1.00)	

4.4.2 Results and Discussion

Figures 4.3a and 4.3b show observed snow depth and snow depth simulated using CRHM, CLASS and CLASS-PBSM for 2007/2008 and 2008/2009, respectively. Table 4.3 shows model evaluation statistics for both periods. In addition to *RMSE*, modelled snow depth was evaluated using the normalized root mean squared error, model bias and coefficient of determination (goodness of fit), given by

$$NRMSE = 100\frac{RMSE}{z_{snow,OBS,Max} - z_{snow,OBS,Min}} \quad [4.29]$$

$$MB = \frac{\sum z_{snow,SIM}}{\sum z_{snow,OBS}} - 1 \quad [4.30]$$

$$R^2 = \left[\frac{\sum \left(\Delta z_{snow,OBS} - \overline{\Delta z_{snow,OBS}} \right) \left(\Delta z_{snow,SIM} - \overline{\Delta z_{snow,SIM}} \right)}{\sqrt{\sum \left(\Delta z_{snow,OBS} - \overline{\Delta z_{snow,OBS}} \right)^2} \sqrt{\sum \left(\Delta z_{snow,SIM} - \overline{\Delta z_{snow,SIM}} \right)^2}} \right]^2 \quad [4.31]$$

where $z_{snow,SIM}$ and $z_{snow,OBS}$ are the simulated and observed snow depth, respectively, $z_{snow,OBS,Max}$ and $z_{snow,OBS,Min}$ are the maximum and minimum observed snow depth, respectively, $\Delta z_{snow,SIM}$ and $\Delta z_{snow,OBS}$ are the change in simulated and observed snow depth from time step to time step, respectively, and $\overline{\Delta z_{snow,OBS}}$ and $\overline{\Delta z_{snow,SIM}}$ are the average change in observed snow depth over the simulation period. The *NRMSE* normalizes the *RMSE* of snow depth with respect to the range of observed values and is expressed as a percentage. Positive and negative *MB* indicate the fraction by which snow depth is either overestimated or underestimated throughout the simulation, respectively. The coefficient of determination gives a measure of the accuracy of the model with R^2 = 1.0 indicating that the model perfectly simulated the variation in change of observed snow depth and R^2 = 0.0 indicating that the model did not simulate any of the variation.

CRHM captured the general trends in snow depth during both periods. There were occasions during both periods where CRHM overestimated snow depth (e.g. late November 2007, late February 2008 and January 2009) and underestimated local peak snow depths (e.g. early December 2007, late January 2008, early April 2008). Not surprisingly since this is a windswept location, CLASS-PBSM provided considerably better results than CLASS. CLASS-PBSM overestimated snow depth throughout the 2007/2008 simulation. CLASS-PBSM overestimated snow depth throughout the 2008/2009 simulation up until snowmelt began to dominate in May.

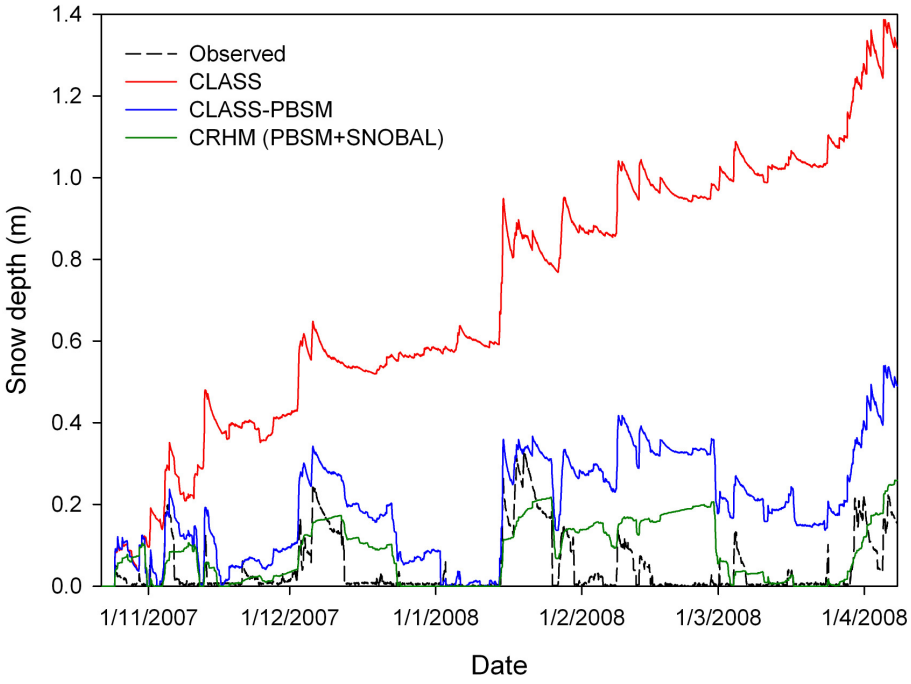

(a)

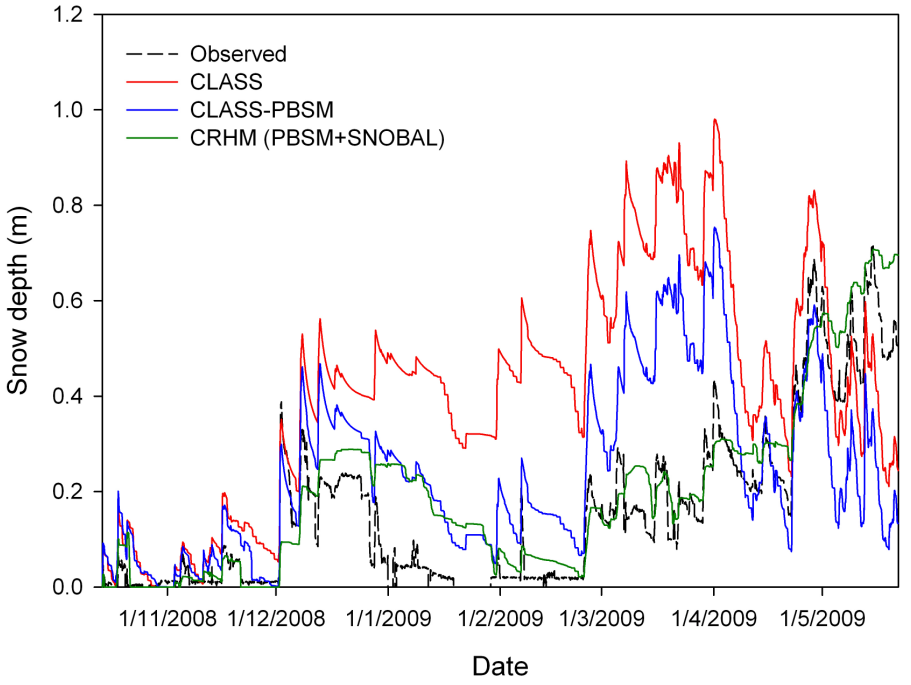

(b)

Figure 4.3 Observed snow and snow depth simulated at Fisera Ridge RT using CRHM (PBSM and SNOBAL), CLASS and CLASS-PBSM for (a) 2007/2008 and (b) 2008/2009.

Table 4.3 Model evaluation statistics for Fisera Ridge RT point simulations

	NRMSE (*RMSE* [cm])			*MB*			R^2		
Year	**CRHM**	**CLASS**	**CLASS-PBSM**	**CRHM**	**CLASS**	**CLASS-PBSM**	**CRHM**	**CLASS**	**CLASS-PBSM**
2007/2008	21.7 (*7.2*)	223 (*73.9*)	55.3 (*18.4*)	0.07	15.2	3.42	0.21	0.21	0.20
2008/2009	11.9 (*8.5*)	47.1 (*33.7*)	26.6 (*19.0*)	0.20	1.57	0.52	0.07	0.06	0.07

Figures 4.4a and 4.4b show cumulative snowfall, blowing snow transport, blowing snow sublimation, snowmelt, snowpack sublimation and snow accumulation for the RT point simulation using CRHM for 2007/2008 and 2008/2009, respectively. SNOBAL simulated approximately equal snowmelt and snowpack sublimation for both 2007/2008 and 2008/2009. Figures 4.5a and 4.5b show cumulative snowfall, blowing snow sublimation, snowmelt, snowpack sublimation and snow accumulation for the RT point simulation using CLASS-PBSM for 2007/2008 and 2008/2009, respectively.

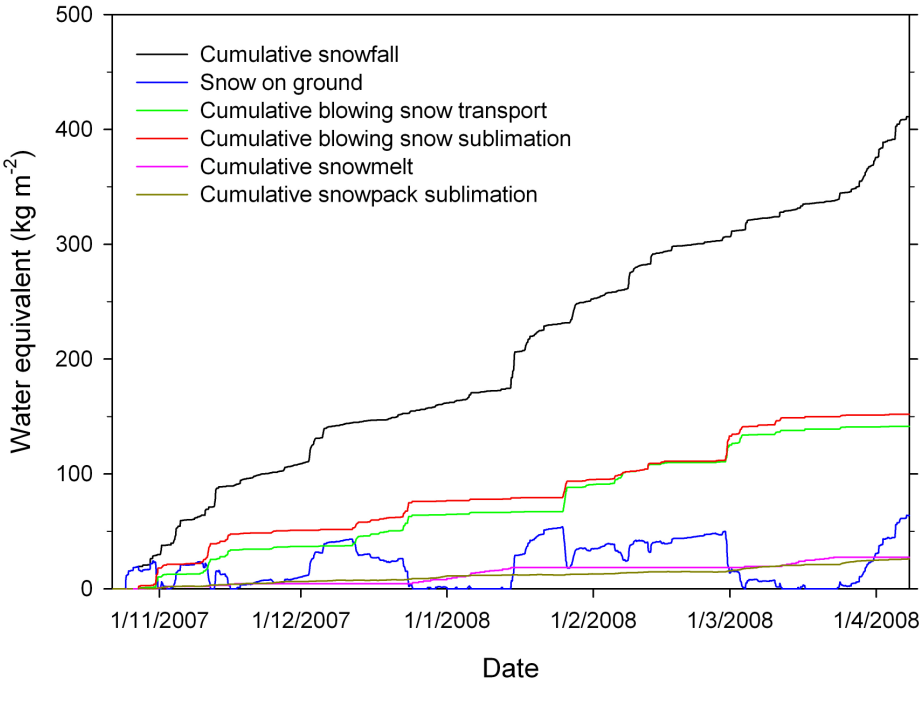

(a)

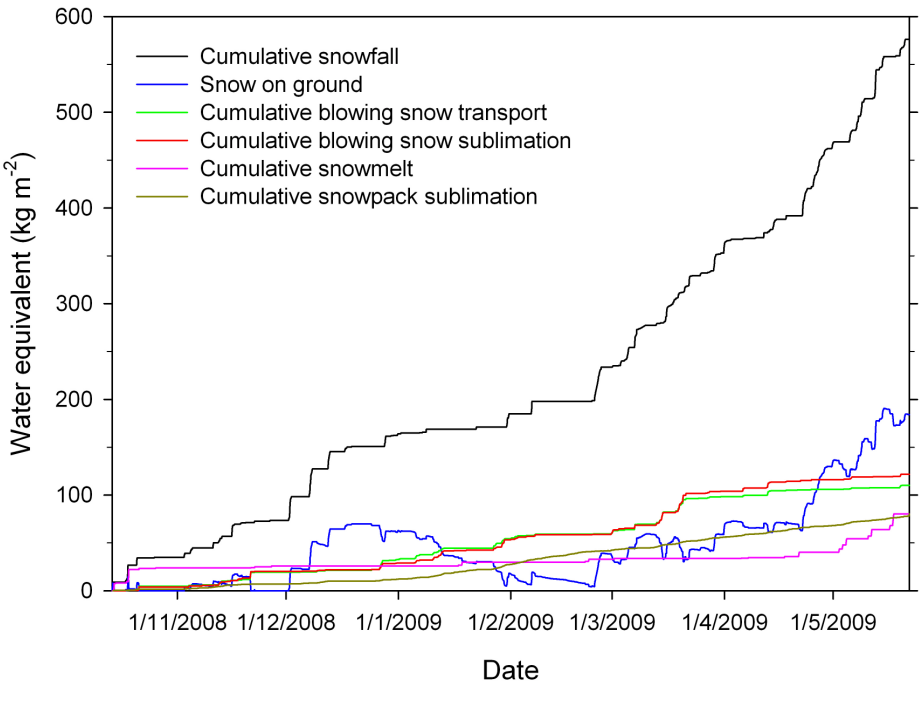

(b)

Figure 4.4 Cumulative snowfall, blowing snow transport, blowing snow sublimation, snowmelt, sublimation of snow on ground and snow accumulation for the Fisera RT point simulation using CRHM for (a) 2007/2008 and (b) 2008/2009.

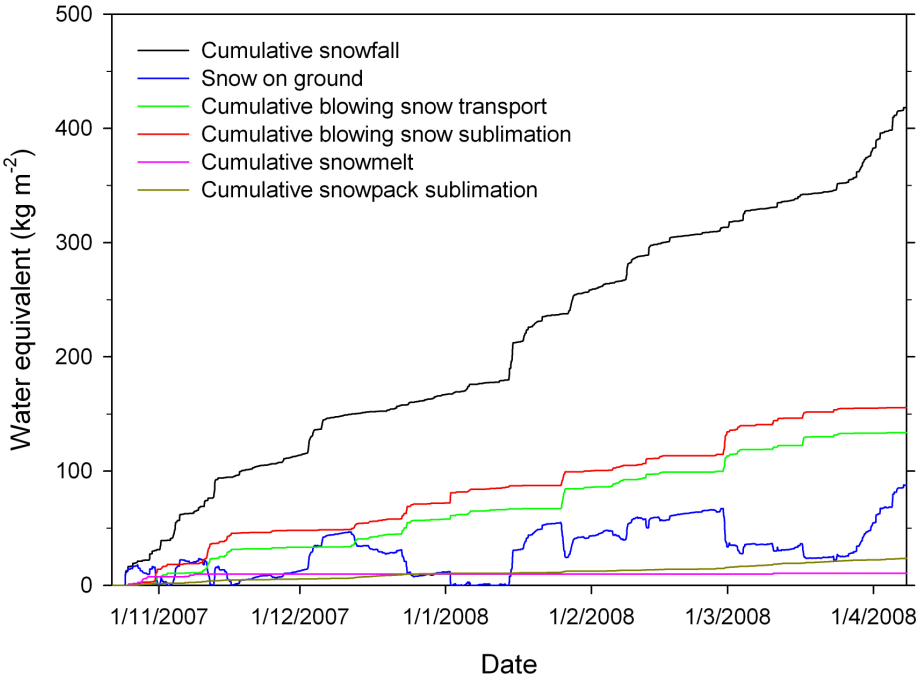

(a)

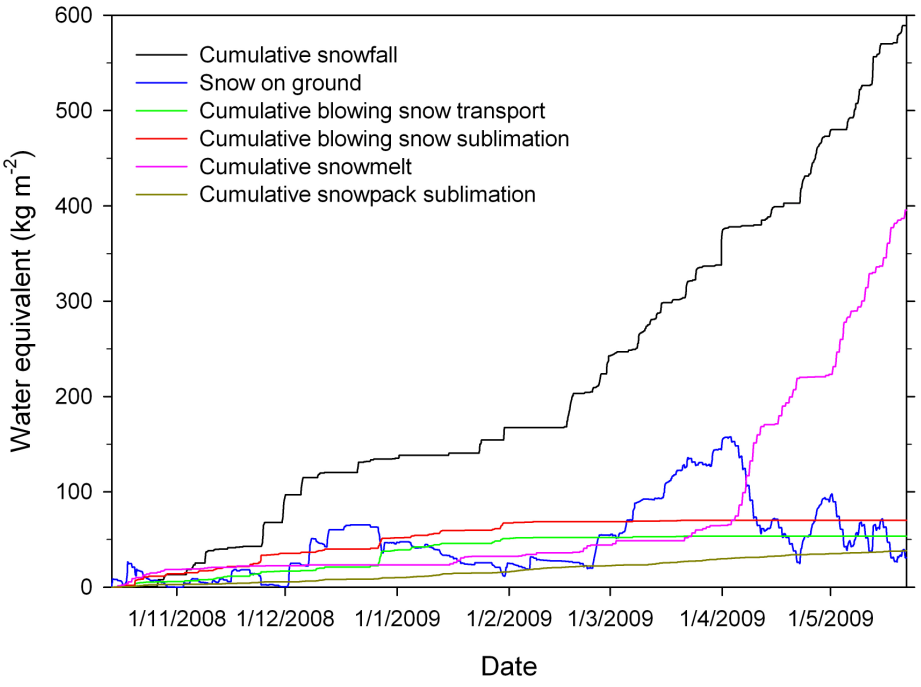

(b)

Figure 4.5 Cumulative snowfall, blowing snow transport, blowing snow sublimation, snowmelt, sublimation of snow on ground and snow accumulation for the Fisera RT point simulation using CLASS-PBSM for (a) 2007/2008 and (b) 2008/2009.

CRHM (PBSM and SNOBAL) provided a better simulated snow depth at the RT than both CLASS and CLASS-PBSM (Table 4.3) and is therefore considered to provide the most realistic simulated fluxes. CLASS-PBSM and CRHM simulated similar quantities of blowing snow transport and sublimation for 2007/2008, whereas for 2008/2009 CLASS-PBSM simulated 49% of the blowing snow transport and 58% of the blowing snow sublimation simulated by CRHM. CLASS-PBSM simulated little snow transport from March 2009 onwards as snowmelt dominated. SNOBAL simulated approximately 17 mm more snowmelt than did CLASS-PBSM for 2007/2008. Conversely, CLASS-PBSM simulated 315 mm more snowmelt than did SNOBAL during 2008/2009, mostly during April and May. Note that only the 2008/2009 period extended beyond early April and it was during this period that CLASS simulated the majority of snowmelt. SNOBAL and CLASS-PBSM simulated similar amounts of snowpack sublimation over 2007/2008 (26 and 24 mm, respectively). SNOBAL simulated 80 mm of snowpack sublimation during 2008/2009. CLASS-PBSM simulated only 38 mm of snowpack sublimation as simulated snowmelt dominated during this period.

There are a number of potential causes for the underestimated snow depth during April and May 2009. The SR50 snow depth data is of good quality as it was verified by checking nearby manual snow depth measurements. The incoming solar radiation observations at the RT station are in line with the clear-sky direct and diffuse solar radiation calculated using the Global module within CRHM (section 4.2.2). There were a few instances, as shown in Figure 4.6, where observed incoming solar radiation was greater than the maximum clear-sky solar radiation. This may be due to slight instrument bias or imperfections in the solar radiation model, but is likely due to reflected shortwave radiation from adjacent snow-covered slopes and patchy cloud cover.

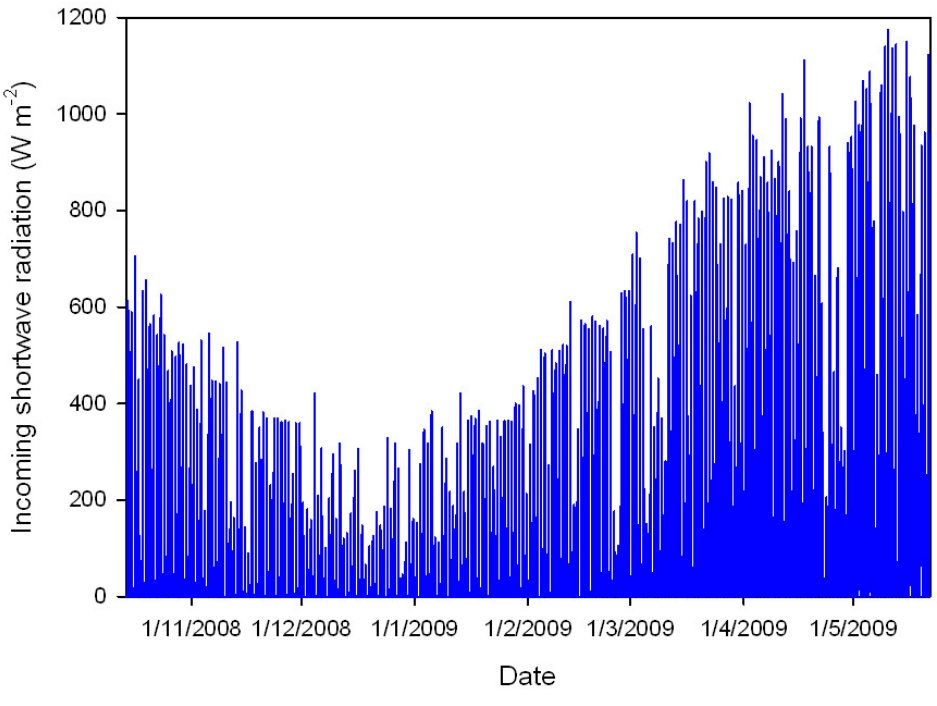

(a)

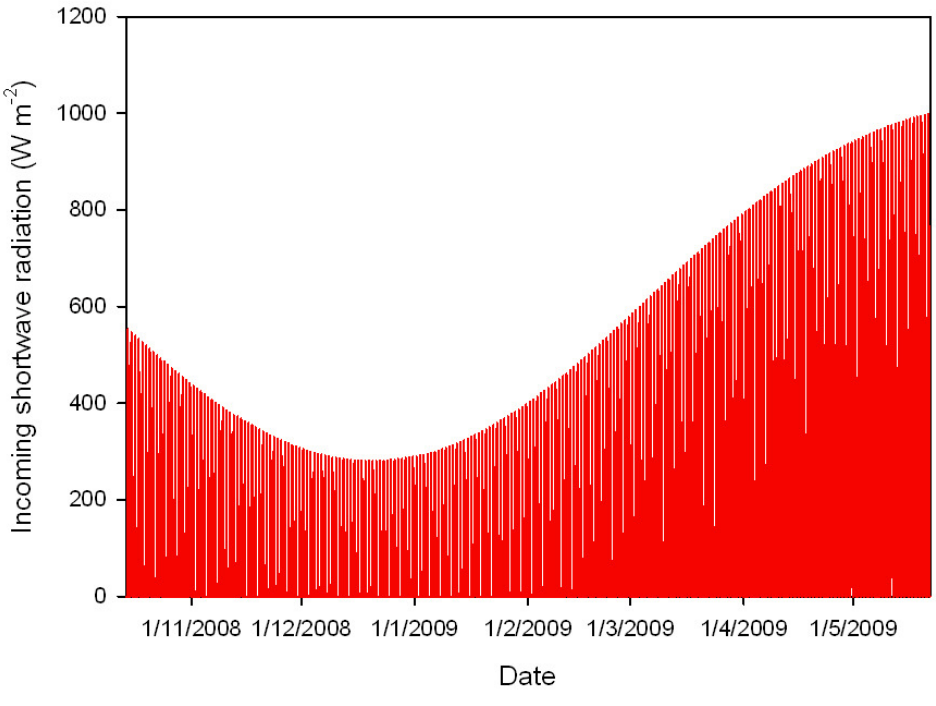

(b)

Figure 4.6 Fisera Ridge-top meteorological station 2008/2009 (a) observed incoming shortwave radiation and (b) sum of calculated of clear-sky direct and diffuse shortwave radiation

To test whether incoming shortwave radiations measurements were higher than actual radiation, incoming shortwave radiation measurements were decreased by 20%. This did not adequately prevent the early snowmelt. Also, both the visible and near-infrared albedo decay functions in CLASS were reduced in an attempt to alleviate the overestimated snowmelt, though this did not improve results significantly. It was examined whether CLASS was overestimating the fraction of precipitation that was rain rather than was actually snow. The code was modified so that all precipitation at air temperatures below 6°C was snow, and this did not improve simulated snow depth significantly.

Overestimated and early simulated snowmelt by CLASS has been observed by a number of modellers (personal conversations with Bruce Davison and Vincent Fortin, Environment Canada) and in other land surface schemes (Slate *et al*., 2001). It is unclear why CLASS overestimated snowmelt during 2008/2009 whereas SNOBAL did not. This issue is more deeply discussed in Section 5.5.1. It should be noted that the underestimated snow depth during this period regardless of the parameter values likely caused the automatic calibration procedure to select less meaningful parameters. It is demonstrated, in Chapter 5, that CLASS considerably overestimates snowmelt over FR HRUs and that the reasonably good point simulations at RT using CLASS-PBSM are due to the presence of a shallow snowpack at this windswept location.

CHAPTER 5
LANDSCAPE-BASED MODEL DEVELOPMENT AND APPLICATION

5.1 Introduction

This chapter presents model parameterization and results for landscape-based distributed simulations over FR and GB. Herein the terms HRU and GRU can represent the same landscape unit, with HRU referring to a CRHM landscape unit and GRU referring to a MESH landscape unit. The algorithm structure developed for inter-GRU snow redistribution within MESH can be generalized for and applied to redistribute other hydrological fluxes such as overland flow. The RMM windflow model was used to attempt to generate HRU-level wind speeds for FR. The HRUs selected for FR follow an aerodynamic sequence; however, the HRUs selected for GB do not. Three approaches for distributing snow transport fluxes over non-spatially contiguous HRUs were developed and tested over GB. Simulations were performed using CRHM, MESH and MESH-PBSM.

5.2 MESH-PBSM Development

CLASS-PBSM (refer to Section 4.3) was incorporated into MESH (herein MESH-PBSM). In addition to the changes discussed in section 4.3, MESH-PBSM redistributes transported snow mass between GRUs. A snow redistribution subroutine (REDISTRIB_SNOW) was coded and is called from the main MESH driver, MESH_driver. Energy and water balance checks (CLASSZZ) are called before and after REDISTRIB_SNOW. CLASSZZ checks that the changes in energy storage in snowpack is equal to the sum of the energy fluxes into and out of them and the change in snow mass storage is equal to the sum of blowing snow fluxes into and out of them.

In addition to the additional parameters required by CLASS-PBSM (section 4.3), MESH-PBSM requires $n + 1$ additional parameters, where n is the number of GRUs (or HRUs for CRHM). The additional parameters are the snow redistribution allocation factors (S_R) for each GRU except the most upwind GRU, a snow redistribution factor for snow transported into the most upwind GRU from "outside the modelled area", and a snow redistribution factor for snow transported "out of the modelled area". The S_R specifies the fraction of snow transport that is transported from upwind GRUs to a given downwind GRU as opposed to other downwind GRUs. At each model time step, the sum of the snow transport from all GRUs is summed. This total snow transport is distributed to GRUs using predetermined S_Rs. The total snow transport from all GRUs is distributed rather than separately distributing the snow transport from individual GRUs because during blowing snow events, a steady-state flow condition can develop across an aggregated fetch composed of multiple GRUs. Snow transport is allowed to enter a catchment via the most upwind GRU (GRU 1) according to the modelled GRU 1 snow transport and S_R specified for basin gain (i.e. snow transport into the catchment is distributed only to GRU 1 and is equal to $S_{R,gain} \cdot p_1 \cdot (F_{salt,1} + F_{susp,1})/x_1$) where the subscript 1 denotes snow transport terms for GRU 1. Snow transport is also allowed to leave the catchment according to $S_{R,basin\ loss}$. Hence, the number S_Rs is equal to $n + 1$ where n is the number of GRUs.

Inclusion of inter-HRU snow transport in the snow mass balance over an HRU results in a discretization of the divergence of transport rates in Equation [2.1]. The snow mass balance over an HRU j that receives snow transport from other HRUs is therefore given by a modification of Equation [2.1] as

$$\frac{dS_j}{dt}(x) = P_j + S_{R,j} \sum \left[p_i \nabla \cdot F_i(x) \right] - p_j \left[\nabla F_j(x) + \frac{\int E_{B,j}(x) dx}{x_j} \right] - E_j - M_j \qquad [5.1]$$

where $S_{R,j}$ is the snow redistribution allocation factor for HRU j.

Figure 5.1 shows the sequential logic for the snow redistribution algorithm, REDISTRIB_SNOW, which is performed for each grid square at each time step there is snow transport.

STEP 1. Calculate aggregated snow transport properties:
- aggregate wind transported snow density, heat capacity, temperature and water equivalent from all GRUs

STEP 2. Remove snow transport out of basin
- IF $S_{R,basin\ loss} > 0$
- remove lost snow from available snow transport

STEP 3. Deposit snow into first GRU
- IF $S_{R,basin\ gain} > 0$
- deposit snow at subarea-level
- recalculate snowpack depth and heat capacity

STEP 4. Deposit snow into other GRUs
- IF S_R for GRU > 0
- deposit snow at subarea-level
- recalculate snowpack depth and heat capacity
- remove deposited snow from available snow transport

STEP 5. Recalculate snowpack properties at GRU-level
- IF snow was deposited into GRU
- recalculate snowpack depth and heat capacity

Figure 5.1 MESH-PBSM Inter-GRU snow redistribution algorithm

If the snow mass is vanishingly small (10^{-3} kg m^{-2}), the snowpack and its liquid water are added to the overland flow. This vanishingly small snowpack check was moved from its original location at the end of CLASSW.

5.3 Aerodynamic Sequence Modelling (FR)

5.3.1 HRU Selection

HRUs were selected by grouping snow depths measured along the FR transect (Figure 5.2). These manual snow depth measurements captured the spatial variability in wind exposure along

the FR transect, which exerts a stronger control on winter snow accumulation at this location than does solar radiation and vegetation. The HRU boundaries were established by subjectively identifying locations where snow depth changed significantly. The boundary between the SF-upper and SF-lower was the most difficult to set. An attempt was made to delineate HRUs using topography and/or vegetation; however, good agreement was not found. The intricacies of alpine snow redistribution by wind and the spatial variability of radiation make it difficult for simple terrain-based HRU delineation.

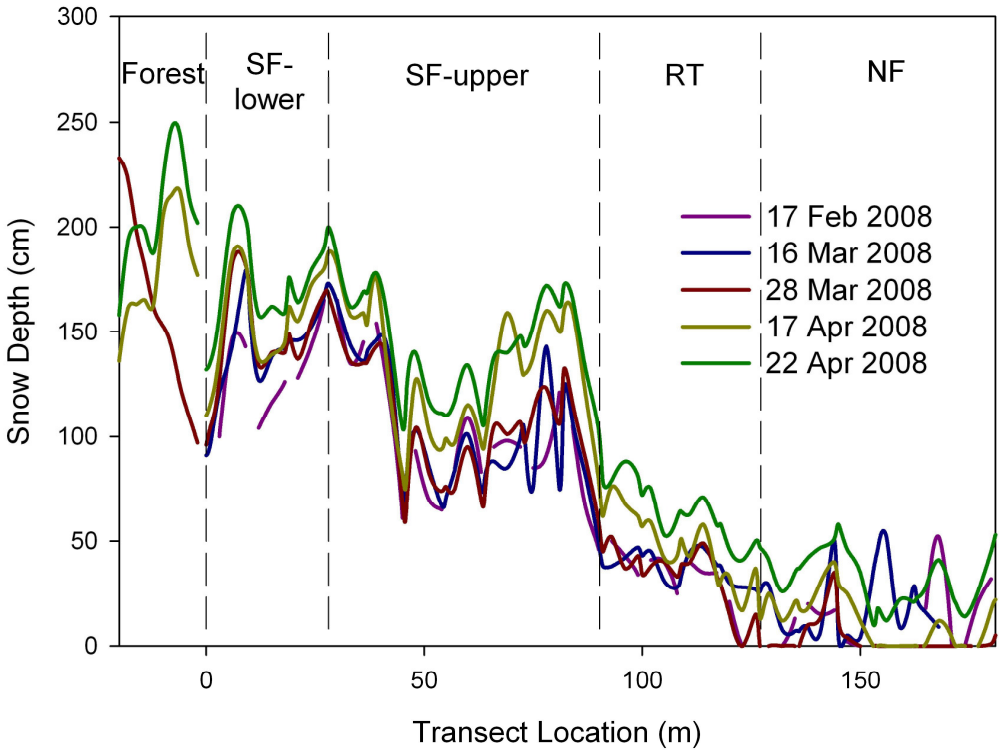

Figure 5.2 Snow depth along Fisera Ridge transect. The boundaries of the five HRUs are indicated by the dashed lines.

Five HRUs were selected based on the observed snow depths shown in Figure 5.2. The north-facing slope HRU (NF) is located from 127 to 181 m, the ridge-top HRU (RT) is located from 90

to 127 m, the upper south-facing slope (SF-upper) is located from 28 to 90 m, the lower south-facing slope (SF-lower) is located from 0 to 28 m and the Forest HRU is located from 0 to -15 m.

5.3.2 Fisera Ridge Parameterization

The HRUs follow an aerodynamic sequence in that the model always transports snow from upwind to downwind HRUs (Figure 5.3). The HRU snow transport sequence is NF → RT → SF-upper → SF-lower → Forest (i.e. NF snow transport reaches all of RT, SF-upper, SF-lower and Forest; SF-upper snow transport only reaches SF-lower and Forest; etc.).

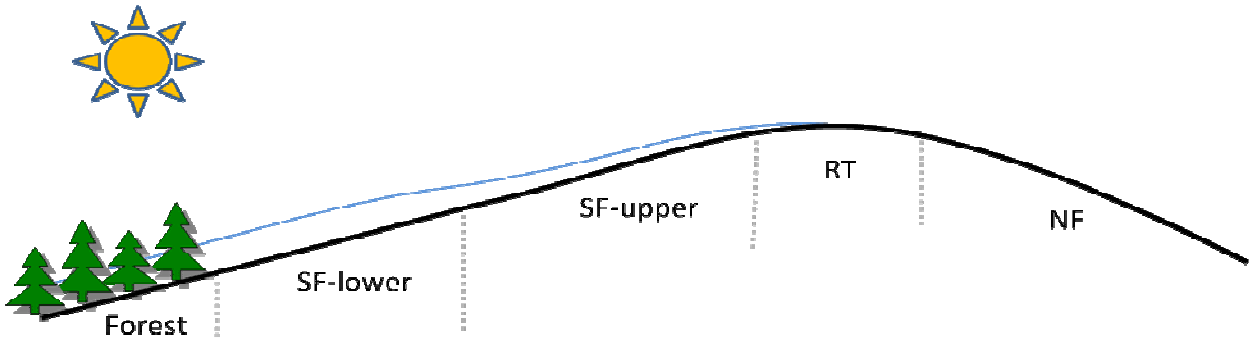

Figure 5.3 Schematic of Fisera Ridge HRUs (not to scale). Blue line indicates typical snow depth distribution over HRUs (not to scale).

The static definition of the HRU locations and relative lengths is a simplification of the actual spatiotemporal snow redistribution patterns. Redistributed snow deposition rates reduce as a land unit fills with more snow, and the maximum snow depth in drift zones is reached before maximum drift length (Tabler, 1975). However, for large-scale hydrological studies, the greatest concern is usually the water equivalence of the snow drift. For this reason it is adequate to simulate snow deposition in statically dimensioned HRUs whose size approaches their maximum drift length. A static definition of HRU locations must also consider the variability of snow

transport directions. Snow transport rates scales approximately with the fourth power of wind speed (Pomeroy *et al*., 1993; Essery *et al*., 1999). Figure 5.4 shows a fourth power of wind speed (u^4) rose (sum of u^4 binned by direction) for the observed wind speed and direction at the Fisera Ridge ridge-top station over the study periods. It is clear that northwesterly blowing snow events dominate snow redistribution at this location. Furthermore, changing HRUs sizes during a model run would add considerable complexity to the calculation of mass balances for HRU.

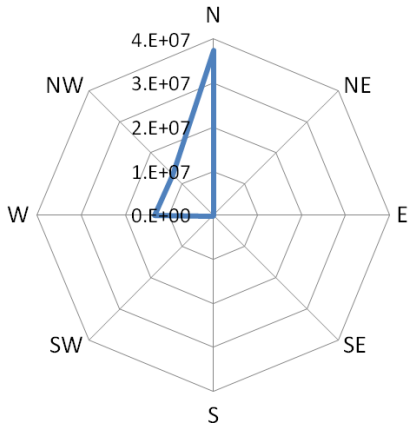

Figure 5.4 u^4 direction for Fisera Ridge-top station for 2007/2008 and 2008/2009. Scale is the fourth power of wind speed (u^4/s^4)

Key CRHM model parameters are presented in Table 5.1. Note that the Canopy module was only applied to the Forest HRU. CRHM model parameters were set based on field measurements with the exception of vegetation height on the NF and RT. Shorter shrub heights than measured were needed to scour enough snow from these HRUs. PBSM is parameterized for densely spaced, narrow crop stalks and grass. Shorter vegetation heights parameters were required to represent sparse shrubs on the NF and RT HRUs. This indicates that the PBSM parameterization for the aerodynamic roughness height may not be appropriate for such shrubs and should be revised. Average HRU aspect and slope were determined from the DEM. A blowing snow fetch

distance of 300 m was specified for each HRU because this is the minimum value required for the fully-developed flow calculations performed by PBSM.

Table 5.1 Fisera Ridge HRUs CRHM model parameters

	NF	RT	SF-upper	SF-lower	Forest
Length (m)	116	37	62	28	15
Aspect (º from north)	345	30	101	93	94
Slope (º)	26	18	20	18	16
Vegetation height (m)	0.1	0.12	0.50	0.90	2.3
Vegetation density (shrubs·m^{-2})	0.1	0.1	0.6	0.6	0.5
Maximum canopy snow load (kg·m^{-2})	-	-	-	-	3
Maximum canopy rain load (kg·m^{-2})	-	-	-	-	2
Leaf Area Index ()	-	-	-	-	0.91
RMM Wind Weight (simulated/reference)	1.49	1.16	0.93	0.92	0.98

MESH and MESH-PBSM parameters were automatically calibrated to 2007/2008 data using DDS for three trials with 3000 objective function evaluations per trial. Table 5.2 shows the optimum parameter values and parameter ranges for the calibrations for MESH and MESH-PBSM. The optimum parameter sets (MESH_parameters_CLASS.ini and MESH_parameters_hydrology.ini) for both MESH and MESH-PBSM are included in Appendix D. CLASS parameters definitions and recommended values are included in Appendix B.

Table 5.2 Optimized parameter values for Fisera Ridge HRU simulations for (a) MESH and (b) MESH-PBSM. Values in parentheses indicate parameter bounds.

(a)

	NF		RT		SF-upper		SF-lower		Forest	
Parameter	**Shrubs**	**Grass**	**Shrubs**	**Grass**	**Shrubs**	**Grass**	**Shrubs**	**Grass**	**Forest**	**Grass**
Veg. roughness length [m]	0.026 (0.025, 0.1)	0.010 (0.005, 0.02)	0.025 (0.025, 0.1)	0.020 (0.005, 0.02)	0.761 (0.05, 0.82)	0.037 (0.005, 0.05)	1.146 (0.165, 0.05)	0.037 (0.008, 0.1)	1.105 (1, 2.5)	0.034 (0.008, 0.1)
Veg. visible albedo ALVC []	0.028 (0.02, 0.1)	0.047 (0.02, 0.08)	0.036 (0.02, 0.1)	0.021 (0.02, 0.08)	0.044 (0.02, 0.1)	0.039 (0.02, 0.08)	0.054 (0.02, 0.1)	0.069 (0.02, 0.08)	0.048 (0.02, 0.1)	0.045 (0.02, 0.08)
Veg. near-	0.161	0.285	0.158	0.201	0.285	0.234	0.293	0.397	0.192	0.310

IR albedo ALIC []	(0.15, 0.3)	(0.2, 0.4)	(0.15, 0.3)	(0.2, 0.4)	(0.15, 0.3)	(0.2, 0.4)	(0.15, 0.3)	(0.25, 0.4)	(0.15, 0.3)	(0.25, 0.4)
Maximum LAI LAMX []	0.359 (0.1, 0.5)	0.312 (0.2, 1)	0.403 (0.1, 0.5)	0.908 (0.2, 1)	0.374 (0.2, 0.6)	0.538 (0.5, 1.5)	0.324 (0.3, 0.7)	0.502 (0.5, 1.5)	0.879 (0.8, 1.1)	1.094 (1, 3)
Minimum LAI LAMN []	0.191 (0.05 0.2)	0.497 (0.1, 0.6)	0.200 (0.05, 0.2)	0.553 (0.1, 0.6)	0.107 (0.1, 0.3)	0.303 (0.3, 1.0)	0.200 (0. 2, 0.5)	0.575 (0.5, 1.0)	0.791 (0.7, 0.9)	0.597 (0.5, 1.5)
Limiting snow depth ZSNL (m)	0.02 (0.01, 1)		0.02 (0.01, 1)		1.00 (0.01, 1)		0.99 (0.01, 1)		0.37 (0.01, 1)	

Table 5.2 continued
(b)

	NF		RT		SF-upper		SF-lower		Forest	
Parameter	**Shrubs**	**Grass**	**Shrubs**	**Grass**	**Shrubs**	**Grass**	**Shrubs**	**Grass**	**Forest**	**Grass**
Veg. roughness length [m]	0.035 (0.025, 0.1)	0.014 (0.005, 0.02)	0.052 (0.025, 0.1)	0.006 (0.005, 0.02)	0.654 (0.05, 0.82)	0.050 (0.005, 0.05)	1.319 (0.165, 0.05)	0.072 (0.008, 0.1)	1.990 (1, 2.5)	0.011 (0.008, 0.1)
Veg. visible albedo ALVC []	0.077 (0.02, 0.1)	0.047 (0.02, 0.08)	0.025 (0.02, 0.1)	0.045 (0.02, 0.08)	0.069 (0.02, 0.1)	0.077 (0.02, 0.08)	0.100 (0.02, 0.1)	0.054 (0.02, 0.08)	0.035 (0.02, 0.1)	0.041 (0.02, 0.08)
Veg. near-IR albedo ALIC []	0.183 (0.15, 0.3)	0.382 (0.2, 0.4)	0.207 (0.15, 0.3)	0.205 (0.2, 0.4)	0.265 (0.15, 0.3)	0.382 (0.2, 0.4)	0.297 (0.15, 0.3)	0.303 (0.25, 0.4)	0.243 (0.15, 0.3)	0.382 (0.25, 0.4)
Maximum LAI LAMX []	0.297 (0.1, 0.5)	0.202 (0.2, 1)	0.171 (0.1, 0.5)	0.284 (0.2, 1)	0.477 (0.2, 0.6)	1.457 (0.5, 1.5)	0.478 (0.3, 0.7)	0.601 (0.5, 1.5)	0.910 (0.8, 1.1)	2.898 (1, 3)
Minimum LAI LAMN []	0.058 (0.05, 0.2)	0.145 (0.1, 0.6)	0.128 (0.05, 0.2)	0.205 (0.1, 0.6)	0.101 (0.1, 0.3)	0.486 (0.3, 1.0)	0.200 (0.2, 0.5)	0.554 (0.5, 1.0)	0.758 (0.7, 0.9)	0.806 (0.5, 1.5)
Vegetation height Ht (m)	0.103 (0.1, 0.6)		0.216 (0.1, 0.6)		0.894 (0.6, 1)		1.174 (0.8, 1.2)		-- ()	
Vegetation density N_S (number m^{-2})	0.68 (0.1, 0.7)		0.57 (0.1, 0.7)		0.73 (0.4, 0.8)		0.48 (0.4, 0.8)		-- ()	
Vegetation silhouette area A_S (m^2)	0.110 (0.1, 1)		0.193 (0.1, 1)		0.307 (0.2, 1)		0.695 (0.2, 1)		-- ()	
Limiting snow depth ZSNL (m)	0.93 (0.01, 1)		0.52 (0.01, 1)		0.25 (0.01, 1)		0.99 (0.01, 1)		0.20 (0.01, 1)	

5.3.3 Windflow Modelling

Simulations were performed for 2007/2008 and 2008/2009 applying the ridge-top station air temperature, relative humidity and incoming longwave radiation observations to all HRUs. Incoming shortwave radiation observations from the ridge-top station (considered a flat plane) were applied to each HRU after adjustments for aspect and slope made by the Global and Slope_Qsi modules. Reflected radiation from adjacent terrain was captured by the radiometer measurements at the ridge-top station, therefore all HRUs received the same contribution of

reflected radiation relative to total incoming radiation. This approach for taking into account reflections deviates somewhat from reality; however this approach produced excellent radiation for snowmelt modelling in the same environment (DeBeer and Pomeroy, 2009). It is not necessary to model topographic shading for this study because it is accounted for in the ridge-top measurements and it is suitable to assume identical effects over this short model transect. Atmospheric pressure, required for MESH and MESH-PBSM simulations, was obtained as discussed in Section 3.2.2. Simulations were performed using two different sets of wind speed forcing data:

(1) FR station observed wind speed data; and

(2) RMM-modelled wind speeds.

For (1), the north-facing meteorological station wind speed data were applied to the NF, the ridge-top meteorological station wind speed data were applied to the RT, and the southeast-facing meteorological station wind speed was applied to the SF-upper, SF-lower and Forest. The ridge-top meteorological station applied to the RT was the same as that used for the point evaluation presented in Section 4.4.

For (2), average RMM-modelled wind speeds were applied to each of the five HRUs. Wind speed and direction observations from an alpine meteorological station were used as reference for RMM (Figure 5.5). This alpine meteorological station was used as the reference in order to reproduce a realistic situation where meteorological observations are sparsely distributed. This alpine meteorological station may be considered a surrogate to a nearby meteorological station operation by the Meteorological Service of Canada.

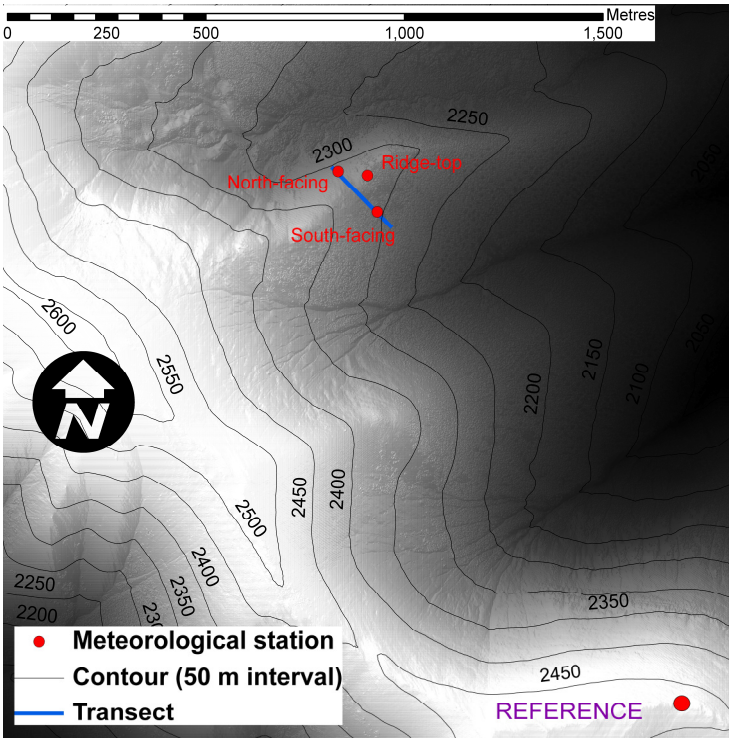

Figure 5.5 Reference alpine meteorological station location relative to Fisera Ridge

RMM was implemented in MATLAB to simulate wind speed over the 10 m LiDAR-derived DEM. A MATLAB m-file containing the DDS algorithm (available at http://www.civil.uwaterloo.ca/btolson/software.htm) was coupled to RMM to automatically calibrate the η (Equation 4.22), γ_s and γ_c (Equation 4.25) parameters. 26,937 non-continuous wind speed and direction measurements from 29 January to 1 May 2009 from the reference alpine station were used to automatically calibrate the parameters to measured wind speed at the three FR stations. The optimum parameter set following 1000 objective function evaluations of the root mean squared error (RMSE) of measured wind speed yield a RMSE of 3.4 m s^{-1} and a model bias of 0.627 (Figure 5.6a). The optimum parameter set was η = 799 m, γ_s = 0.89 and γ_c = 0.11. Though the RMM model performance can be considered poor for simulating wind speed, the near 1:1 (modelled:measured) slope of the regression line suggests that RMM may be

adequate for modelling blowing snow over an entire season. Time series of the RMM-modelled wind speed and the observed wind speed at the ridge-top station also suggests some potential for this application (Figure 5.6b). However, blowing snow transport rates scale approximately with the fourth power of wind speed (u^4; Pomeroy and Male,1992, Essery *et al*., 1999). Figures 5.7a and 5.7b shows a comparison of RMM-modelled and observed u^4. These figures suggest that RMM-modelled u^4 and observed u^4 do not corroborate well and therefore RMM would not likely be adequate for modelling blowing snow in this environment. An evaluation of RMM for distributed blowing snow modelling over FR was made.

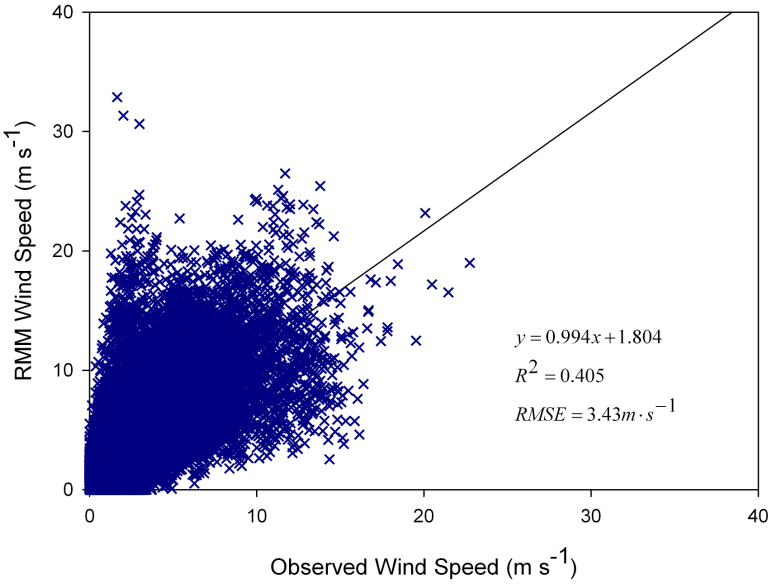

(a)

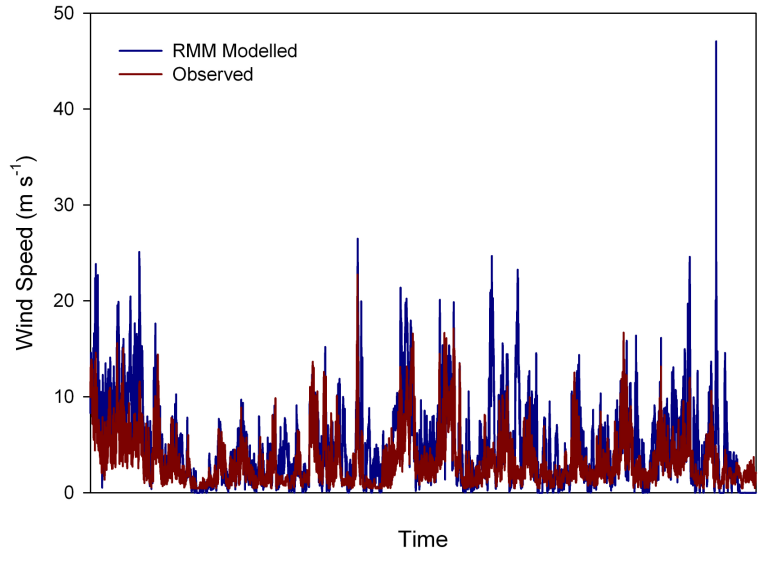

(b)

Figure 5.6 (a) Fisera Ridge observed wind speed versus RMM modelled wind speed (solid lines indicates linear regression), and (b) Non-continuous time series of Ridge-top station observed wind speed and RMM modelled wind speed.

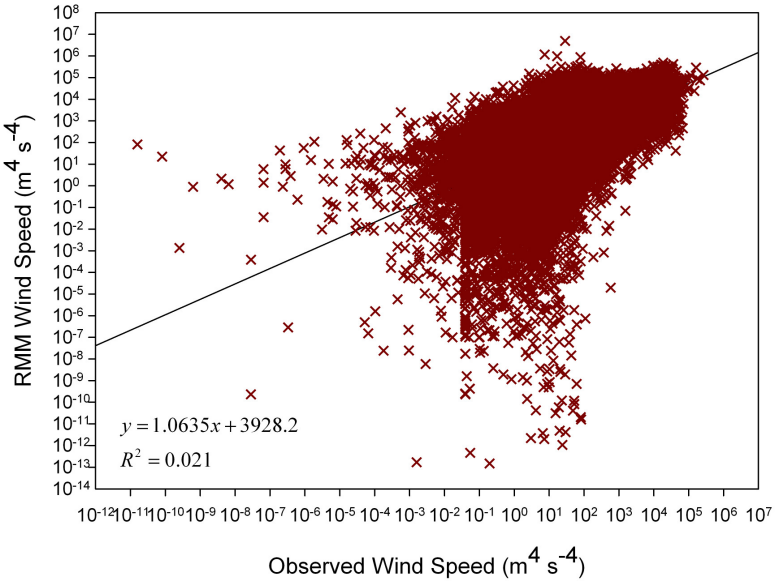

(a)

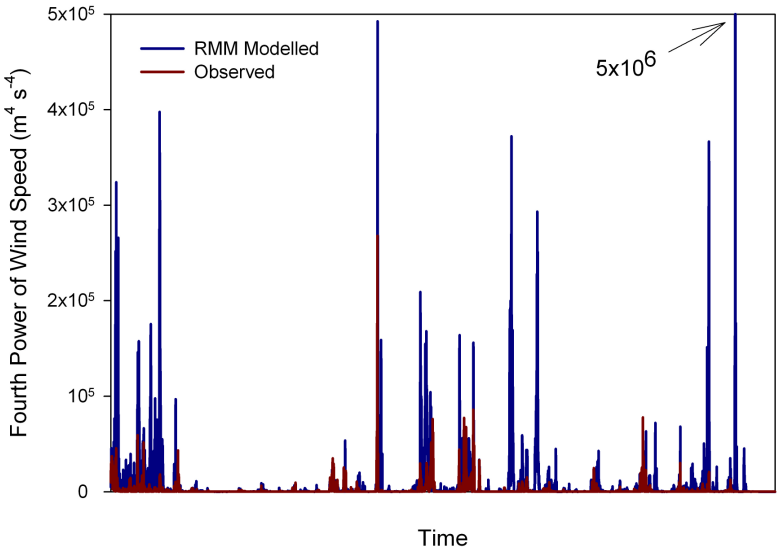

(b)

Figure 5.7 (a) Fisera Ridge observed u^4 versus RMM modelled u^4 on a logarithmic scale (solid lines indicates linear regression), and (b) Non-continuous time series of Ridge-top station observed u^4 and RMM modelled u^4.

For (2) [RMM-modelled wind speeds], the wind speed forcing for each HRU (W_T in Equation [4.24]) was obtained by combining the reference alpine wind speed measurements (W in

Equation [4.24]) and the average RMM W_W over each HRU (W_W in Equations [4.24] and [4.25]). The W_W was calculated for each 10 m cell along the FR transect and the average of all cell W_W values within an HRU (as per the spatial extents defined in Section 5.3.1) was used as W_W in Equation [4.24]. Average RMM W_W for each HRU are presented in Table 5.1. The RMM W_W values along the FR transect do show some corroboration with the observed snow depth (Figure 5.8), suggesting that grouping RMM W_W values spatially (e.g. by HRUs) may be useful for snow redistribution modelling.

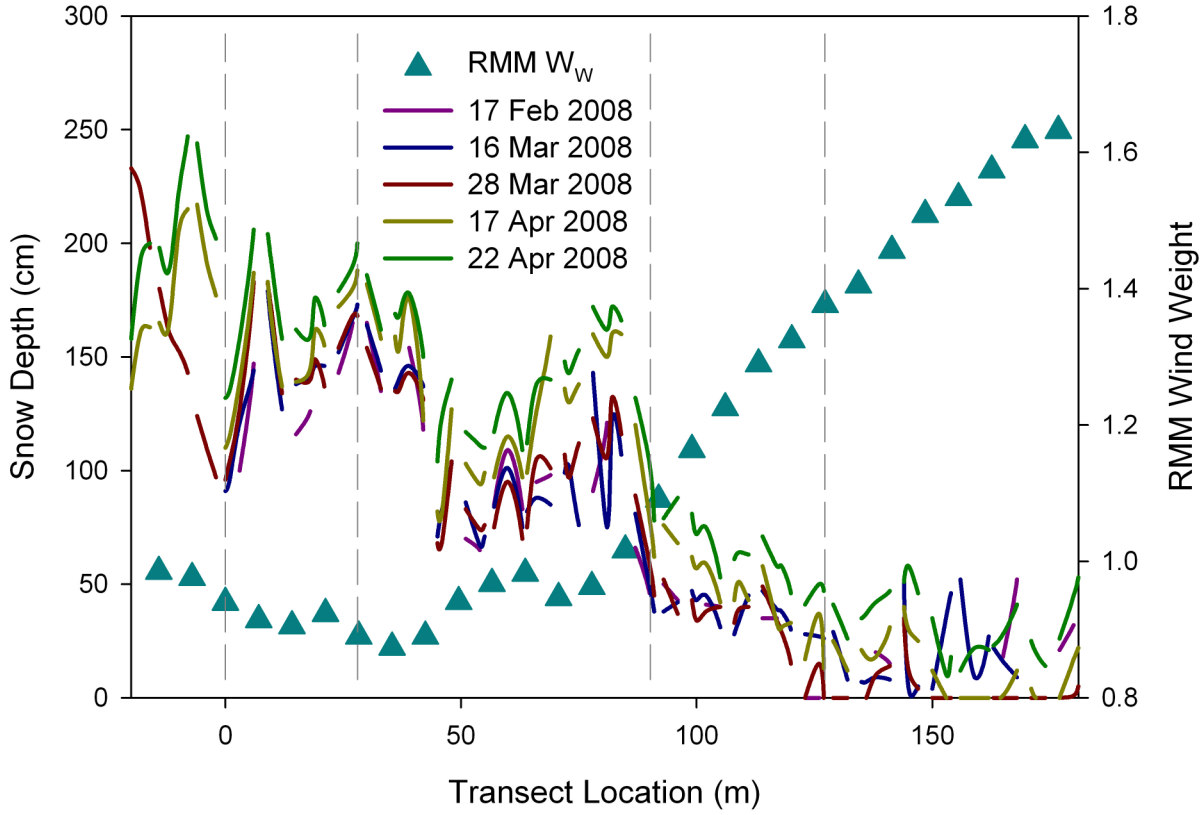

Figure 5.8 RMM wind weights along Fisera Ridge Transect. The boundaries of the five HRUs are indicated by the dashed lines.

5.3.4 Model Evaluation

Simulated snow accumulation was evaluated using model bias, root mean squared error, normalized root mean squared error and coefficient of determination (goodness of fit), given by

$$MB = \frac{\sum \alpha SWE_{sim}}{\sum \alpha SWE_{obs}} - 1 \quad [5.2]$$

$$RMSE = \sqrt{\frac{\sum \left(\alpha SWE_{sim} - \alpha SWE_{obs}\right)^2}{n}} \quad [5.3]$$

$$NRMSE = 100 \frac{RMSE}{SWE_{OBS,Max} - SWE_{OBS,Min}} \quad [5.4]$$

$$R^2 = \left[\frac{\sum \left(\Delta \alpha SWE_{snow,obs} - \overline{\alpha SWE_{snow,obs}}\right)\left(\Delta \alpha SWE_{snow,sim} - \overline{\Delta \alpha SWE_{snow,sim}}\right)}{\sqrt{\sum \left(\Delta \alpha SWE_{snow,obs} - \overline{\Delta \alpha SWE_{snow,obs}}\right)^2} \sqrt{\sum \left(\Delta \alpha SWE_{snow,sim} - \overline{\Delta \alpha SWE_{snow,sim}}\right)^2}} \right]^2 \quad [5.5]$$

where SWE_{sim} and SWE_{obs} are the simulated and observed SWE, respectively. α is the fractional area of the HRU. α is included so that the model evaluation statistics reflect the relative size of different HRUs that make up the FR transect. $\Delta\alpha SWE_{snow,sim}$ and $\Delta\alpha SWE_{snow,obs}$ are the change in simulated and observed SWE from one observation data to the next. $\overline{\alpha SWE_{obs}}$ is the average observed SWE of all HRUs at all observations dates. $\overline{\Delta \alpha SWE_{snow,OBS}}$ and $\overline{\Delta \alpha SWE_{snow,SIM}}$ are the average change in observed SWE over the simulation period. n is the number of observation-simulation pairs used to evaluate *RMSE*. Positive and negative *MB* indicate the fraction by which SWE is either overestimated or underestimated throughout the simulation, respectively, and describes the reproduction of total snow mass over all the HRUs. The *RMSE* gives a measure of the variation of residuals between observed and simulated SWE in mm SWE and describes how well the snow mass is distributed on the various HRUs. The *NRMSE* normalizes the *RMSE* with respect to the range of observed SWE and is expressed as a percentage. Positive and negative

MB indicate the fraction by which snow depth is either overestimated or underestimated throughout the simulation, respectively. The coefficient of determination gives a measure of the accuracy of the model in simulating the change in observed SWE. R^2 = 1.0 indicates that the model perfectly simulated the variation in change of observed SWE and R^2 = 0.0 indicates that the model did not simulate any of the variation.

5.4 Inter-HRU Snow Redistribution Modelling (GB)

5.4.1 Inter-HRU Snow Redistribution Allocation

Three snow redistribution allocation factor (S_R) schemes were evaluated for GB:

1) All HRUs received the same amount of snow transport (all S_Rs equal);
2) S_Rs were assigned to HRUs considering the predominant seasonal measured wind direction(s), HRU aerodynamic and topographic characteristics and the spatial arrangement of HRUs;
3) S_Rs were binned by wind direction considering the spatial arrangement of HRUs and therefore can change with each time step. Eight binned directions were used (the four cardinal and the four primary inter-cardinal directions).

For S_R scheme 1, all S_Rs (including $S_{R,basin\ loss}$) are equivalent. S_R scheme 1 is the most rudimentary approach to inter-HRU snow redistribution. Its application disregards the direction of blowing snow events, the actual drift accumulation capability of the HRUs, as well the proximity and size of HRUs.

Application of S_R schemes 2 and 3 require wind direction and speed data and a pre-established spatial arrangement of the HRUs. First, it must be determined which HRUs are sources and which are sinks of snow transport (resulting in positive and negative snow erosion rates, respectively). This is accomplished by simulating snow transport fluxes in point mode for each

HRU using PBSM. When HRUs are selected based upon the characteristics that govern snow accumulation (i.e. wind exposure and aerodynamic roughness) it is usual that snow transport source and sink HRUs can be distinctly identified (e.g. Pomeroy *et al*., 1997). Scheme 2 and 3 S_Rs were parameterized using interface lengths, d, between source and sink HRUs perpendicular to the wind direction (d determinations are explained in Section 5.4.3). Pomeroy and Male (1992) showed that snow transport fluxes scale approximately with the fourth power of wind speed (u^4) and Essery *et al*. (1999) used this expression to parameterize a simplified version of PBSM. For S_R scheme 2, the predominant u^4 resultant direction over a winter is used to determine the interface lengths, d_i, between source and sink HRUs. Therefore, S_R scheme 2 assumes that all snow transport occurs in the predominant u^4 resultant direction. For S_R scheme 3, the wind direction at each time step is used to determine d_i. An illustration of the d_i concept is shown on Figure 5.9 for GB.

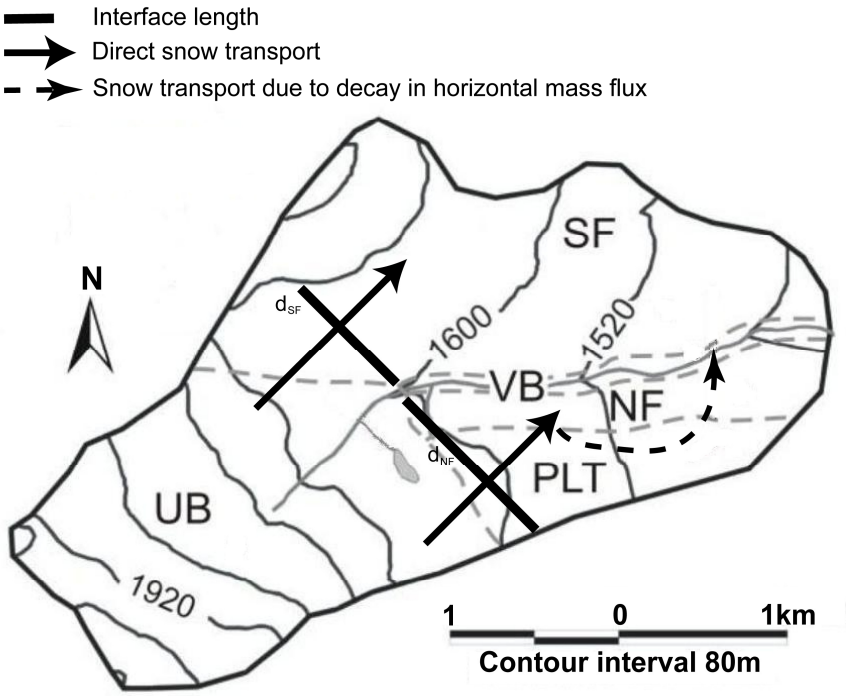

Figure 5.9 Granger Basin interface lengths (d) for S_R scheme 2 (southwest wind)

The S_R parameterization presumes that all snow transported from source to sink HRUs occurs across and perpendicular to d_i. The S_R for total snow transported to HRU j is given by

$$S_{R,j} = L_{C,j} \frac{d_j}{\sum d_i} \quad [5.6]$$

for sink HRUs adjacent to source HRUs, and by

$$S_{R,j} = \left(1 - L_{C,k}\right) \frac{d_k}{\sum d_i} \quad [5.7]$$

for sink HRUs not adjacent to sources HRUs, where d_j is the length of the interface between source HRUs and HRU j perpendicular to the predominant u^4 (or wind) direction, and d_i is the length of the interface between source HRUs and all sink HRUs, i, to which snow is transported, perpendicular to the predominant u^4 direction. d_k is the interface length between source HRUs and HRU k that is upwind of HRU j which is adjacent to source HRUs. L_C is a fractional term that accounts for the "snow trapping efficiency" of a leeward slope.

Over hilly and mountainous terrain snow can be transported from an upwind HRU and deposited into a downwind HRU that is not directly adjacent to the upwind HRU. For instance, snow can be transported from over a leeward slope and deposited in a downwind valley bottom. A leeward slope represents an increase in landscape aerodynamic roughness that reduces the downwind boundary layer wind speed or flow separation occurs. If the step-change in leeward slope elevation and slope is sufficient, a positive snow erosion regime can abruptly become negative resulting in deposition. The decay in the horizontal flux of snow transport from this "boundary" of positive/negative snow erosion rates can be used to estimate the fraction of snow transport that is deposited into a leeward slope as opposed to a downwind valley bottom. Takeuchi (1980) measured the downwind increase in the horizontal flux of snow transport from a wooded boundary. Results were presented for various snow transport threshold conditions and

wind speeds at a vertical scale of 0.3m. A hyperbolic increase in snow transport rate was observed until fully-developed flow was established from 200-300 m downwind from the wooded boundary. To the author's knowledge Takeuchi's measurements remain the best field measurements of the horizontal development of snow transport rates. The fraction of snow transport that is deposited into a leeward slope as opposed to a downwind valley bottom can be estimated presuming that the decrease in the horizontal flux of snow transport follows the same profile as the increase in the horizontal flux as measured by Takeuchi. Pomeroy and Male (1986) developed a hyperbolic function, which approximates the shape of Takeuchi's horizontal profiles given by

$$L_C = \frac{\tanh\left(4\frac{L}{300} - 2\right)}{2} + 0.5 \qquad [5.8]$$

where L_C is the horizontal mass flux as a fraction of the fully-developed flux at L, the distance downwind from an aerodynamic barrier (m). The distance required to attain fully-developed flow was taken to be Takeuchi's upper value of 300 m, since measurements were limited to a vertical scale of 0.3 m. Figure 5.10 shows values of L_C calculated using Equation [5.8].

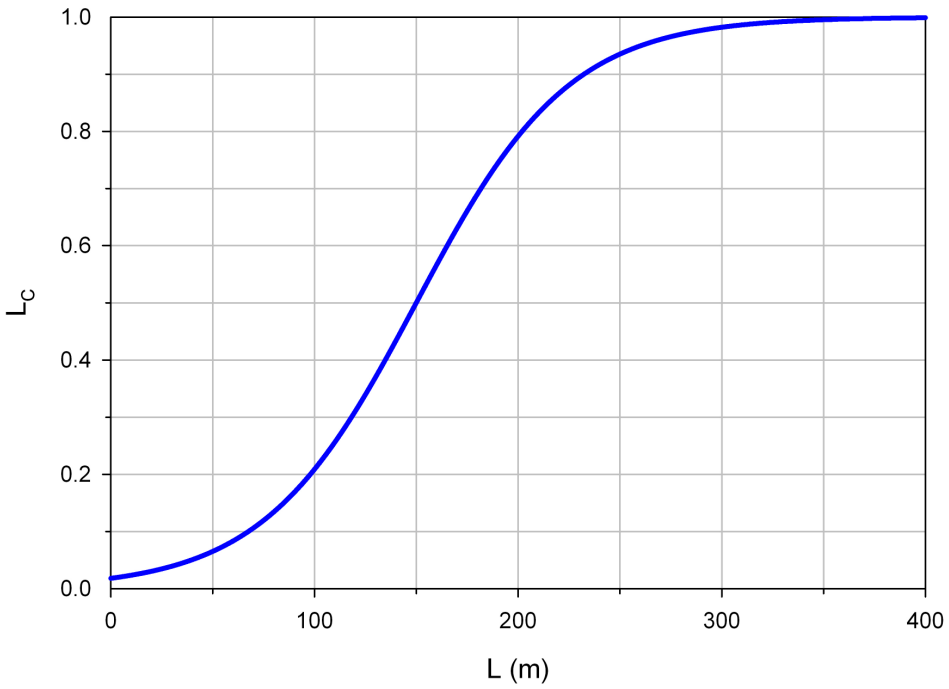

Figure 5.10 Horizontal mass flux as a fraction of the fully-developed flux at distance downwind from an aerodynamic barrier as per Pomeroy and Male (1986)

In the proposed method, L_C is the parameterization of the fraction of snow transport that is deposited into a leeward slope HRU and $1 - L_C$ is the fraction of snow transport that is deposited into the adjacent downwind HRU, such as a valley bottom. This method assumes that the snow transport regime upwind of the leeward slope HRU is fully-developed, and that a negligible quantity of snow is eroded from the leeward slope and thus all airborne snow particles above a leeward slope are a result of snow transport from an upwind location (except during snowfall). Flow separation over the crest of a leeward slope is not accounted for. Equation [5.8] is independent of wind speed and turbulent effects on snow particle vertical velocity are ignored.

5.4.2 HRU Selection

Five HRUs were selected to represent GB (Figure 5.11, Table 5.3): Upper Basin (UB), Plateau (PLT), North-facing Slope (NF), South-facing Slope (SF) and Valley Bottom (VB). These five HRUs were selected based on field observations of sun and wind exposure, slope, vegetation cover and soil type (McCartney *et al*., 2006), usefulness in modelling snowcover ablation (Dornes *et al*., 2008a, 2008b; Dornes, 2009) and consideration of the landscape features that govern snow accumulation and redistribution (Pomeroy *et al*., 1999; 2006). The HRUs were delineated as per Dornes *et al*. (2008a). These HRUs each contain one of the GB meteorological stations presented in Section 3.3.2.

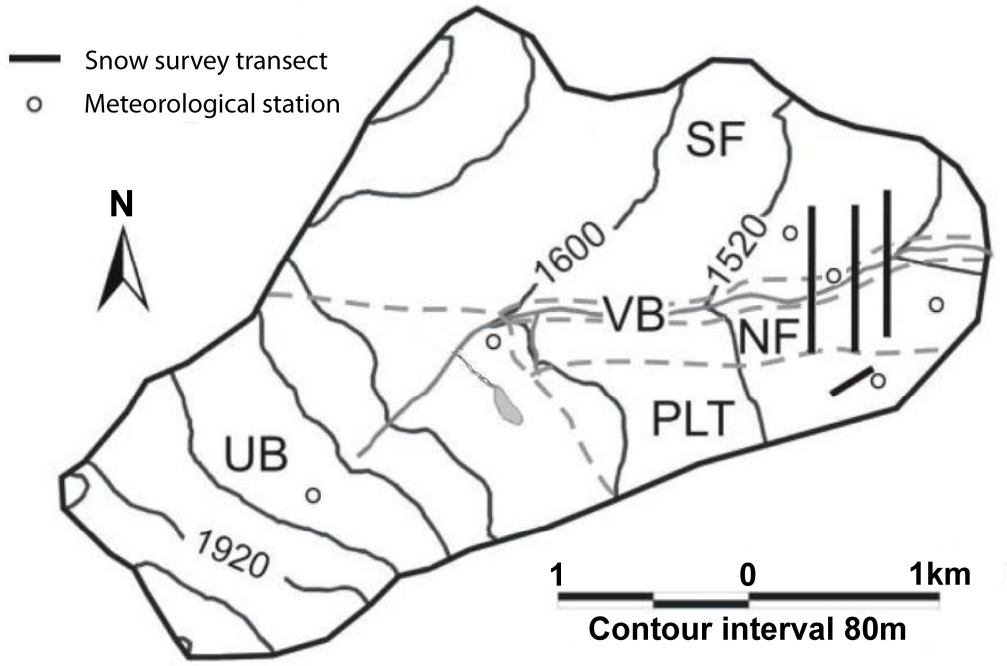

Figure 5.11 Granger Basin Hydrological Response Units

Table 5.3 Granger Basin HRUs physiographic characteristics

HRU	Area (km^2)	Elevation range (m ASL)	Vegetation cover
UB	3.1	1600-2100	bare ground and rocks
PLT	0.8	1460-1520	short shrubs

NF	0.6	1350-1460	mixed shrubs
SF	3.2	1350-1760	mixed shrub
VB	0.3	1310-1350	tall shrubs

5.4.3 Granger Basin Parameterization

Wind direction and speed measurements from the UB meteorological station were used to sum u^4 values binned by direction to determine the predominant u^4 direction(s) (S_R scheme 2) and to activate S_R changes (S_R scheme 3). UB wind speed and direction measurements were only available for 2003/2004. To qualitatively ascertain that the predominant u^4 direction was also the same for 1998/1999 and 2000/2001, wind measurements from a nearby alpine meteorological station at a similar elevation were examined. The predominant u^4 directions measured at this alpine station were the same for 1998/1999, 2000/2001 and 2003/2004 (southerly wind); therefore, it is assumed that the predominant u^4 directions measured at UB during 2003/2004 can also be applied to 1998/1999 and 2000/2001 simulations. Figure 5.12 shows the u^4 summation binned by direction for November 2003 to March 2004. This figure shows that there were two predominant u^4 directions measured over 2003/2004, from the northwest and from the southwest.

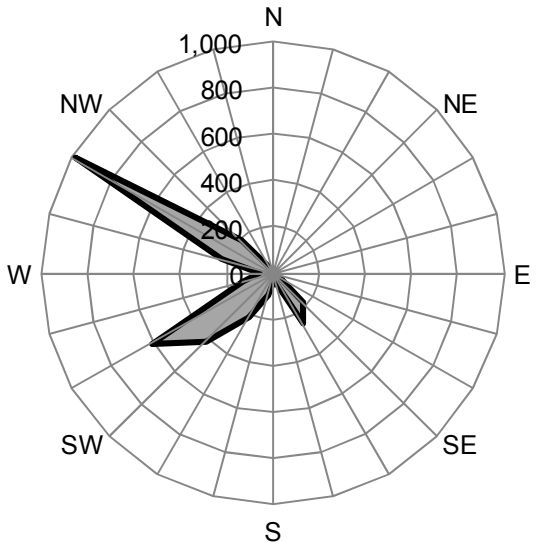

Figure 5.12 u^4 direction for GB 2003/2004. Scale is the fourth power of wind speed (u^4/s^4)

Interface lengths, d_i, were drawn manually and measured on a 30 m × 30 m DEM and are presented on Figure 5.9 for S_R scheme 2 for a southwest predominant u^4 direction. For a northwest predominant u^4, all snow transport from UB and PLT is blown out of the basin ($S_{R,basin\ loss}$ = 1.0). S_R values used for scheme 2 are the average of the northwest- and southwest-derived values. Fetch distances for each HRU were computed by applying the FETCHR program (Lapen and Martz, 1993) to the 30 m x 30 m DEM. Fetch, as measured by the FETCHR program, is the distance from a cell to the nearest cell that is considered to be a topographic obstacle. A topographic obstacle is defined as

$$Z_{test} \geq Z_{core} + NI \qquad [5.9]$$

where Z_{core} is the elevation of the cell for which the fetch distance is being measured, Z_{test} is the elevation of the cell tested as a topographic obstacle, N is the distance from Z_{core} to Z_{test} and I is the obstacle height increment. FETCHR performs fetch analysis in the compass directions: N, NE, E, SE, S, SW, W and NW. The HRU fetch distances used in the simulations were the mean of the fetch distance measured for each cell within an HRU. For this application, I = 15 cm provided mean HRU fetch distances that seemed appropriate based on visual observations during site visits in February 2008. For S_R schemes 1 and 2, the average of the computed fetch distances for the NW and SW directions was used as presented in Table 5.4a. For S_R scheme 3, the fetch distance varied according to the eight binned wind directions as presented in Table 5.4b.

Table 5.4 Granger Basin fetch distances for (a) S_R schemes 1 and 2, and (b) S_R scheme 3

(a)

UB	PLT	NF	SF	VB
734	319	300*	631	300*

(b)

Wind direction	UB	PLT	NF	SF	VB
North	1010	300*	300*	627*	300*
Northeast	1276	420	344	815	300*
East	1287	724	1133	1351	449
Southeast	1090	374	305	771	459
South	1024	300*	300*	627	300*
Southwest	770	427	335	798	300*
West	1133	691	1137	1356	458
Northwest	1066	300*	509*	775*	441

* Set to 300 m because measured fetch distance was less than the minimum required by PBSM (300m).

By applying PBSM in point mode over each HRU, it was determined that UB and PLT are the snow transport source HRUs and NF, SF and VB are the sink HRUs. The three S_R scheme resulting values are presented in Table 5.5. For S_R scheme 1, all S_Rs (including $S_{R,basin\ loss}$) are equivalent (Table 5.5a). For S_R scheme 2, the average of S_Rs determined for NW and SW winds was used (Table 5.5b). For S_R scheme 3, S_Rs were different for each of the eight binned wind directions (Table 5.5c). For S_R schemes 2 and 3, since UB and PLT are snow transport sources and the snow transport is fully developed across UB and PLT, $S_{R,PLT} = 0$. $L_{C,NF}$ calculated using Equation [5.8] was applied to d_{NF} to calculate NF and VB S_R values. The length of NF in the northeast-southwest direction, L, was measured to be approximately 205 m on the DEM, which for Equation [5.8] yields $L_{C,NF} = 0.81$. It was assumed, therefore, that 19% of the snow that was transported to the NF reached was rather deposited in the VB. Thus, $S_{R,NF}$ was calculated using Equation [5.6] and $S_{R,VB}$ was calculated using Equation [5.7] with $(1 - L_{C,NF})$. $S_{R,SF}$ was calculated using Equation [5.6] with $L_{C,SF} = 1.0$.

The use of interface lengths to parameterize GB S_R values is suitable because quantities of snow transport are similar upwind from different interface lengths. For instance consider Figure

5.9 and the interface lengths d_{SF} and d_{NF}. In reality the UB fetch distance is greater upwind d_{SF} than it is upwind d_{NF}. However, once the PLT snow transport is also considered, there is similar snow transport per unit width across both d_{SF} and d_{NF}. Thus the interface lengths alone are able to consolidate the different quantities of snow transported across d_{SF} and d_{NF}.

Table 5.5 Granger Basin snow redistribution allocation factors for (a) S_R scheme 1, (b) S_R scheme 2, (c) S_R scheme 3

(a)

Basin gain	PLT	NF	SF	VB	Basin loss
1.0	0.20	0.20	0.20	0.20	0.20

(b)

Basin gain	PLT	NF	SF	VB	Basin loss
1.0	0.00	0.28	0.16	0.06	0.60

(c)

Wind direction	Basin gain	PLT	NF	SF	VB	Basin loss
North	0.47	0.00	0.00	0.00	0.00	1.00
Northeast	0.00	0.00	0.00	0.00	0.00	1.00
East	1.00	0.00	0.00	0.00	0.00	1.00
Southeast	1.00	0.00	0.35	0.22	0.08	0.35
South	1.00	0.00	0.41	0.28	0.09	0.22
Southwest	1.00	0.00	0.51	0.37	0.12	0.00
West	1.00	0.00	0.12	0.00	0.06	0.82
Northwest	0.50	0.00	0.00	0.00	0.00	1.00

An apparent mismatch of scales must be addressed, with respect to the locations of the snow survey transects that are used to characterise snow conditions across the entire HRU in which they lie. Of particular concern is the location and extent of the SF transects, which were located near the eastern end of the SF HRU. Applying either S_R scheme results in snow being transported into the SF HRU. Modelling results presented in this manuscript show that the UB is the source of the majority of the blown snow deposited into the SF. This transported snow would be deposited over the western portion of the SF. As a result, it is anticipated that simulated SF mean SWE slightly exceeds observed SWE.

Winter snow transport and redistribution calculations were performed using CRHM with PBSM. PBSM was not coupled with a melt model because snowmelt over winters in this

environment is negligible. Table 5.6 shows CRHM model parameters. Vegetation height and diameter were set to 0.1 m for the UB to represent the roughness effects of sparse vegetation and rocks. Vegetation height on the NF and SF were set based on the February 2008 measurements on these HRUs (87 cm height), assuming some growth over the years. Fetch distances used were the average of northwest and southwest fetch distance calculated using FETCHR. The fetch distance for the NF and VB were set to the PBSM minimum of 300 m because the fetch distance calculated for these HRUs using FETCHR was less than the minimum required by PBSM.

Table 5.6 Granger Basin CRHM model parameters

Wind direction	Vegetation height (m)	Vegetation diameter (m)	Vegetation density (number m^{-2})	Fetch (m)
UB	0.1	0.1	0.5	734
PLT	0.3	0.3	1	319
NF	0.8	0.8	1	300
SF	0.8	0.8	1	631
VB	1.5	0.8	1	300

Snow redistribution simulations over GB were also simulated using MESH and MESH-PBSM. As opposed to the CRHM GB simulations, the snow ablation period was also simulated using MESH and MESH-PBSM. MESH and MESH-PBSM simulations were only performed using S_R scheme 2 for two reasons: 1) S_R scheme 3 is difficult to apply using MESH because wind direction is not a MESH input and thus adds another degree of complexity to the model, and 2) CRHM model results show that S_R scheme 2 is adequate (section 5.5.2 and MacDonald *et al*., 2009). Calibration was performed using DDS on the 2003/2004 data because it is the only period where snow surveys where performed on the PLT. Root mean squared error (*RMSE*) of SWE was used as the objective function.

$$RMSE = \sqrt{\frac{\sum \left(SWE_{SIM} - SWE_{OBS} \right)^2}{n}} \quad [5.10]$$

where n is the number of simulated-observed pairs, and SWE_{SIM} and SWE_{OBS} are the simulated and observed snow water equivalent in mm, respectively. Three optimization trials of 2000 objective functions evaluations were performed for both MESH and MESH-PBSM. The optimal parameter sets had an *RMSE* of 35.6 mm SWE and 21.9 mm SWE for MESH and MESH-PBSM, respectively. Table 5.7 shows the optimum parameter values and parameter ranges for the calibrations for MESH and MESH-PBSM. Parameter ranges were set based on prior work by Dornes *et al*. (2008b). Shrub LAI parameter ranges were set based on in situ measurements taken at GB by Bewley (2006). The optimum parameter sets (MESH_parameters_CLASS.ini and MESH_parameters_hydrology.ini) for both CLASS and CLASS-PBSM are included in Appendix E. CLASS parameters definitions and recommended values are included in Appendix B.

Table 5.7 Optimized parameter values for Granger Basin simulations using S_R scheme 2 for (a) MESH and (b) MESH-PBSM. Values in parentheses indicate parameter bounds.

(a)

	UB		PLT		NF		SF		VB	
Parameter	**Shrubs**	**Grass**	**Shrubs**	**Grass**	**Shrubs**	**Grass**	**Shrubs**	**Grass**	**Shrubs**	**Grass**
Veg. roughness length [m]	0.036 (0.022, 0.045)	0.005 (0.005, 0.025)	0.043 (0.025, 0.041)	0.029 (0.008, 0.03)	0.024 (0.022, 0.165)	0.013 (0.008, 0.03)	0.199 (0.025, 0.165)	0.009 (0.008, 0.03)	0.176 (0.15, 0.273)	0.015 (0.008, 0.03)
Veg. visible albedo ALVC []	0.035 (0.03, 0.2)	0.181 (0.02, 0.2)	0.216 (0.03, 0.2)	0.219 (0.02, 0.2)	0.198 (0.03, 0.2)	0.097 (0.02, 0.2)	0.246 (0.03, 0.2)	0.159 (0.02, 0.2)	0.130 (0.03, 0.2)	0.127 (0.02, 0.2)
Veg. near-IR albedo ALIC []	0.540 (0.3, 0.7)	0.438 (0.2, 0.5)	0.358 (0.3, 0.7)	0.398 (0.2, 0.4)	0.682 (0.3, 0.7)	0.290 (0.2, 0.5)	0.692 (0.3, 0.7)	0.468 (0.2, 0.5)	0.696 (0.3, 0.7)	0.551 (0.2, 0.6)
Maximum LAI LAMX []	0.141 (0.1, 0.31)	1.080 (0.5, 2)	0.284 (0.1, 0.52)	1.013 (0.5, 3)	0.369 (0.3, 0.5)	2.118 (0.5, 4)	0.354 (0.3, 0.5)	2.864 (0.5, 4)	0.353 (0.3, 0.8)	2.140 (0.5, 4)
Minimum LAI LAMN []	0. 463 (0.05, 0.2)	0. 146 (0.1, 2)	0. 368 (0.05, 0.2)	1. 512 (0.5, 2)	0. 263 (0.1, 0.3)	1.947 (0.5, 2)	0. 245 (0.1, 0.3)	0.445 (0.5, 2)	0.204 (0.1, 0.3)	1.997 (0.5, 2)
Limiting snow depth ZSNL (m)	0.69 (0.01, 1.0)		0.96 (0.01, 1.0)		0.40 (0.01, 1.0)		0.28 (0.01, 1.0)		0.78 (0.01, 1.0)	

Table 5.7 continued
(b)

	UB		PLT		NF		SF		VB	
Parameter	**Shrubs**	**Grass**	**Shrubs**	**Grass**	**Shrubs**	**Grass**	**Shrubs**	**Grass**	**Shrubs**	**Grass**
Veg. roughness length [m]	0.022 (0.022, 0.045)	0.007 (0.005, 0.025)	0.067 (0.025, 0.041)	0.026 (0.008, 0.03)	0.099 (0.022, 0.165)	0.011 (0.008, 0.03)	0.187 (0.025, 0.165)	0.009 (0.008, 0.03)	0.266 (0.15, 0.273)	0.012 (0.008, 0.03)
Veg. visible albedo ALVC []	0. 110 (0.03, 0.2)	0. 022 (0.02, 0.2)	0. 142 (0.03, 0.2)	0. 200 (0.02, 0.2)	0. 089 (0.03, 0.2)	0. 146 (0.02, 0.2)	0. 227 (0.03, 0.2)	0. 094 (0.02, 0.2)	0. 218 (0.03, 0.2)	0. 193 (0.02, 0.2)
Veg. near-IR albedo ALIC []	0. 364 (0.3, 0.7)	0. 383 (0.2, 0.5)	0. 463 (0.3, 0.7)	0. 274 (0.2, 0.4)	0. 346 (0.3, 0.7)	0. 301 (0.2, 0.5)	0. 691 (0.3, 0.7)	0. 564 (0.2, 0.5)	0. 686 (0.3, 0.7)	0. 590 (0.2, 0.6)
Maximum LAI LAMX []	0.408 (0.1, 0.31)	1.694 (0.5, 2)	0.374 (0.1, 0.52)	1.392 (0.5, 3)	0.422 (0.3, 0.5)	1.014 (0.5, 4)	0.436 (0.3, 0.5)	2.185 (0.5, 4)	0.662 (0.3, 0.8)	3.161 (0.5, 4)
Minimum LAI LAMN []	0.226 (0.05, 0.2)	0.227 (0.1, 2)	0.301 (0.05, 0.2)	0.597 (0.5, 2)	0.218 (0.1, 0.3)	0.513 (0.5, 2)	0.252 (0.1, 0.3)	0.557 (0.5, 2)	0.252 (0.1, 0.3)	1.374 (0.5, 2)
Vegetation height Ht (m)	0.104 (0.01, 0.15)		0. 394 (0.1, 0.4)		0. 715 (0.7, 0.9)		0. 721 (0.7, 0.9)		-- ()	
Vegetation density N_S (number m^{-2})	0.15 (0.1, 0.8)		0.62 (0.5, 1.0)		-- ()		-- ()		-- ()	
Vegetation silhouette area A_S (m^2)	0.149 (0.01, 0.5)		0.493 (0.1, 0.5)		-- ()		-- ()		-- ()	
Fetch distance fetch (m)	674.8 (661, 807)		332.7 (300, 351)		-- ()		-- ()		-- ()	
Limiting snow depth ZSNL (m)	0.03 (0.01, 1.0)		0.95 (0.01, 1.0)		0.29 (0.01, 1.0)		0.19 (0.01, 1.0)		0.33 (0.01, 1.0)	

5.4.4 Model Evaluation

Simulated snow accumulation was evaluated using model bias (Equation [5.2]), root mean squared error (Equation [5.3]), the normalized root mean squared error (Equation [5.4]), the coefficient of determination (Equation [5.5]) and a modification of the Nash-Sutcliffe efficiency coefficient (*MNS*) given by

$$MNS = 1 - \frac{\sum\left(\alpha SWE_{sim} - \alpha SWE_{obs}\right)^2}{\sum\left(\alpha SWE_{obs} - P\right)^2} \qquad [5.11]$$

where SWE_{sim} and SWE_{obs} are the simulated and observed SWE, respectively. α is the fractional area of the HRU. α is included so that the model evaluation statistics reflect the relative size of different HRUs that make up GB. The original Nash-Sutcliffe coefficient (Nash and Sutcliffe, 1970) quantifies the accuracy of a streamflow model with respect to the mean observed discharge over a model period i.e. all terms in Equation [5.11] would be discharge and P would be mean observed discharge over the model period. Here a *MNS* equal to one indicates best fit and a *MNS* equal to zero indicates that the model performed no better than only using cumulative snowfall to represent snow accumulation in HRUs. The *MNS* was only used for evaluating the GB CRHM model. Assuming that snowmelt over GB during the winter is negligible and therefore a snowmelt model need not be coupled to PBSM in CRHM, the only other predictor of snow accumulation in HRUs aside from the blowing snow redistribution model would be snowfall. Conversely, owing to its non-modular structure, MESH potentially calculates snowmelt at each time step.

5.5 Distributed Model Results and Discussion

5.5.1 Fisera Ridge

CRHM simulations were performed at 15-minute intervals from 20 October 2007 to 30 April 2008 and from 24 September 2008 to 19 April 2009. Figures 5.13 and 5.14 show observed and simulated snow accumulation over HRUs using observed station wind speed data and using RMM-modelled wind speeds, respectively. Tables 5.8 and 5.9 show end-of-winter snow accumulation, cumulative snowmelt, transport in to and out of HRUs, blowing snow sublimation, snowpack sublimation and sublimation of intercepted snow in the Forest HRU for simulations using observed wind speed data and using RMM-modelled wind speeds, respectively. Table 5.10 shows CRHM model evaluation statistics for all simulations over the entire simulation period.

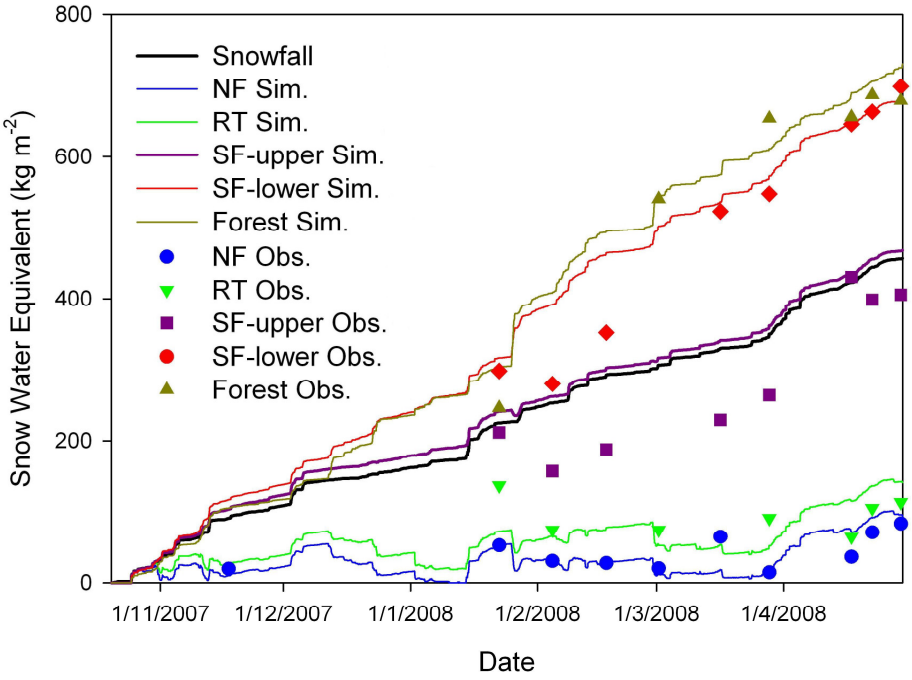

(a)

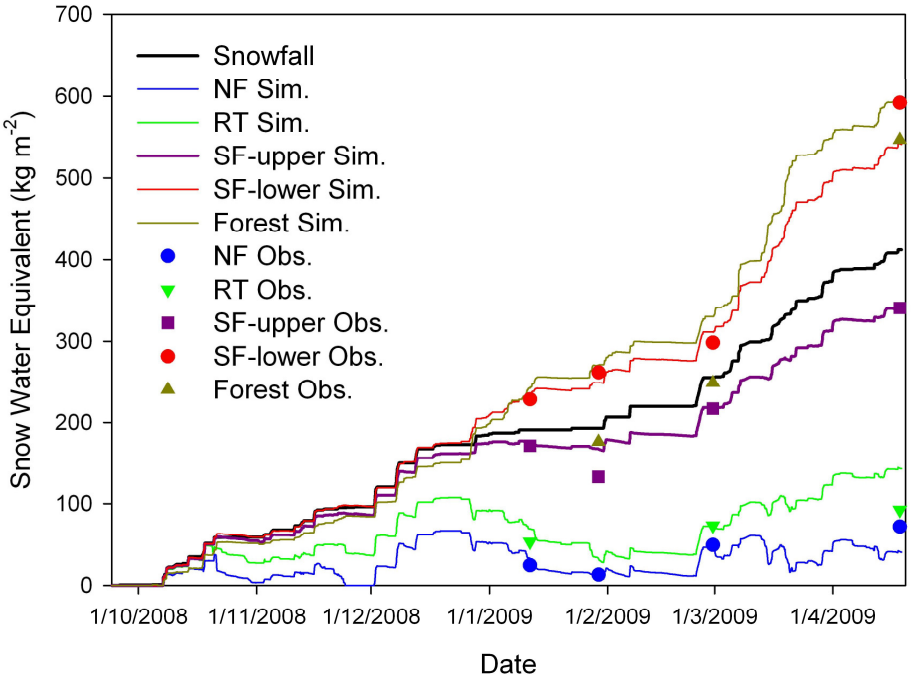

(b)

Figure 5.13 Fisera Ridge HRUs observed and simulated snow accumulation using CRHM with observed wind speeds for (a) 2007/2008 and (b) 2008/2009

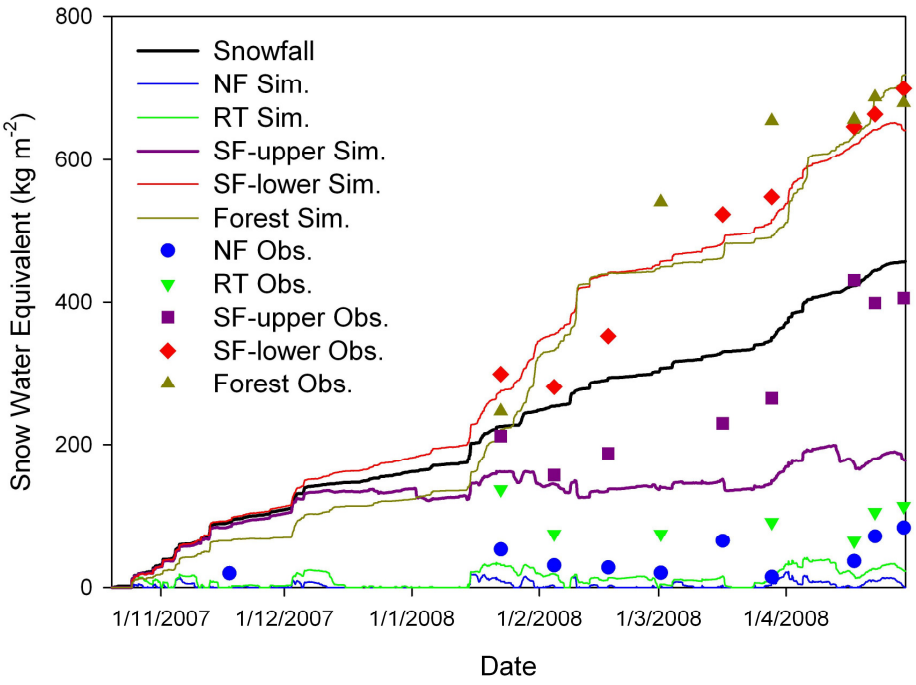

(a)

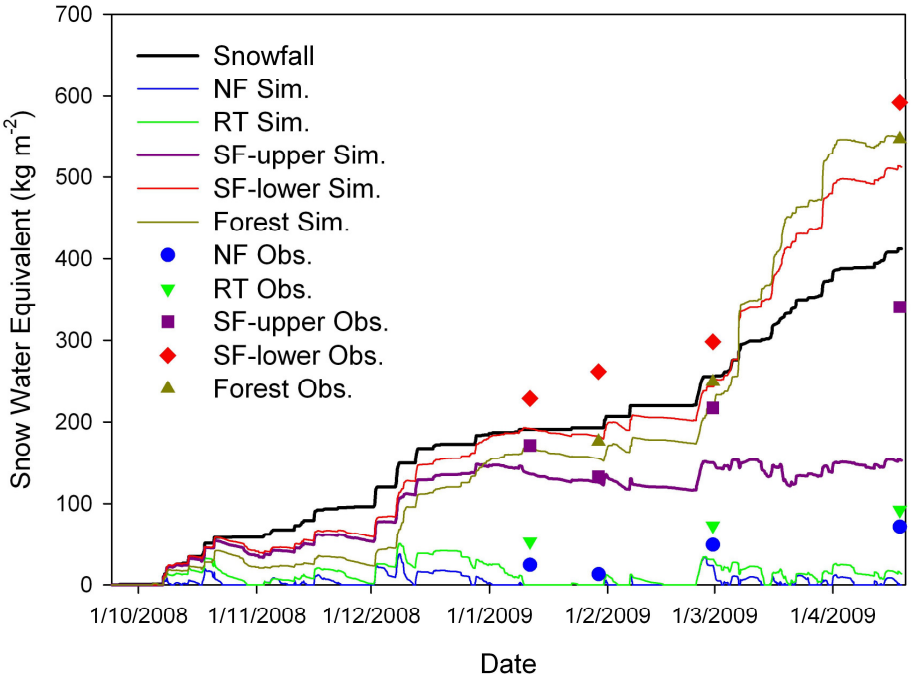

(b)

Figure 5.14 Fisera Ridge HRUs observed and simulated snow accumulation using CRHM with RMM-modelled wind speeds for (a) 2007/2008 and (b) 2008/2009

Table 5.8 Summary of Fisera Ridge cumulative model results using CRHM with observed wind speed data for (a) 2007/2008 and (b) 2008/2009 (quantities are in kg m^{-2}; values in parentheses indicate quantity as percentage of snowfall)

(a)

	Snow on ground		Snowmelt		Snow Transport In		Snow Transport Out		Blowing Snow Sublimation		Snowpack Sublimation		Intercepted Snow Sublimation	
NF	95	(20)	4.4	(0.9)	0	(0)	145	(31)	187	(40)	31	(6.7)	-	-
RT	141	(30)	1.6	(0.3)	13	(2.8)	149	(32)	175	(38)	9.8	(2.1)	-	-
SF-upper	468	(103)	1.6	(0.4)	13	(2.8)	5.9	(1.3)	5.3	(1.2)	-14	(-3.0)	-	-
SF-lower	679	(150)	1.6	(0.4)	213	(47)	0	(0)	0	(0)	-15	(-3.2)	-	-
Forest	731	(161)	0.3	(0.1)	437	(96)	0	(0)	0	(0)	-15	(-3.3)	152	(34)
Transect	*353*	(*78*)	*2.3*	(*0.5*)	-	-	-	-	*86*	(*19*)	*2.8*	(*0.6*)		

(b)

	Snow on ground		Snowmelt		Snow Transport In		Snow Transport Out		Blowing Snow Sublimation		Snowpack Sublimation		Intercepted Snow Sublimation	
NF	40	(9.8)	7.0	(1.7)	0	(0)	127	(31)	152	(37)	85	(21)	-	-
RT	142	(34)	1.2	(0.3)	2.3	(0.5)	101	(24)	114	(27)	63	(15)	-	-
SF-upper	342	(82)	3.7	(0.9)	18	(4.3)	16	(3.8)	17	()	55	(13)	-	-
SF-lower	542	(133)	1.4	(0.3)	188	(46)	0	(0)	0	(0)	52	(13)	-	-
Forest	597	(147)	2.8	(0.7)	346	(85)	0	(0)	0	(0)	29	(7.2)	82	(20)
Transect	*269*	(*65*)	*3.8*	(*0.9*)	-	-	-	-	*69*	(*17*)	*62*	(*15*)		

Table 5.9 Summary of Fisera Ridge HRUs cumulative model results using CRHM with RMM-modelled wind speeds for (a) 2007/2008 and (b) 2008/2009 (quantities are in kg m^{-2}; values in parentheses indicate quantity as percentage of snowfall).

(a)

	Snow on ground		Snowmelt		Snow Transport In		Snow Transport Out		Blowing Snow Sublimation		Snowpack Sublimation		Intercepted Snow Sublimation	
NF	0.0	(0.0)	112	(24)	0.0	(0.0)	113	(24)	175	(38)	60	(13)	-	-
RT	23	(4.9)	44	(9.5)	104	(22)	172	(37)	246	(53)	82	(18)	-	-
SF-upper	178	(39)	1.6	(0.4)	37	(8.2)	129	(28)	150	(33)	34	(7.4)	-	-
SF-lower	641	(142)	1.6	(0.4)	238	(52)	6.2	(1.4)	11	(2.2)	31	(6.8)	-	-
Forest	720	(159)	0.1	(0.0)	525	(116)	0.0	(0.0)	0.0	(0.0)	42	(9.2)	200	(44)
Transect	*206*	(*45*)	*40*	(*8.6*)	-	-	-	-	*144*	(*31*)	*50*	(*11*)		

(b)

	Snow on ground		Snowmelt		Snow Transport In		Snow Transport Out		Blowing Snow Sublimation		Snowpack Sublimation		Intercepted Snow Sublimation	
NF	0	(0)	46	(11)	0	(0)	141	(34)	144	(35)	79	(19)	-	-
RT	14	(3.2)	11	(2.6)	94	(22)	171	(41)	190	(45)	127	(30)	-	-
SF-upper	153	(37)	11	(2.8)	46	(11)	90	(22)	80	(19)	127	(31)	-	-
SF-lower	512	(126)	10	(2.5)	239	(59)	0	(0)	0	(0)	123	(30)	-	-
Forest	552	(136)	14	(3.4)	439	(108)	0	(0)	0	(0)	135	(33)	107	(26)
Transect	*165*	(*40*)	*21*	(*5.0*)	-	-	-	-	*101*	(*24*)	*114*	(*28*)		

Table 5.10 Fisera Ridge HRUs CRHM model evaluation statistics

	Observed Wind			RMM-modelled Wind		
Year	***NRMSE* (*RMSE* [kg m^{-2}])**	***MB***	***R^2***	***NRMSE* (*RMSE* [kg m^{-2}])**	***MB***	***R^2***
2007/2008	1.9 (*13.2*)	0.13	0.69	3.6 (*24.3*)	-0.31	0.58
2008/2009	0.9 (*5.1*)	0.05	0.89	3.0 (*17.3*)	-0.32	0.63

Snow accumulation was generally well simulated with CRHM when using the observed wind speed data. 2007/2008 was not simulated to the same accuracy as 2008/2009 as snow accumulation was overestimated on the SF-upper throughout the simulation and snow accumulation was overestimated on the SF-bottom during February but matched observed snow

accumulation at the end of the simulation in April 2008. Observed SF-upper snow accumulation was lower than cumulative snowfall in 2007/2008 whereas simulated snow accumulation in this HRU slightly exceeded cumulative snowfall. Simulations show that snow accumulation on the NF and RT were reduced to roughly one-quarter of cumulative snowfall whereas snow accumulation on the SF-lower and Forest increased by approximately half compared to cumulative snowfall due to snow redistribution by wind. Simulated snowmelt and snowpack sublimation resulted in an approximately equal loss of snow mass during 2007/2008, with the net condensation simulated on the SF-upper, SF-lower and Forest nearly balancing the sublimation simulated on the NF and RT. Simulated snowpack sublimation significantly exceeded simulated snowmelt during 2008/2009. Sublimation of intercepted snow in the Forest was significant as 34% and 20% of snowfall was calculated to sublimate from this HRU during 2008/2008 and 2008/2009, respectively.

Snow accumulation was not as well simulated when using the RMM wind speeds. RMM wind speeds were typically greater than the measured wind speeds. This caused much greater erosion of the SF-upper as well as greater erosion of the RT. This increased snow transport balanced the higher modelled blowing snow sublimation rates to yield satisfactory simulated snow accumulation on the SF-lower and Forest through the winter. Much higher snowmelt and snowpack sublimation were simulated on most HRUs when using the RMM wind speeds because the higher RMM wind speeds increased turbulent transfer of sensible heat towards the snowpack. As well, greater melt rates were calculated due to shallower snowpacks, which were caused by greater snow erosion rates. The higher RMM wind speeds caused higher simulated intercepted snow sublimation rates in the Forest HRU.

Estimated blowing snow sublimation losses were 19% for 2007/2008 and 17% for 2008/2009 over the transect when using the observed wind speed data. These blowing snow sublimation losses were substantial and important to the winter water balance of the alpine ridge. Satisfactory FR snow mass balance closure suggests that the use of the minimum PBSM fetch distance parameter (300 m) is adequate in this environment. Boundary layer development for fetches shorter than this in complex terrain are poorly understood and so the parameter is left to its minimum value (based on the limits of PBSM physics) until a more realistic parameterization is be developed.

The observed SF-lower snow accumulation was greater than the Forest snow accumulation in 2008/2009, whereas the opposite was true during 2007/2008 and for the simulations. It is difficult to elucidate why this was the case. Observed wind speeds were generally higher during 2008/2009 than 2007/2008 (higher mean and less positive skew of wind speed), so it is not a case of downwind transport distance increasing with increasing wind speed; in fact the inverse seems to have occurred.

It will be worthwhile testing other empirical, terrain-based windflow models (e.g. Winstral *et al*., 2009). However, it is not expected that empirical windflow models can be as accurate as the much more computational expensive computational fluid dynamic models. It is worth mentioning that Bernhardt *et al*. (2009) applied a computationally inexpensive approach to use wind fields generated from the MM5 atmospheric model to drive a snow transport model by generating a library of the 220 most common windfields.

Figure 5.15 shows MESH results for (a) 2007/2008 and (b) 2008/2009 using the observed wind speeds and Figure 5.16 shows MESH-PBSM results for a) 2007/2008 and (b) 2008/2009 using the observed wind speeds. Model evaluation statistics are shown on Table 5.11. The

MESH results are not surprisingly very poor because the model does not capture the wind erosion of snow on the NF and RT and the deposition of transported snow into the SF-lower and Forest. MESH was not even able to simulate the variation in observed SWE as shown by the poor R^2 scores. MESH-PBSM provided a markedly better simulated snowcover than MESH. MESH simulated snow accumulation in the HRUs fairly accurately for both periods until snowmelt began to dominate in March 2008 and April 2009. As done for the FR point simulations presented in section 4.4.2, incoming shortwave radiation measurements were decreased by 20% to determine if reflected shortwave radiation from adjacent was the cause of overestimated snowmelt. This did not improve simulated snow accumulation significantly. The albedo decay functions in CLASS were reduced in an attempt to alleviate the overestimated snowmelt, though this did not improve results much either. Also, the hard-coded parameters that control turbulent transfer of sensible and latent heat (the roughness length of snow and the ratio of roughness length for momentum to that for heat) were adjusted but this did not alleviate the early snowmelt issue. To investigate whether CLASS was overestimating the ground heat flux to the snowpack, the soil temperature simulated by CLASS for each HRU was put into the CRHM model runs. This does not affect the CRHM simulated snowcover significantly. A newer version of MESH with CLASS 3.5 was evaluated over the Fisera Ridge HRUs, and snowmelt was just as severely overestimated as with CLASS 3.4. Cumulative blowing snow transport and sublimation quantities estimated by CRHM (PBSM) and MESH-PBSM were similar. Oddly, CLASS predicted net condensation on the Forest HRU canopy.

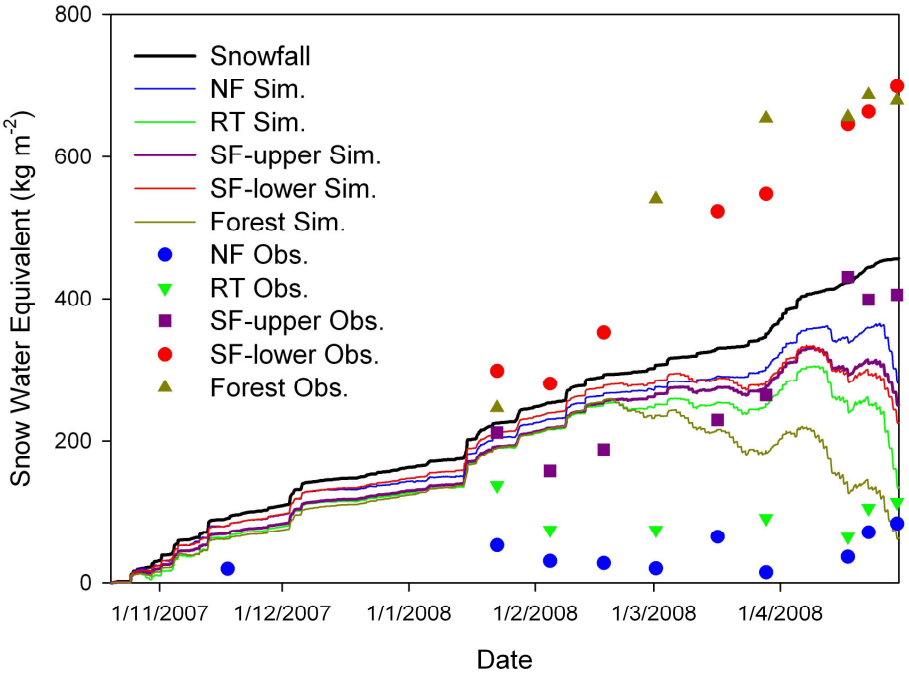

(a)

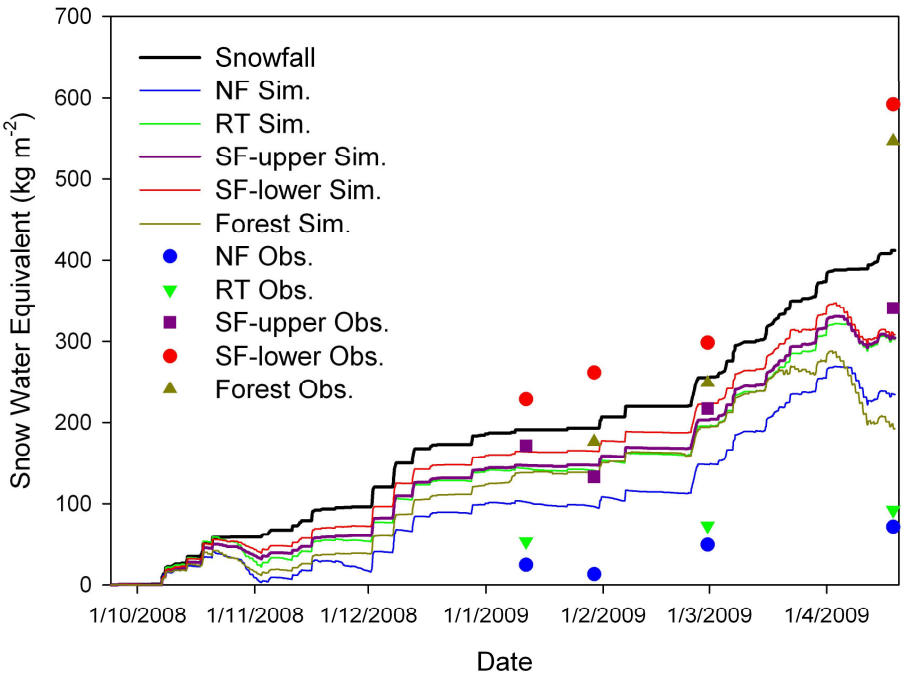

(b)

Figure 5.15 Fisera Ridge HRUs observed and simulated snow accumulation using MESH for (a) 2007/2008 and (b) 2008/2009

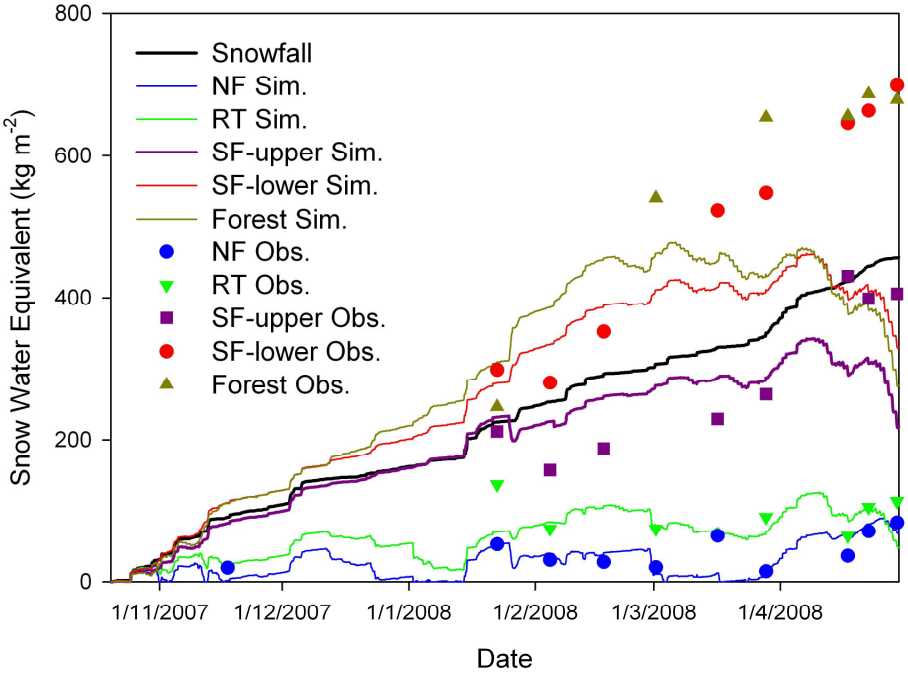

(a)

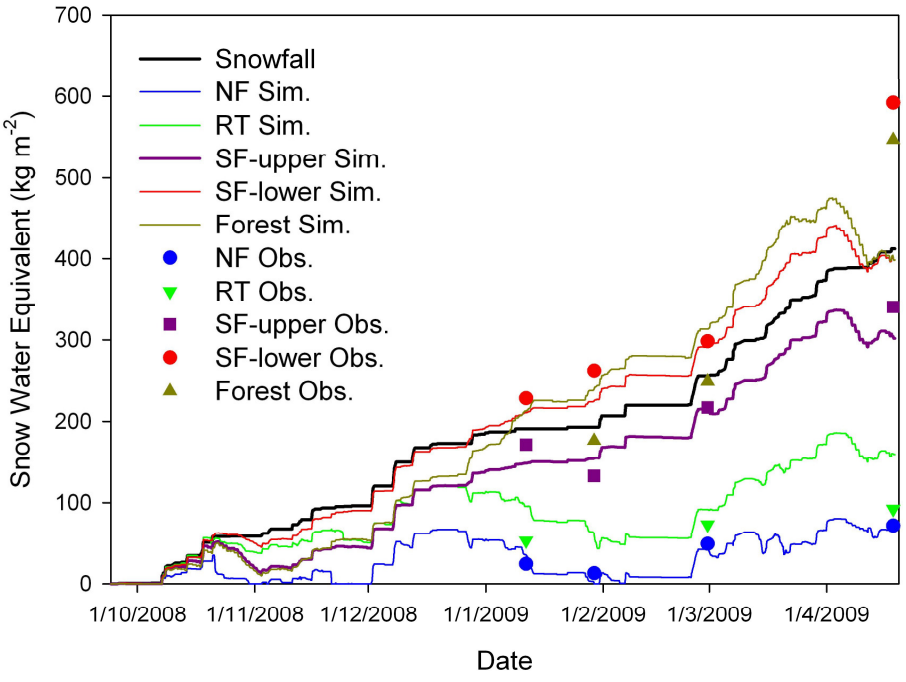

(b)

Figure 5.16 Fisera Ridge HRUs observed and simulated snow accumulation using MESH-PBSM for (a) 2007/2008 and (b) 2008/2009

Table 5.11 Fisera Ridge HRUs MESH and MESH-PBSM model evaluation statistics

Year	MESH			MESH-PBSM		
	NRMSE (***RMSE*** [kg m^{-2}])	***MB***	R^2	***NRMSE*** (***RMSE*** [kg m^{-2}])	***MB***	R^2
2007/2008	6.3 (43.0)	0.14	0.32	3.0 (20.6)	-0.18	0.48
2008/2009	3.9 (22.5)	0.11	0.39	1.5 (8.9)	-0.05	0.71

Table 5.12 Summary of Fisera Ridge HRUs cumulative model results using MESH-PBSM for (a) 2007/2008 and (b) 2008/2009 (quantities are in kg m^{-2}; values in parentheses indicate quantity as percentage of snowfall).

(a)

	Snow on ground		Snowmelt		Snow Transport In		Snow Transport Out		Blowing Snow Sublimation		Snowpack Sublimation		Intercepted Snow Sublimation	
NF	69	(15)	29	(6.3)	0	(0)	163	(35)	191	(41)	9.0	(1.9)	-	-
RT	50	(11)	145	(31)	107	(23)	159	(34)	184	(39)	33	(7.1)	-	-
SF-upper	219	(47)	226	(48)	63	(14)	19	(4.0)	38	(8.2)	22	(4.7)	-	-
SF-lower	331	(71)	12	(2.6)	143	(31)	0.03	(0.0)	0.03	(0.0)	12	(2.6)	-	-
Forest	277	(59)	430	(92)	265	(57)	0	(0)	0	(0)	9.4	(2.0)	1.9	(0.4)
Transect	*166*	(*35*)	*142*	(*30*)	-	-	-	-	*100*	(*21*)	*18*	(*3.9*)		

(b)

	Snow on ground		Snowmelt		Snow Transport In		Snow Transport Out		Blowing Snow Sublimation		Snowpack Sublimation		Intercepted Snow Sublimation	
NF	66	(16)	17	(4.1)	0	(0)	134	(33)	173	(43)	8.8	(2.2)	-	-
RT	160	(37)	50	(12)	83	(19)	119	(28)	148	(35)	31	(7.3)	-	-
SF-upper	308	(73)	116	(27)	49	(2.0)	8.6	(2.0)	14	(3.3)	20	(4.6)	-	-
SF-lower	400	(95)	96	(23)	111	(26)	5.3	(1.3)	6.2	(1.5)	16	(3.8)	-	-
Forest	402	(96)	227	(54)	206	(49)	0	(0)	0	(0)	7.4	(1.8)	-10	(-2.4)
Transect	*234*	(*55*)	*82*	(*19*)	-	-	-	-	*81*	(*20*)	*17*	(*4.1*)		

Overestimated and early simulated snowmelt by CLASS has been observed by other modellers (personal conversation with Bruce Davison, Environment Canada). Simulated early and mid-season snowmelt was also reported by Slater *et al*. (2001) in the Project for the Intercomparison of Land-surface Parameterization Schemes (PILPS) Phase 2(d) comparison of

snowcover simulations by a number of LSSs, and by Rutter *et al*. (2009) in the Snow Model Intercomparison Project 2 (SnowMIP2) comparison of snowcover simulations by a number of snow models, including some LSSs. Slater *et al*. (2001) observed that the divergence of simulated snowcover amongst the LSSs tended to persist throughout the simulations and largely attributed that to internal model feedback (Slater *et al*., 2001). Rutter *et al*. (2009) showed that inter-model divergence in simulated snowcover and the greatest underestimation of snow accumulation was dominated by the simulation of melt events during accumulation periods when air temperatures rose above 0ºC. This may have been the case for the FR simulations because it is located within Canada's Chinook belt, which is characterized by unseasonable air temperature increases of, on average, 5-6 °C during approximately 44-48 days per winter (Nkemdirim, 1996). It is unclear why CLASS overestimated snowmelt whereas SNOBAL did not. Though it is outside the scope of this thesis to perform a detailed analysis to determine the reason(s), it is suspected that the early and overestimated snowmelt by CLASS may have been caused by the numerical method in CLASS or by a process parameterization. To examine this issue in a preliminary manner and to provide an impetus for a deeper examination of this issue, Figure 5.17 shows 12-hour averages of observed air temperature, CRHM (i.e. SNOBAL-simulated) and MESH-PBSM (i.e. CLASS-simulated) simulated snowpack temperature for the SF-bottom HRU for (a) 2007/2008 and (b) 2008/2009. Only the SF-bottom HRU is presented in this demonstration because it has a continuous, deep snowpack compared to the upwind HRUs and the effects of vegetation are less compared to the Forest HRU.

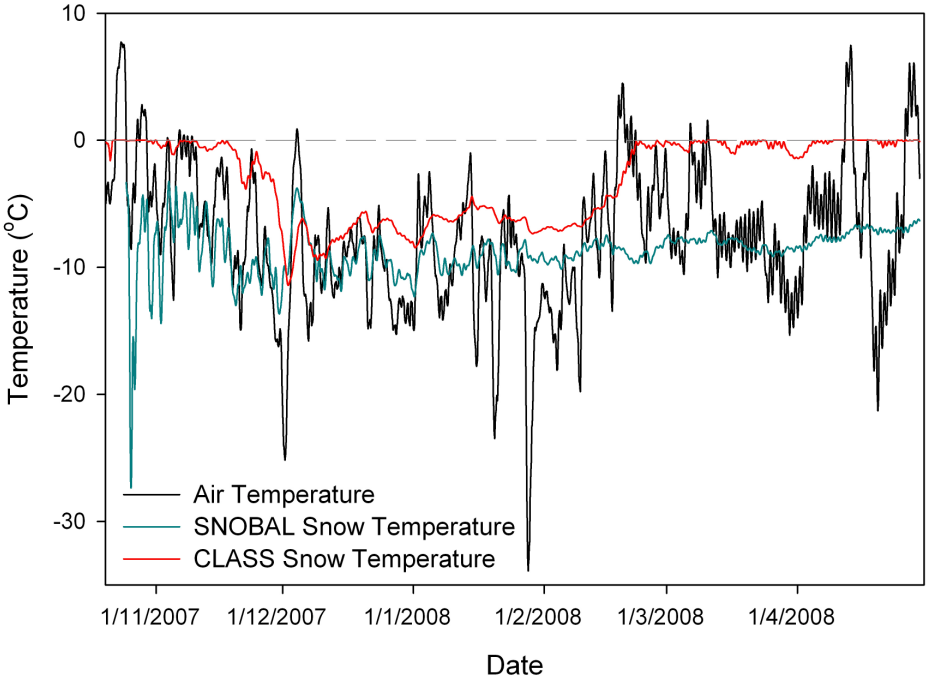

(a)

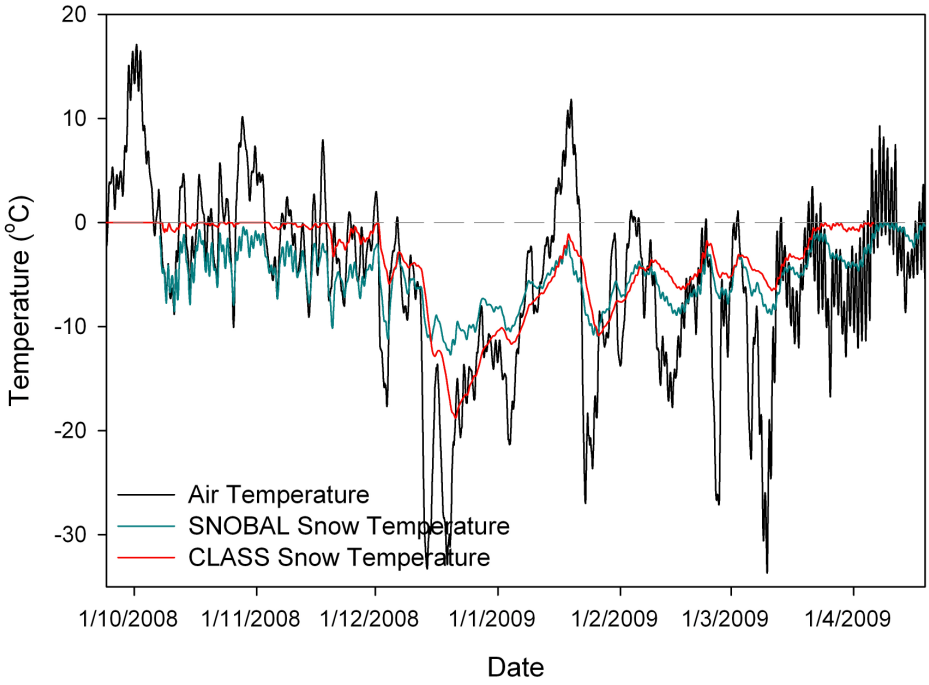

(b)

Figure 5.17 Observed air temperature, CRHM (SNOBAL)-simulated average snowpack temperature and MESH-PBSM (CLASS)-simulated snowpack temperature for the Fisera Ridge SF-bottom HRU for (a) 2007/2008 and (b) 2008/2009. Dashed grey line indicates 0 °C.

Figure 5.17a shows that CLASS simulated a warmer snowpack than SNOBAL throughout nearly all of the winter 2007/2008 period. In late February 2008, CLASS simulated the average snowpack temperature to rise to near 0ºC and the snowpack temperature remained at around this temperature through to the end of the simulation. The rise in snowpack temperature coincides with air temperatures above 0ºC for over two days. Conversely, the average snowpack temperature simulated by SNOBAL remained at around -6 to -9 ºC during this period. For the 2008/2009 simulation (Figure 5.17b), CLASS and SNOBAL simulated a similar snowpack temperature up until mid-late March 2009. This rise in snowpack temperatures coincides with three consecutive days of above 0 ºC air temperatures (evenings excluded). The air temperature was above 0ºC, and as high as 12 ºC, during mid-January 2009 for seven consecutive days. CLASS did not simulate the average snowpack temperature to reach 0ºC during this period. CLASS uses an explicit time-stepping scheme with a finite difference approximation of the snowpack temperature over 30-minute time steps. This approach can lead to the temperature evolution being systematically overestimated or underestimated as errors accumulate. This is a common difficulty amongst snow models of varying degrees of complexity (Etchevers *et al*., 2004). The results of the original SnowMIP (Etchevers *et al*., 2004) show that even a particular model does not exhibit a systematic bias in simulated snow temperature from site to site. It is possible that CLASS systematically overestimated the snowpack temperature and the early snowmelt was finally simulated to occur as too much of the snowpack was projected to be warmed to 0ºC and melted. An implicit scheme would be better able to simulate the thermal evolution of the snowpack. Conversely to CLASS, SNOBAL uses a variable time-stepping scheme that is dependent on the snowpack specific mass (Marks *et al*., 1998; Marks *et al*., 1999). SNOBAL has three snow mass thresholds (60, 10 and 1 kg m^{-2} or mm SWE) that activate the use

of different time step durations. The longest time step used when the snow mass is above 60 kg m^{-2} and the shortest time step is used when the snow mass is below 1 kg m^{-2}.

Both CLASS and SNOBAL use physically based energy and mass balances. The most glaring difference in physical parameterizations between CLASS and SNOBAL is the way in which the snowpack is represented. CLASS represents the snowpack as a single layer with the variation of temperature with depth calculated using a quadratic equation (Verseghy, 2008). SNOBAL represents the snowpack as two layers with separate thermal calculations for each layer and allowing energy transfer by conduction and diffusion between the two snow layers (Marks *et al*., 1998).

Further diagnostics should be performed on the FR data set to during determine the reason(s) for CLASS overestimating snowmelt. Depending on the results of a further analysis, CLASS developers should consider: 1) implementing an implicit scheme for the thermal calculations, 2) revising the manner in which CLASS calculates the thermal evolution of the snow pack by i) revising the way in the variation of temperature with depth is calculated, and ii) implementing a two-layer snow model.

5.5.2 Granger Basin

CRHM was used to simulate snow accumulation and redistribution over GB HRUs. Table 5.13 shows model evaluation statistics for the CRHM model for all three S_R schemes for all three periods. The model evaluation statistics show that Schemes 2 and 3 provide the best simulated snow accumulation. Despite there being bias and error in all simulations, all model runs were able to simulate the variation in observed SWE as shown by the high coefficient of determination scores.

Table 5.13 Model evaluation statistics for Granger Basin simulations using CRHM

S_R	*MNS*			*MB*			*NRMSE* (*RMSE* [kg m^{-2}])			R^2		
Scheme	**1999**	**2001**	**2004**	**1999**	**2001**	**2004**	**1999**	**2001**	**2004**	**1999**	**2001**	**2004**
1	0.14	-0.24	0.59	0.03	0.12	0.08	4.4 (*3.7*)	6.1 (*6.2*)	1.9 (*2.1*)	0.99	0.97	0.99
2	0.43	0.08	0.98	0.00	0.08	0.02	3.6 (*3.0*)	5.4 (*5.4*)	0.5 (*0.5*)	1.00	0.99	1.00
3	-	-	0.84	-	-	-0.05	-	-	1.2 (*1.3*)	-	-	1.00

Figure 5.18 shows mean measured and simulated snow accumulation using CRHM for the NF, SF, VB and PLT (2004 only) for (a) 17 March 1999, (b) 3 April 2001 and (c) 15 April 2004, using S_R Scheme 1. The horizontal dashed lines represent total precipitation over the simulation period. Simulated NF, SF and VB snow accumulation exceeded total precipitation in each simulation period, whereas simulated PLT snow accumulation was below total precipitation in 2004. Model performance with S_R Scheme 1 is considered inadequate, indicating that the assumption that all HRUs receive the same snow transport is not met. However, *MNS* scores are greater than zero with the exception of 2001, suggesting that the model with this simple redistribution parameterization performed better than a model without consideration of blowing snow. Poor model performance is best demonstrated by the considerably overestimated VB snow accumulation and underestimated NF snow accumulation in 1999 and 2001 (Figure 5.18). It is noted that NF snow accumulation was closely simulated in 2004, suggesting that either the predominant u^4 direction was different over 2003/2004 than the other simulation periods, and/or differences in snow survey transects from year to year.

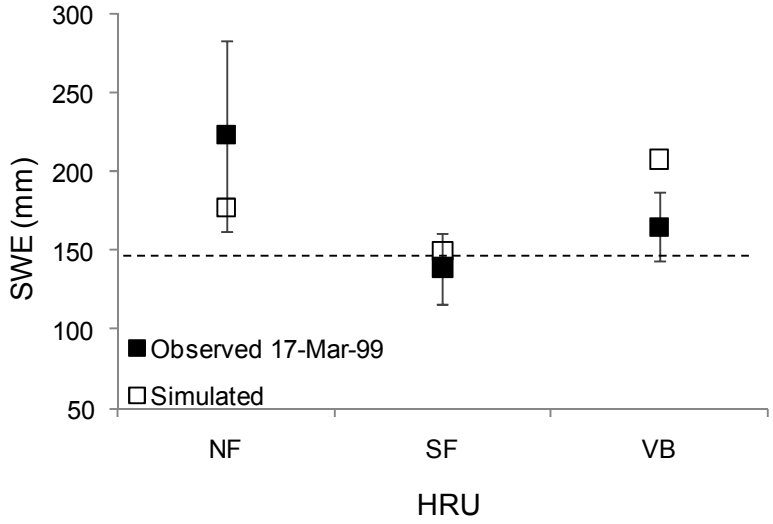

(a)

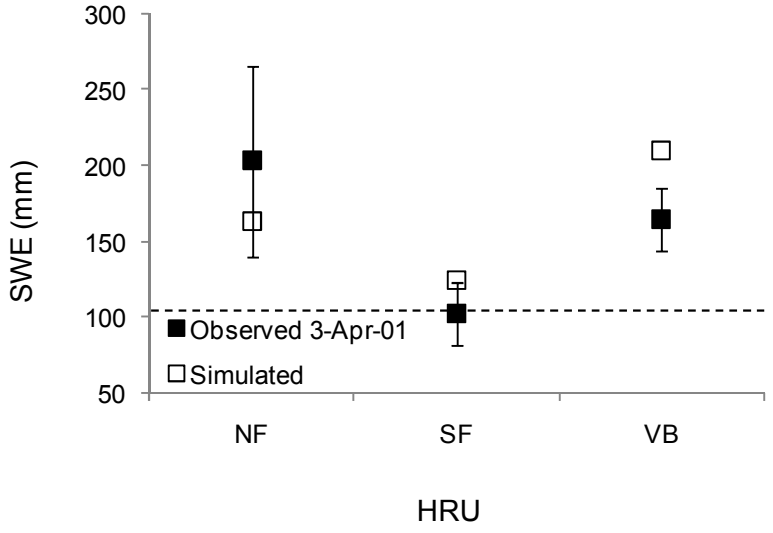

(b)

Figure 5.18 Granger Basin measured and simulated snow accumulation using CRHM with S_R Scheme 1 for the NF, SF and VB for (a) 17 March 1999, (b) 3 April 2001 and (c) 15 April 2004. ±1/2 standard deviation of observed SWE is included. Dashed line represents cumulative snowfall.

Figure 5.18 continued

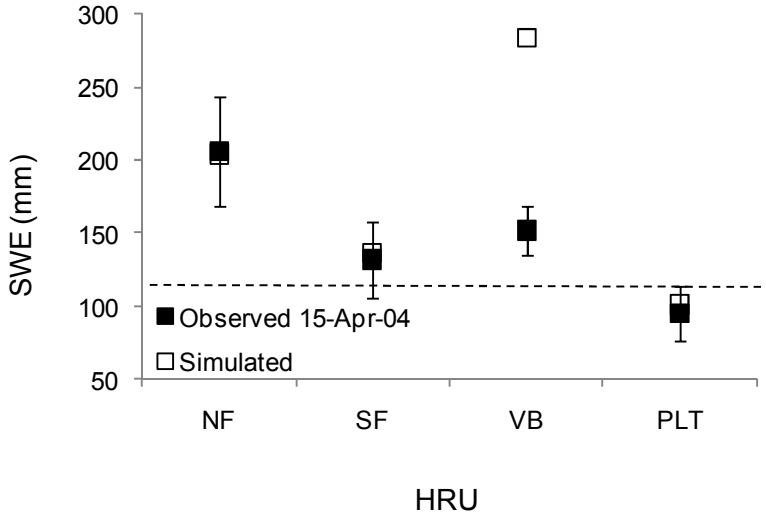

(c)

Figure 5.19 shows mean measured and simulated snow accumulation using CRHM for the NF, SF, VB and PLT (2004 only) for (a) 17 March 1999, (b) 3 April 2001 and (c) 15 April 2004, using S_R Scheme 2. The horizontal dashed lines represent cumulative precipitation over the simulation period. All simulated snow accumulation fell within 1/2 standard deviation of observed SWE except for VB in 2001. CRHM model performance with S_R Scheme 2 is considered good for 1998/1999 and 2000/20001 and excellent for 2003/2004. This suggests that redistributing snow with regard to predominant seasonal wind direction as well as the spatial arrangement, topography and vegetation of HRUs can be successful in estimating snow accumulation. As for model performance using S_R Scheme 1, there was considerable divergence between 1998/1999 and 2000/2001, and 2003/2004 model performance.

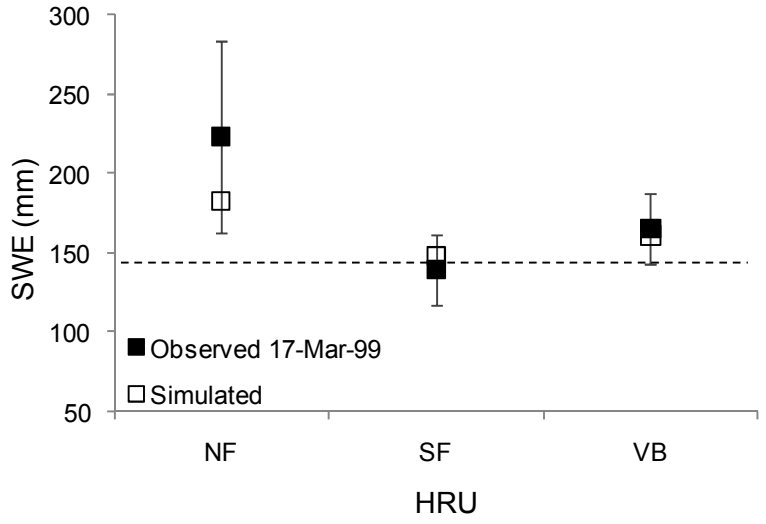

(a)

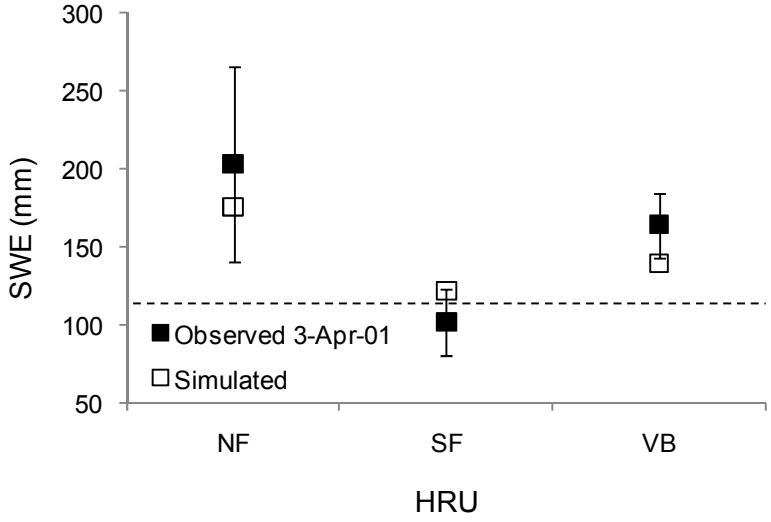

(b)

Figure 5.19 Granger Basin measured and simulated snow accumulation using CRHM with S_R scheme 2 for the NF, SF and VB for (a) 17 March 1999, (b) 3 April 2001 and (c) 15 April 2004. ±1/2 standard deviation of observed SWE is included. Dashed line represents cumulative snowfall.

Figure 5.19 continued

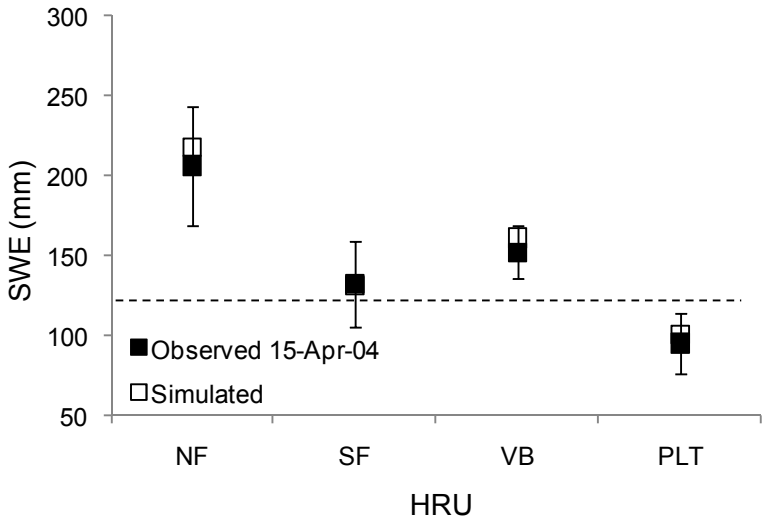

(c)

Figure 5.20 shows mean measured and simulated snow accumulation using CRHM for the NF, SF, VB and PLT for 15 April 2004, using S_R Scheme 3. The horizontal dashed line represents cumulative precipitation over the simulation period. All simulated snow accumulation fell within 1/2 standard deviation of observed SWE. Model performance with S_R Scheme 2 is considered excellent for 2003/2004 (Table 5.13), though wind direction data for 1998/1999 and 2000/2001 could have provided additional insight and validation. This suggests that redistributing snow by blowing snow event-based wind direction, as well as the spatial arrangement, topography and vegetation of HRUs can successfully estimate snow accumulation.

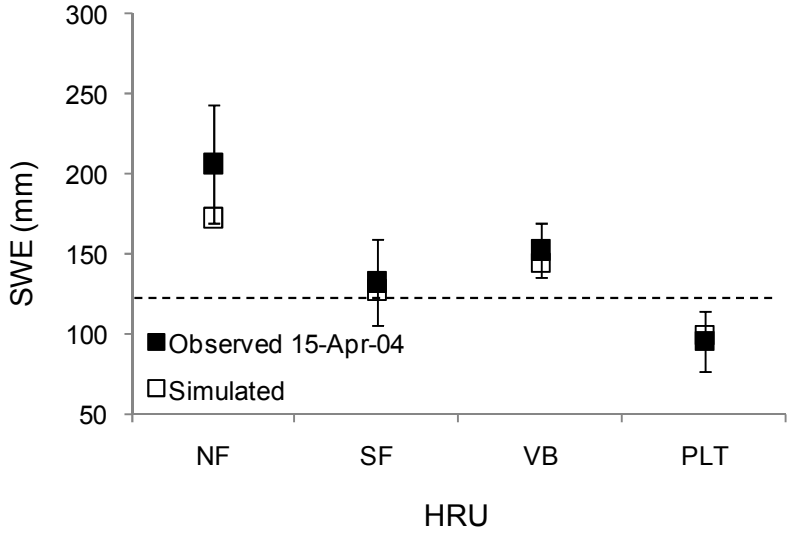

Figure 5.20 Granger Basin measured and simulated snow accumulation using CRHM with S_R Scheme 3 for the NF, SF and VB for 15 April 2004. ±1/2 standard deviation of observed SWE is included. Dashed line represents cumulative snowfall.

CRHM model evaluation statistics presented in Table 5.13 show that applying PBSM with any of the S_R schemes improved simulated snow accumulation as compared to a model without a blowing snow parameterization (all $MSN > 0$ with the exception of S_R Scheme 2 applied to 2000/2001). Even the most rudimentary snow redistribution scheme (S_R Scheme 1) improved simulated snow accumulation. S_R Scheme 2 (defining S_R values based on a predominant u^4 direction) provided the most accurately modelled snow accumulation. It is unclear how S_R Scheme 3 would have performed over 1998/1999 and 2000/2001. In view of the S_R Scheme 2 and 3 results, it is evident that a snow redistribution parameterization that incorporates wind direction, interface lengths and snow trapping efficiency can adequately simulate snow accumulation in HRUs over complex terrains such as this mountainous sub-Arctic catchment.

Having established that S_R Scheme 2 provided good to excellent simulated snow accumulation, and that results are available for all three simulation periods, simulated snow

accumulation and blowing snow sublimation results using CRHM for UB and PLT are presented and discussed in Figure 5.21. This figure shows cumulative area-weighted average snowfall, simulated snow transport into UB from outside GB, simulated cumulative SWE and simulated cumulative blowing snow sublimation for the UB and PLT for (a) 1998/1999, (b) 2000/2001 and (c) 2003/2004 to the same end dates as Figures 5.18, 5.19 and 5.20, using S_R Scheme 2. UB and PLT simulated snow accumulation were both less than cumulative snowfall for each simulation period, as snow was blown from these HRUs downwind. Simulated snow accumulation for the UB was 130, 12 and 50 mm for 1998/1999, 2000/2001 and 2003/2004, respectively. Simulated snow accumulation for the PLT was 84, 70 and 99 mm for 1998/1999, 2000/2001 and 2003/2004, respectively. Unfortunately snow survey data was not available for the UB and PLT for 1999 and 2001. However, surveys and aerial photography of nearby terrain in 2001 showed complete snow erosion from high exposed ridges in spring 2001. A snow survey across the east side of the PLT on 16 April 2004 (Figure 5.11) provided a mean SWE of 95 mm; therefore PLT cumulative SWE was well simulated for 2004. The relative amount of simulated blowing snow sublimation varied widely over each simulation period. Simulated cumulative blowing snow sublimation as a fraction of cumulative snowfall over and snow transport into UB was 19, 81 and 51% for 1999, 2001 and 2004, respectively. Simulated UB cumulative sublimation for 2004 and, in particular, 2001 was higher than is normally reported in the literature for more level environments (Pomeroy *et al*., 1993, 1997; Pomeroy and Li, 2000; Liston and Sturm, 2002; Bowling *et al*., 2004). Simulated cumulative blowing snow sublimation as a fraction of cumulative snowfall over PLT was 21, 23 and 9% for 1999, 2001 and 2004, respectively. These blowing snow sublimation quantities correspond to 10, 37 and 24% of cumulative snowfall for all of GB using CRHM, which corresponds well with estimates in the low-Arctic tundra

(Pomeroy *et al*., 1997; Essery *et al*., 1999) and northern Alaska (Bowling *et al*., 2004). Difficulties simulating UB snow accumulation and sublimation for the 2000/2001 simulation period are attributed to the high observed wind speeds and the assumption that this could be evenly applied uniformly to irregular high alpine terrain. The UB wind speed itself is considered realistic and during 2000/2001 was on average 1.1 m s^{-1} faster than during 1998/1999. UB wind speed measurements were less right-skewed during 2000/2001 than during 1998/1999 (skewness of 0.9 vs. 1.4). The higher mean wind speed and greater proportion of higher wind speed measurements during 2000/2001 cause the blowing snow model to almost completely ablate the UB snowpack, as the low UB roughness element density and height were unable to retain a snowpack under such wind regimes. It is possible that breaking the UB HRU into an exposed and a sheltered HRU would reduce the very high erosion and sublimation rates modelled over this season and permit greater snow retention in the UB during high wind speed winters. However, it should be noted that nearly complete ablation of snow by wind was observed over much of the UB in 2001.

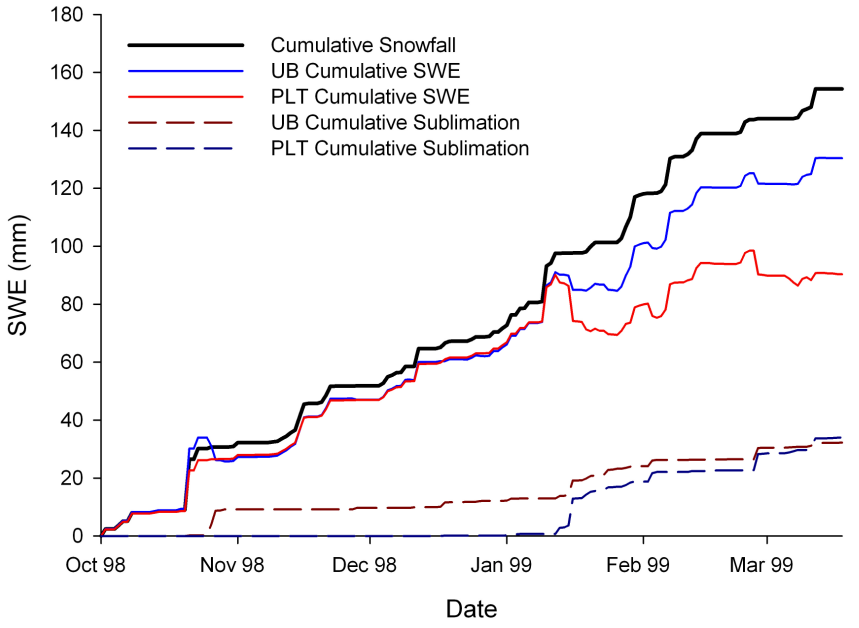

(a)

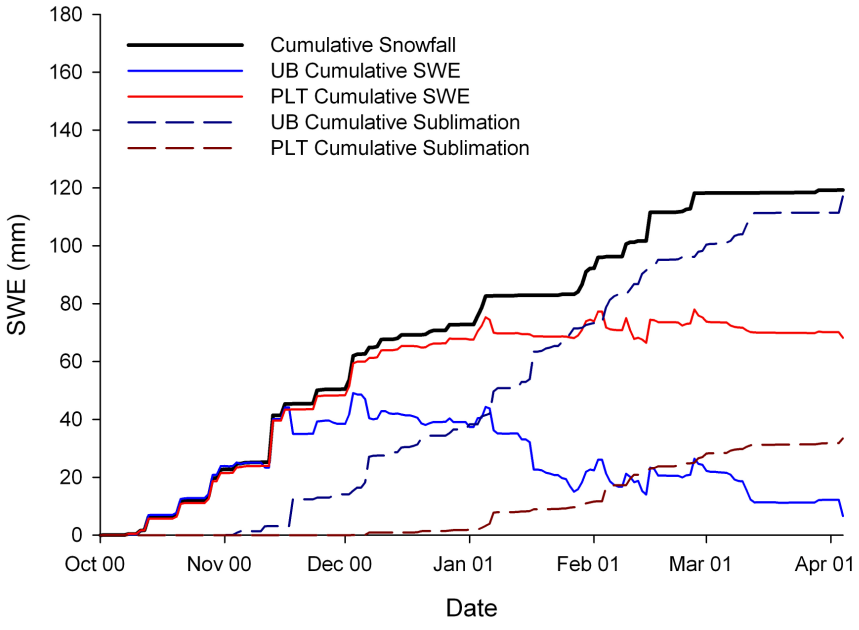

(b)

Figure 5.21 Granger Basin average cumulative snowfall, simulated snow accumulation and cumulative sublimation for UB and PLT using S_R Scheme 2 for (a) 1998/1999, (b) 2000/2001 and (c) 2003/2004

Figure 5.21 continued

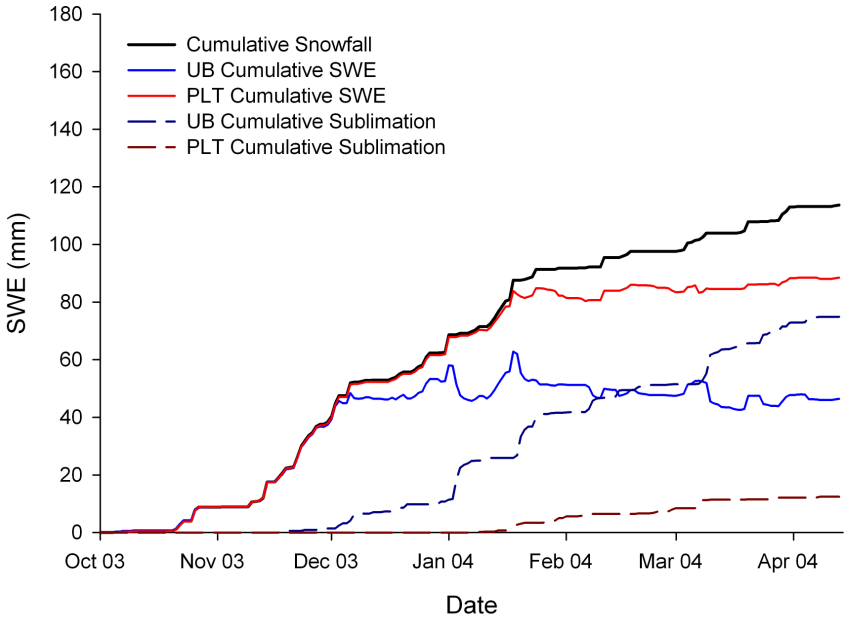

(c)

MESH and MESH-PBSM were used to simulate snow accumulation, redistribution and ablation over GB HRUs using S_R Scheme 2. Table 5.14 shows MESH and MESH-PBSM model evaluation statistics for the GB simulations.

Table 5.14 Model evaluation statistics for Granger Basin simulations using MESH and MESH-PBSM

Year	MESH			MESH-PBSM		
	***NRMSE* (*RMSE* [kg m^{-2}])**	***MB***	***R^2***	***NRMSE* (*RMSE* [kg m^{-2}])**	***MB***	***R^2***
1998/1999	21.9 (*18.4*)	0.24	0.70	20.6 (*17.3*)	0.27	0.68
2000/2001	23.1 (*23.3*)	-0.23	0.86	19.7 (*19.9*)	-0.18	0.86
2003/2004	16.6 (*18.4*)	-0.84	0.94	13.6 (*15.1*)	-0.82	0.92

Table 5.14 shows that MESH-PBSM provided slightly better simulated snowcover as compared to MESH. A qualitative visual examination of the simulated snowcover compared to observed snowcover indicates that MESH-PBSM provides a more marked improvement over MESH than the evaluation statistics in Table 5.14 suggest. Figures 5.22 and 5.23 show MESH and MESH-PBSM simulated snowcover, respectively, for (a) 1998/1999, (b) 2000/2001 and (c) 2003/2004. The cumulative snowfall shown in these figures is the average snowfall of all GB HRUs. MESH results (Figure 5.22) show that UB has the greatest snow accumulation throughout most of the three simulation periods. Though manual snow measurements are not available for UB, field observations show that UB is predominantly windswept. Thus the model evaluation statistics in Table 5.14 do not reflect this MESH shortcoming. Similarly, MESH evaluation statistics do not capture PLT snowpack for 1998/1999 and 2000/2001. PLT manual snow surveys were only performed during 2004. MESH-PBSM adequately simulated scouring of the UB and PLT, and accumulation in the NF and VB. Like the CRHM simulations, blowing snow sublimation was likely overestimated over the UB during 2000/2001.

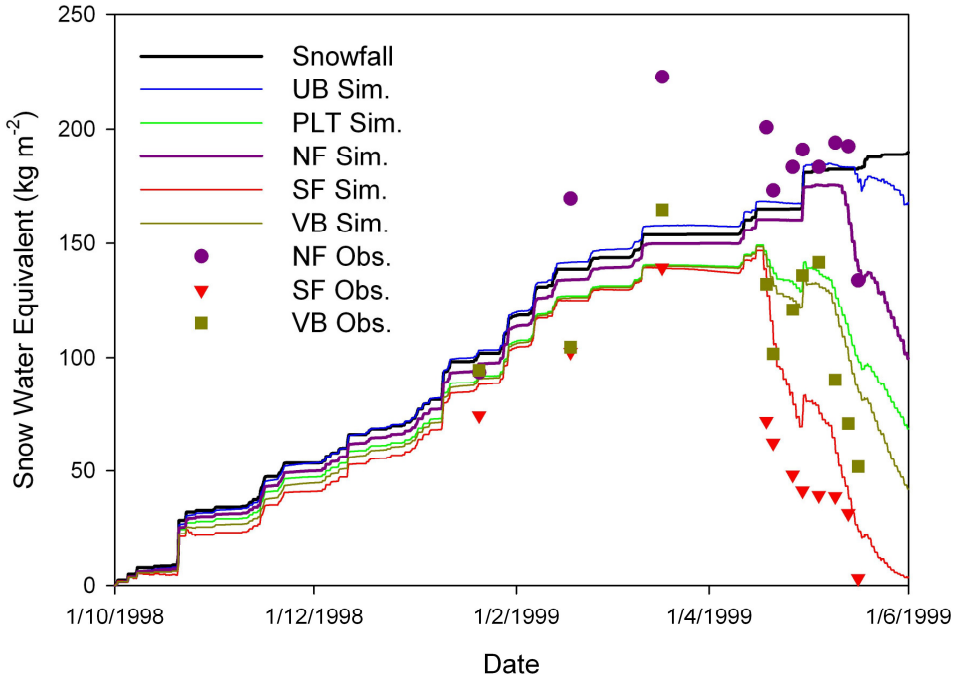

(a)

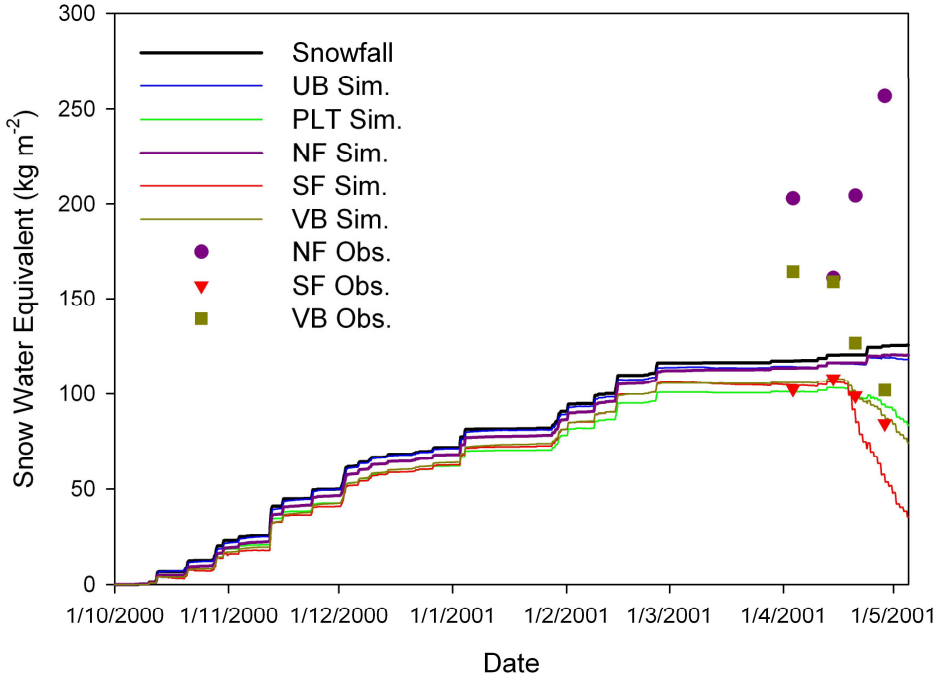

(b)

Figure 5.22 Granger Basin observed and simulated snow accumulation using MESH for (a) 1998/1999, (b) 2000/2001 and (c) 2003/2004.

Figure 5.22 continued

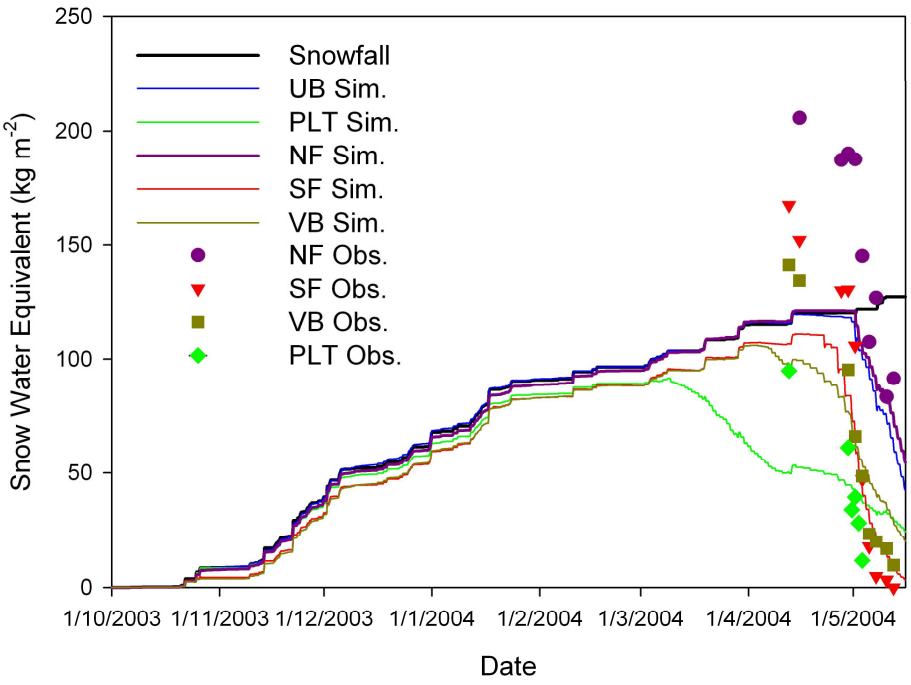

(c)

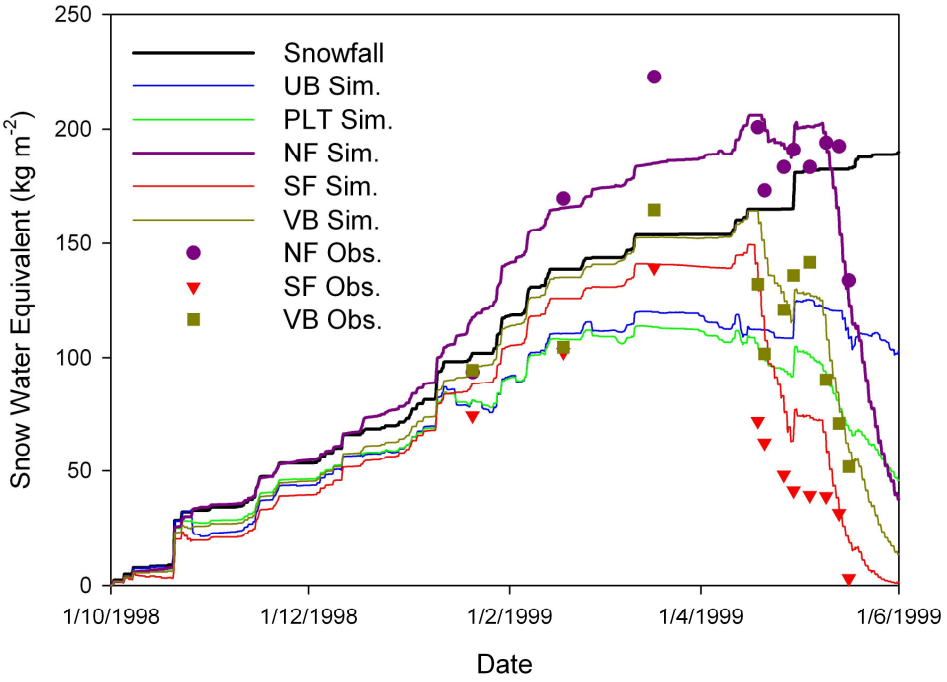

(a)

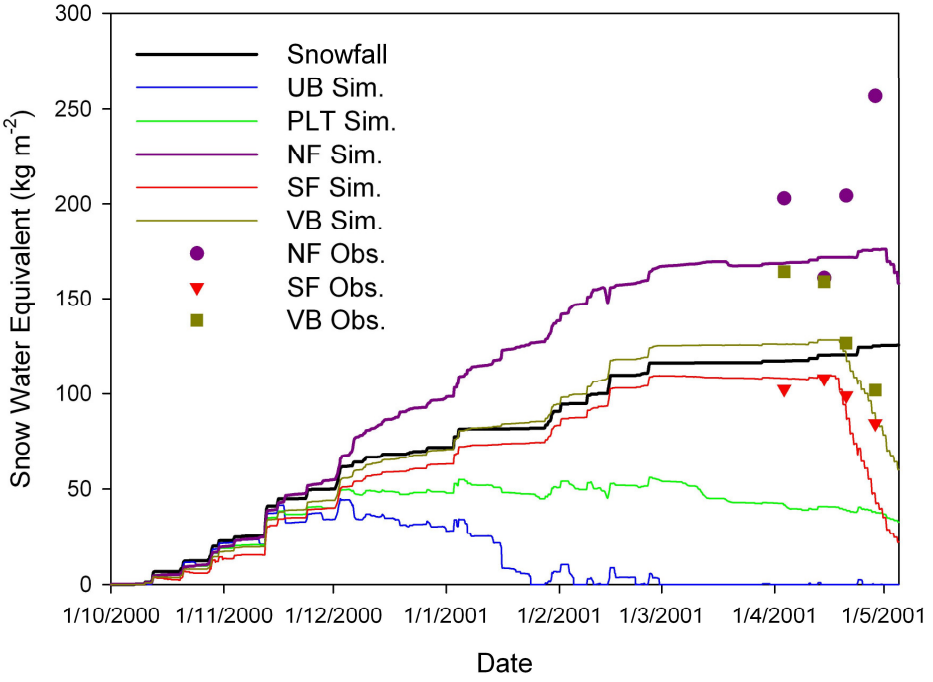

(b)

Figure 5.23 Granger Basin observed and simulated snow accumulation using MESH-PBSM for (a) 1998/1999, (b) 2000/2001 and (c) 2003/2004.

Figure 5.23 continued

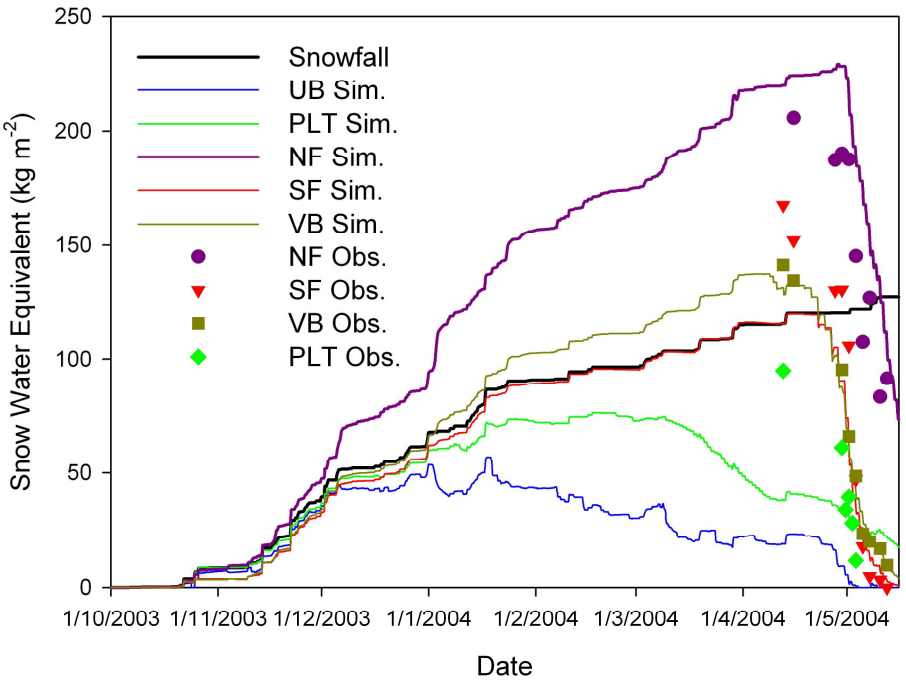

(c)

Like the CRHM model results, the relative amount of simulated blowing snow sublimation varied over each simulation period. MESH-PBSM simulated cumulative blowing snow sublimation as a percentage of cumulative snowfall over UB was 28, 85 and 81% for 1999, 2001 and 2004, respectively, compared to 20, 90 and 60%, using CRHM. Simulated UB cumulative sublimation for 2001 and 2004 was higher than is normally reported in the literature for more level environments (Pomeroy *et al*., 1993, 1997; Pomeroy and Li, 2000; Liston and Sturm, 2002; Bowling *et al*., 2004). MESH-PBSM simulated cumulative blowing snow sublimation as a percentage of cumulative snowfall over PLT was 7, 26 and 8% for 1999, 2001 and 2004, respectively, compared to 21, 23 and 9%, using CRHM. These blowing snow sublimation quantities correspond to 12, 36 and 33% of cumulative snowfall for all of GB using MESH-

PBSM for 1999, 2001 and 2004, respectively, which corresponds well with estimates in the low-Arctic tundra (Pomeroy *et al*., 1997; Essery *et al*., 1999) and northern Alaska (Bowling *et al*., 2004). The GB blowing snow sublimation as a percent of snowfall as simulated using MESH-PBSM is quite similar to that estimated using CRHM (10, 37 and 24% for 1999, 2001 and 2004, respectively). Like the CRHM simulations, MESH-PBSM difficulties simulating UB snow accumulation and sublimation for the 2000/2001 simulation period are attributed to the high observed wind speeds and the assumption that this could be evenly applied uniformly to irregular high alpine terrain.

5.6 Limitations and Directions for Future Research

This section includes discussions of the limitations of applying PBSM in mountain environments, and priorities for future research on blowing snow with a particular focus on modelling windflow and snow transport. Future research on windflow in mountain environments should focus on developing flow over short fetches, flow separation and spatially distributed modelling approaches. Future research on blowing snow in mountain environments should focus on the effect of developing flow on saltation dynamics and the upper boundary for suspension, as well the effects of flow separation and high turbulence on snow transport and sublimation rates. Other snow transport and redistribution processes deserve research attention, namely the modelling preferential deposition of snowfall and avalanche redistribution. A discussion of the application of the modelling approach employed in this study to larger domains is made.

5.6.1 Boundary Layer Development Over Short Fetches

PBSM calculations are made assuming conditions of fully developed flow. For this reason it is recommended that PBSM be applied to areas with a minimum fetch distance of 300 m. This

condition is not satisfied in most alpine areas. For developing flow, the vertical wind speed profile is variable over time. Pomeroy (1988) showed that the mass flux of saltating snow is strongly related to the friction velocity: the maximum height of saltating snow particle trajectories is proportional to the square of friction velocity, the mean horizontal velocity of saltating particles is proportional to the friction velocity, and the efficiency of saltation is inversely proportional to the friction velocity. PBSM uses coefficients derived from fully developed flow conditions to account for these relationships. Under conditions of not fully developed flow, PBSM estimates of the friction velocity, and thus the saltation mass flux may not be accurate. Given that suspension occurs as a result of turbulent diffusion from the saltation layer, developing flow also affects the suspension layer. For suspension calculations, PBSM calculates turbulent diffusion upwards from a variable reference height near the mean maximum trajectory height of saltating particles and a constant reference drift density at this height. This approach can be violated during developing flow conditions because the trajectory height of saltating particles is proportional to the square of friction velocity which may not be accurately estimated during developing flow. Furthermore, the constant reference drift density used in PBSM is assumed to be appropriate for fully developed flow. The upper boundary for suspension is often limited by the vertical gradient of drift density, which PBSM assumes to obey steady state conditions. This can be violated during developing flow. The upper boundary for suspension increases with fetch distance (Pomeroy, 1988), thus a lower upper boundary can be expected for developing flow conditions. However, turbulence can be greater over mountain landscapes than over flat landscapes. Greater fluctuating vertical components of the wind speed in mountain environments make compensate for the lack of fully developed flow in PBSM-estimates of the upper boundary for suspension. In general it is difficult to elucidate the effects

that the fully developed flow assumptions in PBSM calculations have on applying this model in alpine environments where flow is not fully developed.

5.6.2 Turbulence in Mountain Environments

As mentioned in the previous section, windflow over mountain landscapes is more turbulent than that over flat landscapes. The greater fluctuating vertical components of wind speed in mountains can cause higher upper boundaries for suspension over short fetches compared to the upper boundaries over similar short fetches in flat landscapes. In addition, greater turbulence can cause higher blowing snow sublimation rates since it is controlled by fluctuating components of the particle velocity and ventilation velocity (Lee, 1975).

5.6.3 Flow separation

Flow separation is the separation of streamlines from the surface at high Reynolds numbers. Flow separation of wind is common in areas of sharp topography, such as mountains. Streamlines can be separated as flow passes over a sharp ridge, with a portion of the flow remaining parallel to the surface and an upper portion diverging from the surface. Flow separation can occur during blowing snow events. This complicates blowing snow modelling over alpine terrain. Greater sublimation quantities of suspended snow particles in the separated flow field could be expected because the particles are in transit for a longer duration and are subject to higher wind speeds. In addition, suspended snow in the separated flow field could bypass adjacent terrain (e.g. an HRU) and be deposited further downwind, precluding the use of the aerodynamic sequence approach (i.e. that used for FR). There are no published guidelines for the conditions under which flow separation occurs (e.g. wind speed and terrain characteristics). Intensive observations in mountains could provide empirical relationships that relate flow

separation to surface wind speed and terrain characteristics such as slope and curvature. Computational fluid dynamic models compute flow separation; however, they are computationally expensive to run in coupled mode with a snow transport model over a large domain. A possible solution to this would be to run a computational fluid dynamic model for a collection of reference conditions (i.e. wind speed and direction) and generate a library of flow separation conditions. Different snow redistribution parameterizations (e.g. S_R values) can be developed for flow separation and non-flow separation conditions. A snow transport model can be run offline from the computational fluid dynamic model using reference wind data, and the library of flow separation conditions can trigger the different snow redistribution parameterizations. Flow separation was not observed at the either the Fisera Ridge or Granger Basin sites and therefore is not a concern in this study.

5.6.4 Windflow Modelling in Mountain Enviroments

The estimation of spatially distributed wind fields in mountainous terrain remains a research challenge. The results from the RMM model presented in this study show that it is difficult to accurately model windflow in alpine environments using terrain-based empirical windflow models. In light of the sparse distribution of alpine meteorological observations and that these models are computationally efficient; these models could be applied carefully. Other empirical terrain-based models should be evaluated, such as that presented by Winstral et al. (2008).

Another approach to obtain spatially distributed wind fields in mountainous terrains could be to run a computational fluid dynamic model for a collection of reference conditions (i.e. wind speed and direction) and generate a library of spatially distributed wind fields. Bernhardt et al. (2009) used this approach for fully-distributed (i.e. gridded) snow transport modelling. The

computational fluid dynamic model wind fields could be scaled to the HRU-level, and could be used to delineate HRUs.

5.6.5 Other Phenomena

Two snow transport processes were not considered in this study: preferential deposition and avalanches.

Recently, preferential deposition of snowfall has received research attention as a snow transport process (Lehning et al., 2008; Dadic et al., 2010; Mott and Lehning, 2010; Mott et al., 2010). Preferential deposition is the non-uniform deposition of snowfall over alpine topography as a result of near-ground spatially heterogeneous windflow. Preferential deposition results in increased snowfall on leeward slopes due to reduced deposition velocities on windward slopes as a result of high wind velocities and updraft (Lehning et al., 2008). Model results suggest that in-slope drifts, like cornices and dunes, were mainly formed due to saltation, whereas larger-scale (i.e. ridge scale) leeslope drifts were due to preferential deposition of snowfall (Mott and Lehning, 2010; Mott et al., 2010). Results presented do not show great correlation between measured and modelled changes in snow depth, suggesting that the processes influencing, and the importance of, preferential deposition are not adequately understood. A study of its importance at the sites considered in this study is warranted.

Avalanches redistribute snow from upper elevations in alpine areas to lower elevations, and can significantly influence the spatial distribution of snow mass. Relative simple models of snow redistribution by avalanches should be further developed and implemented in land surface hydrology models (e.g. Bernhardt and Schulz, 2010).

5.6.6 Operational/Large-scale Application of Landscape-based Approach

The application of the HRU-based approach to snow redistribution modelling for operational large-scale hydrological and couple atmospheric-hydrological simulations would require careful selection of HRUs. Snow distribution and many hydrological fluxes are controlled by combinations of radiation input, wind, vegetation cover and soil type. Therefore, HRU selection should be based on a combination of the aforementioned features. A LiDAR map of snow depth can be used to generalize HRUs based on terrain characteristics. A promising option would be to run a high-resolution hydrological model over a large domain over a limited time period, and to to delineate HRUs based on common hydrological responses of the high-resolution grid cells. A similar approach could be taken for wind speed modelling as discussed in the previous section.

CHAPTER 6
CONCLUSIONS

This thesis focused on HRU-based modelling of snow redistribution by wind over mountainous terrain. Hydrological and atmospheric models require some description of blowing snow redistribution and sublimation that is suitable for complex terrain. The large scale application of these models in mountain and polar environments precludes a finely distributed approach such as employed for small basins. Some form of landscape aggregation is necessary for mountain topography in northern Canada.

A physically based blowing snow model, PBSM, which was initially developed for application over the Canadian Prairies, was used to simulate snow transport and sublimation over two sites representative of mountainous regions in Canada (Fisera Ridge in the Marmot Creek Research Basin, Alberta and Granger Basin in the Wolf Creek Research Basin, Yukon Territory). The only modification made to PBSM was to account for the difference in partitioning of the wind shear stress due to the geometry and density of tundra shrubs compared to that due to crop stalks. Two hydrological models were evaluated in this study, CRHM and MESH. PBSM algorithms were incorporated into CLASS and MESH to create CLASS-PBSM and MESH-PBSM, respectively. The calculated blowing snow sublimation loss is removed from the mass balance and thermodynamic feedback is not included as it is in some other blowing snow models. The addition of PBSM to CLASS required four additional parameters per GRU, and the addition of PBSM to MESH required five additional parameters per GRU. A novel component of MESH-PBSM is the model structure of the inter-GRU snow redistribution algorithm, which can be generalized to route other hydrological fluxes between GRUs.

CRHM, CLASS and CLASS-PBSM were evaluated in point mode at a windswept location on Fisera Ridge over two winter periods. PBSM was coupled with the snowcover energy and mass-

balance model (SNOBAL) within CRHM. CRHM was able to effectively simulate snow depth at this location. CLASS-PBSM provided considerably better results than CLASS, though the presence of a shallow snowpack at this windswept location hides that CLASS overestimated snowmelt at Fisera Ridge.

PBSM (in CRHM) was used to simulate end-of-winter snow accumulation in HRUs over Granger Basin during three winter periods. Snow transport fluxes were distributed across Granger Basin demarcated by multiple HRUs using the inter-HRU snow redistribution allocation factors, S_R. Three S_R schemes of varying complexity were evaluated. Even the most rudimentary snow redistribution scheme improved simulated snow accumulation when compared to a model without any blowing snow parameterization. Model results showed that end-of-winter snow accumulation can be accurately simulated using a physically based blowing snow model when S_R values are established that take into account wind direction and speed, HRU slope and aspect, along with the spatial arrangement of the HRUs in the catchment. MESH-PBSM was used to simulate Granger Basin snow accumulation, redistribution and ablation. Results showed marked improvement when compared to MESH without PBSM algorithms. Similar blowing snow sublimation quantities were estimated using CRHM and MESH-PBSM.

PBSM was combined with SNOBAL, and forest energy and water balance modules within CRHM to simulate snow redistribution and the resulting accumulation regimes over HRUs that represent Fisera Ridge over two winter periods. HRUs were selected by examining manual snow depth measurements. The HRUs followed an aerodynamic sequence in that the model always transported snow from upwind to downwind HRUs. Simulations were performed using two different sets of wind speed forcing data: observed wind speed data, and modelled wind speeds from a widely applied empirical windflow model (RMM). The RMM wind speeds were upscaled

by spatial averaging to the HRU-level. The RMM model performed poorly in estimating wind speed at Fisera Ridge. Best snowcover results were obtained when using the observed wind speeds. The empirical RMM model underestimated the end-of-winter snow accumulation that governs snowmelt runoff. The wind speed overestimation gave rise to a blowing snow transport and sublimation overestimation, which resulted in an underestimation of end-of-winter snow accumulation on windswept HRUs. Greater snowmelt and snowpack sublimation quantities were estimated using the RMM wind speeds. This would cause further difficulties in accurately simulating snowcover ablation and runoff during snowmelt-dominated periods. MESH-PBSM was also used to simulate snow accumulation and redistribution over these same HRUs. Snow accumulation was well simulated during both periods up until snowmelt was grossly overestimated during spring. It remains indeterminate as to why snowcover simulations with MESH are difficult at this location. The most substantial difference between the physical parameterizations in the CLASS snowcover model and SNOBAL is that CLASS represents the snowpack as a single layer with the variation of temperature with depth calculated using a quadratic equation, whereas SNOBAL represents the snowpack as two layers. In addition, explicit time stepping schemes that are employed in many snow models, including that in CLASS, have been shown to be problematic in accurately simulating surface seasonal snowpack temperatures. Further diagnostics should be performed on the FR data set to determine the reason(s) for CLASS overestimating snowmelt. CRHM and MESH model results at both Fisera Ridge and Granger Basin showed that it is critical that snow transport, sublimation and redistribution calculations be included in mesoscale models in these environments. Seasonal blowing sublimation losses were shown to be considerable (10-37% of snowfall).

A limitation of this study was the rather subjective definition and discretization of HRUs. Future work should involve improving snowmelt simulations at Fisera Ridge using CLASS and MESH, better discretizing HRUs based on terrain attributes, developing a computationally-efficient windflow model for mountainous terrain, and evaluating the regionalization of model parameters for blowing snow modelling in mountains environments. Future research on windflow in mountain environments should focus on developing flow over short fetches, flow separation and spatially distributed modelling approaches. Future research on blowing snow in mountain environments should focus on the effect of developing flow on saltation dynamics and the upper boundary for suspension, as well the effects of flow separation and high turbulence on snow transport and sublimation rates. Other snow transport and redistribution processes deserve research attention, namely the modelling preferential deposition of snowfall and avalanche redistribution.

LIST OF REFERENCES

Abbott MB, Bathurst JC, Cunge JA, O`Connell PE, Rasmussen J. 1986. An introduction to the European Hydrologic System - Système Hydrologique Européen, ``SHE``, 1, History and philosophy of a physically-based, distributed modelling system. *Journal of Hydrology* **87**: 45-49.

Anderson RS, Haff PK. 1991. Wind modification and bed response during saltation of sand in air. *Acta Mechanica* (Suppl.) **1**, 21-51.

Anderton SP, White SM, Alvera B. 2002. Evaluation of the spatial variability of snow water equivalent for a high mountain catchment. *Hydrological Processes* **18**: 435-453.

Bernhardt M, Schulz K. 2010. SnowSlide: a simple routine for calculating gravitational snow transport. *Geophysical Research Letters* **37**: L11502.

Hopkinson C, Fox A. 8 January 2008. IP3 LiDAR collaborative research data report. Applied Geomatics Research Group.

Auld H. 1995.Dependence of ground snow loads on elevation in western Canada. *Proceedings of the 63rd Western Snow Conference* **63**: 143-146.

Avissar R. 1992. Conceptual aspects of a statistical-dynamic approach to represent the landscape subgrid-scale heterogeneities in atmospheric models. *Journal of Geophysical Research – Atmospheres* **97**: 2729-2742.

Bagnold RA. 1941. The physics of blown sand and desert dunes. *Methuen*. London. 265 p.

Bagnold RA. 1966. An approach to the sediment transport problem from general physics. *U.S. Geological Survey Professional Paper 411, 37 p.*

Bernhardt M, Zängl G, Liston GE, Strasser U, Mauser W. 2009. Using wind fields from a high-resolution atmospheric model for simulating snow dynamics in mountainous terrain. *Hydrological Processes* **23**: 1064-1075.

Beven KJ, Kirkby MJ. 1979. A physically-based, variable contributing area model of basin hydrology. *Hydrological Sciences Bulletin* **24**: 43-69.

Beven KJ. 1989. Changing ideas in hydrology – the case of physically-based models. *Journal of Hydrology* **105**: 157-172.

Bewley D. 2006. Shrub-tundra effects on snowmelt energetic and the atmospheric interaction with snow. Ph.D. Thesis, Institute of Geography and Earth Sciences, University of Wales, Aberystwyth, UK. 196 p.

Bintanja R. 1998. The contribution of snowdrift sublimation to the surface mass balance of Antarctica. *Annals of Glaciology* **27**: 251-259.

Bintanja R. 2000. Snowdrift suspension and atmospheric turbulence. Part I: theoretical background and model description. *Boundary-Layer Meteorology* **95**: 343-368.

Bintanja R 2001. Modelling snowdrift sublimation and its effects on the moisture budget of the atmospheric boundary layer. *Tellus Serie A, Dynamic Meteorology and Oceanography* **53**: 215-232.

Bintanja R, Reijmer CH. 2001. A simple parameterization for snowdrift sublimation over Antarctic snow surfaces. *Journal of Geophysical Research – Atmospheres* **106**: 31739-31748.

Bowling LC, Pomeroy JW, Lettenmaier, DP. 2004. Parameterization of blowing snow sublimation in a macroscale hydrology model. *Journal of Hydrometeorology* **5**: 745-762.

Budd WF. 1966. The drifting of non-uniform snow particles. *Studies in Antarctic Meteorology, American Geophysical Union Antarctic Research Series* **9**: 59-70.

Budd WF, Dingle WRJ, Radok U. 1966. The Byrd snow drift project: outline and basic results. *Studies in Antarctic Meteorology, American Geophysical Union Antarctic Research Series*, **9**: 71-134.

Carey SK, Quinton WL. 2004. Evaluating snowmelt runoff generation in a discontinuous permafrost catchment using stable isotope, hydrochemical and hydrometric data. *Nordic Hydrology* **35**: 309-324.

Crawford NH, Linsley RS. 1966. Digital simulation in hydrology: The Stanford Watershed model IV. Technical Report No. 39. Department of Civil Engineering, Stanford University, Palto Alto, CA.

Dadic R, Mott R, Lehning M, Burlando P. 2010. Parameterization of wind-induced preferential deposition of snow. *Hydrological Processes* **24**: 1994-2006.

Davison B, Pohl S, Dornes P, Marsh P, Pietroniro A, MacKay M. 2006.Characterizing snowmelt variability in a land-surface-hydrological model. *Atmosphere-Ocean* **44**: 271-287.

DeBeer CM, Pomeroy JW. 2009. Modelling snow melt and snowcover depletion in a small alpine cirque, Canadian Rocky Mountains. *Hydrological Processes* **23**: 2584-2599.

Déry SJ, Taylor PA, Xiao J. 1998. The thermodynamic effects of sublimating, blowing snow in the atmospheric boundary layer. *Boundary-Layer Meteorology* **89**: 251-283.

Déry SJ, Yau MK. 1999. A bulk blowing snow model. *Boundary-Layer Meteorology* **93**: 237-251.

Déry SJ, Yau MK. 2001. Simulation of blowing snow in the Canadian Arctic using a double-moment model. *Boundary-Layer Meteorology* **99**: 297-316.

Déry SJ, Crow WT, Stieglitz M, Wood EF. 2004. Modeling snow-cover heterogeneity over complex arctic terrain for regional and global climate models. *Journal of Hydrometeorology* **5**: 33-48.

Dingle WRJ, Radok U. 1961. Antarctic snow drift and mass transport. *International Association of Scientific Hydrology Publication* **55**: 77-87.

Donald JR, Soulis ED, Kouwen N, Pietroniro A. 1995. Snowcover depletion curves and satellite snowcover estimates for snowmelt runoff modelling. *Water Resources Research* **31**: 995-1009.

Doorschot J, Raderschall N, Lehning M. 2001. Measurements and one-dimensional model calculations of snow transport over a mountain ridge. *Annals of Glaciology* **32**: 153-158.

Doorschot J, Lehning M. 2002. Equilibrium saltation: mass fluxes, aerodynamic entrainment and dependence on grain properties. *Boundary Layer Meteorology* **104**: 111-130.

Doorschot JJ, Lehning M, Vrouwe A. 2004. Field measurements of snow-drift threshold and mass fluxes, and related model simulations. *Boundary Layer Meteorology* **113**: 347-368.

Dornes PF, Pomeroy JW, Pietroniro A, Carey SK, Quinton WL. 2008a. Influence of landscape aggregation in modelling snow-cover ablation and snowmelt runoff in a subarctic mountainous environment. *Hydrological Sciences Journal* **53**: 725-740.

Dornes PF, Pomeroy JW, Pietroniro A, Verseghy, DL. 2008b. Effects of spatial aggregation of initial conditions and forcing data on modeling snowmelt using a land surface scheme. *Journal of Hydrometeorology* **9**: 789-803.

Dornes PF, Tolson BA, Davison B, Pietroniro A, Pomeroy JW, Marsh P. 2008. Regionalisation of land surface hydrological model parameters in subarctic and arctic environments. *Physics and Chemistry of the Earth* **33**: 1081-1089.

Dornes PF. 2009. An approach for modelling snowcover ablation and snowmelt runoff in cold region environments. Ph.D. Thesis, Department of Geography and Planning (Centre for Hydrology), University of Saskatchewan, Saskatoon, SK. 183 p.

Dyunin AK. 1954. Solid flux of snow-bearing air flow. *Trudy Transportno-Energicheskogo Instituta* **4**: 71-88. (trans. Belkov G. 1963. National Research Council of Canada Technical Translation 1102. 25 p.)

Dyunin AK. 1959. Fundamentals of the theory of snowdrifting. *Isvestia Sibirski Otdeleniya Akademii Nauk SSSR* **12**: 11-24. (trans. Belkov G. 1961. National Research Council of Canada Technical Translation 952. 26 p.)

Dyunin AK. 1974. Mekhanika silnykh meteley (Mechanics of strong snow storms). *Novosibirsky Institut Ingenerov Zheleznodorozhnnogo Transport, Trudy* **159**: 3-110.

Elder K, Dozier J, Michaelsen J. 1991. Snow accumulation and distribution in an alpine watershed. *Water Resources Research* **27**: 1541-1552.

Ellis CR, Pomeroy JW, Brown T, MacDonald J. 2010. Simulation of snow accumulation and melt in needleleaf forest environments. *Hydrology and Earth System Sciences* **14**: 925-940.

Essery R, Pomeroy J. 2004. Vegetation and topographic control of wind-blown snow distributions in distributed and aggregated simulations for an Arctic tundra basin. *Journal of Hydrometeorology* **5**: 735-744.

Essery R, Li L, Pomeroy J. 1999. A distributed model of blowing snow over complex terrain. *Hydrological Processes* **13**: 2423-2438.

Etchevers P, Martin E, Brown R, Fierz C, Lejeune Y, Bazile E, Boone A, Dai Y-J, Essery R, Fernandez A, Gusev Y, Jordan R, Koren V, Kowalcyk E, Nasonova NO, Pyles RD, Schlosser A, Shmakin AB, Smirnova TG, Strasser U, Verseghy D, Yamazaki T, Yang, Yang Z-L. 2004. Validation of the energy budget of an alpine snowpack simulated by several snow models (SnowMIP project). *Annals of Glaciology* **38**: 150-158.

Fang X, Pomeroy JW. 2009. Modelling blowing redistribution to prairie wetlands. *Hydrological Processes* **23**: 2557-2569.

Frazer GW, Canham CD, Lertzman KP. 1999. Gap Light Analyzer GLA, Version 2.0: Imaging software to extract canopy structure and gap light transmission indices from true-color fisheye photographs, Users manual and program documentation. Institute of Ecosystem Studies, Simon Fraser University, Burnaby, BC, and Milbrook, NY. 40 p.

Gauer P. 2001. Numerical model of blowing and drifting snow in alpine terrain. *Journal of Glaciology* **47**: 97-110.

Gill MK, Kaheil YH, Khalil A, McKee M, Bastidas L. 2006. Multiobjective particle swarm optimization for parameter estimation in hydrology. *Water Resources Research* **42**: W07417.

Goodison BE, Metcalfe JR, Louie PYT. 1998. Summary of country analyses and results, Annex 5.B Canada. In *The WMO Solid Precipitation Measurements Intercomparison Final Report*, *Instrum. Obs. Methods rep. 67, WMO/TD 872*. 105-112.

Gordon M, Savelyev S, Taylor PA. 2009. Measurements of blowing snow, part II: mass number and density profiles and saltation height at Franklin Bay, NWT, Canada. *Cold Regions Science and Technology* **55**: 75-85.

Gordon M, Simon K, Taylor PA. 2006. On snow depth predictions with the Canadian Land Surface Scheme including a parameterization of blowing snow sublimation. *Atmosphere-Ocean* **44**: 239-255.

Granger RJ, Gray DM, Dyck GE. 1984. Snowmelt infiltration to frozen prairie soils. *Canadian Journal of Earth Sciences* **21**: 669-677.

Gray DM, Landine PG. 1987. Albedo model for shallow prairie snowcovers. *Canadian Journal of Earth Sciences* **24**: 1760-1768.

Gray DM, Landine PG. 1988. An energy-budget snowmelt model for the Canadian Prairies. *Canadian Journal of Earth Sciences* **25**: 1292-1303.

Gray DM and others. 1979. Snow accumulation and distribution. In *SC Colbeck and M Ray (eds.), Proceedings, Modeling Snow Cover Runoff*. U.S. Army Cold Region Research Laboratory, Hanover, NH. 3-33.

Grayson R, Blöschl G. 2001. Spatial modelling of catchment dynamics. In *R Grayson and G Blöschl (eds.), Spatial Patterns in Catchment Hydrology – Observations and Modelling*. Cambridge University Press: Cambridge, UK. 51-81.

Greene EM, Liston GE, Pielke RA. 1999. Simulation of above treeline snowdrift transport using a numerical snow-transport model. *Cold Regions Science and Technology* **30**: 135-144.

Gupta HV, Sorooshian S, Yapo PO. 1998. Toward improved calibration of hydrologic models: optimization algorithms, catchment conditions, and model structure. *Water Resources Research* **32**: 751-763.

Hasholt B, Liston GE, Knudsen NT. 2003. Snow-distribution modelling in the Ammassalik Region, South East Greenland. *Nordic Hydrology* **34**: 1-16.

Helgason WD, Pomeroy JW. 2005. Uncertainties in estimating turbulent fluxes to melting snow in a mountain clearing. *Proceedings of the 62nd Eastern Snow Conference*: 129-138.

Helgason, WD. 2010. Energy fluxes at the air-snow interface. Ph.D. Thesis, Department of Geography and Planning (Centre for Hydrology), University of Saskatchewan, Saskatoon, SK. 186 p.

Hiemstra CA, Liston GE, Reiners WA. 2002. Snow redistribution by wind an interactions with vegetation at upper treeline in the Medicine Bow Mountains, Wyoming, U.S.A. *Arctic, Antarctic, and Alpine Research* **34**: 26-273.

Jackson PS, Hunt JCR. 1975. Turbulent wind flow over a low hill. *Quarterly Journal of the Royal Meteorological Society* **101**: 929-955.

Jaedicke C, Gauer P. 2005. The influence of drifting snow on the location of glaciers on western Spitsbergen, Svalbard. *Annals of Glaciology* **42**: 237-242.

Jones HG, Pomeroy JW, Walker DA, Hoham RW. 2001. Snow ecology: an interdisciplinary examination of snow-covered ecosystems. Cambridge University Press: Cambridge, UK. 394 p.

Kasten F, Young AT. 1989. Revised optical air-mass tables and approximation formula. *Applied Optics* **28**: 4735-4738.

Kite GW. 1975. Performance of two deterministic hydrological models. *ASH-AISH Publication* **115**: 136-142.

Kouwen N. 1988. WATFLOOD: a microcomputer-based flow forecasting system based on real-time weather data. *Canadian Water Resources Association Journal* **13**: 62-77.

Kouwen N, Mousavi SF. 2002. WATFLOOD/SPL9 hydrological model and flood forecasting system. In *VP Singh and DK Freverts (Eds.), Mathematical Models of Large Watershed Hydrology,* Water Resources Publications: Colorado, USA. 649-686.

Kuchment LS, Gelfan AN, Demidov VN. 2000. A distributed model of runoff generation in the permafrost region. *Journal of Hydrology* **240**: 1-22.

Lapen DR, Martz LW. 1993. The measurement of two simple topographic indices of wind sheltering-exposure from raster digital elevation models. *Computers & Geosciences* **19**: 769-779.

Lapen DR, Martz LW. 1996. An investigation of the spatial association between snow depth and topography and in a Prairie agricultural landscape using digital terrain analysis. *Journal of Hydrology* **184**: 277-298.

Leavesley GH, Stannard LG. 1995. The precipitation-runoff modelling system – PRMS. In *VP Singh (Ed.), Computer Models of Watershed Hydrology*. Water Resources Publications, Highlands Rand, CO. 281-310.

Lee LW. 1975. Sublimation of snow in turbulent atmosphere. Ph.D. Thesis, University of Wyoming, Laramie, WY. 162 p.

Lehning M, Lowe H, Ryser M, Raderschall N. 2008. Inhomogeneous precipitation distribution and snow transport in steep terrain. *Water Resources Research* **44**: W07404.

Lemelin DR, Surry D, Davenport AG. 1988. Simple approximations for wind speed-up over hills. *Journal of Wind Engineering and Industrial Aerodynamics* **28**: 117-127.

Lettau H. 1969. Note on aerodynamic roughness-parameter estimation on the basis of roughness element description. *Journal of Applied Meteorology* **8**: 828-832.

Li L, Pomeroy JW. 1997a. Estimates of threshold wind speeds for snow transport using meteorological data. *Journal of Applied Meteorology* **36**: 205-213.

Li L, Pomeroy JW. 1997b. Probability of occurrence of blowing snow. *Journal of Geophysical Research* **102**: 21955-21964.

Liston GE, Sturm M. 1998. A snow transport model for complex terrain. *Journal of Glaciology* **44**: 498-516.

Liston GE, Sturm M. 2002. Winter precipitation patterns in arctic Alaska determined from a blowing-snow model and snow-depth observation. *Journal of Hydrometeorology* **3**: 646-659.

Liston GE, Elder K. 2006. A meteorological distribution system for high-resolution terrestrial modeling (MicroMet). *Journal of Hydrometeorology* **7**: 217-234.

Loewe F. 1956. Études de Glaciologie en Terre Adélie, 1951-1952. *Actualités Scientifiques et Industrielles, 1247*. Hermann: Paris. 159 p.

Luce CH, Tarboton DG, Cooley KR. 1998. The influence of the spatial distribution of snow on basin-averaged snowmelt. *Hydrological Processes* **12**: 1671-1683.

MacDonald JP, Pomeroy JW. 2007. Gauge undercatch of two common snowfall gauges in a prairie environment. *Proceedings of the 64th Eastern Snow Conference*: 119-124.

MacDonald MK, Pomeroy JW, Pietroniro A. 2009. Parameterizing redistribution and sublimation of blowing snow for hydrological models: tests in a mountainous subarctic catchment. *Hydrological Processes* **23**: 2570-2583.

Manabe S. 1969. Climate and ocean circulation: 1. The atmospheric circulation and the hydrology of the earth`s surface. *Monthly Weather Review* **97**: 739-774.

Marks D, Kimball J, Tingey D, Link T. 1998. The sensitivity of snowmelt process to climate conditions and forest cover during rain-on-snow: a case study of the 1996 Pacific Northwest flood. *Hydrological Processes* **12**: 1569-1587.

Marks D, Domingo J, Susong D, Link T, Garen D. 1999. A spatially distributed energy balance snowmelt model for application in mountain basins. *Hydrological Processes* **13**: 1935-1959.

Mason PJ, Sykes RI. 1979. Flow over an isolated hill of moderate slope. *Quarterly Journal of the Royal Meteorological Society* **105**: 383-395.

Mellor M, Radok U. 1960. Some properties of drifting snow. *Symposium on Antarctic Meteorology*. London: Pergamon Press. 347-354.

McCartney SE, Carey SK, Pomeroy JW. 2006. Intra-basin variability of snowmelt water balanced calculations in a subarctic catchment. *Hydrological Processes* **20**: 1001-1016.

Molotch NP, Colee MT, Bales RC, Dozier J. 2005. Estimating the spatial distribution of snow water equivalent in an alpine basin using binary regression tree models: the impact of digital elevation data and independent variable selection. *Hydrological Processes* **19**: 1459-1479.

Monteith JL. 1965. Evaporation and environment. *Symposia of the Society for Experimental Biology* **19**: 205-234.

Mott R, Lehning M. 2010. Meteorological modeling of very high-resolution wind fields and snow deposition for mountains. *Journal of Hydrometeorology* **11**: 934-949.

Mott R, Schirmer M, Bavay M, Grünewal T, Lehning M. 2010. Understanding snow-transport processes shaping the mountain snow-cover. *The Cryosphere Discussions* **4**: 865-900.

Nash JE, Sutcliffe JV. 1970. River flow forecasting through conceptual model. Part 1 – a discussion of principles. *Journal of Hydrology* **10**: 282-290.

Nemoto M, Nishimura K. 2004. Numerical simulation of snow saltation and suspension in a turbulent boundary layer. *Journal of Geophysical Research – Atmospheres* **109**: D18206.

Neumann N, Marsh P. 1998. Local advection in the snowmelt landscape of Arctic tundra. *Hydrological Processes* **12**: 1547-1560.

Nkemdirim LC. 1996. Canada's chinook belt. *International Journal of Climatology* **16**: 441-462.

Owen PR. 1964. Saltation of uniform grains in air. *Journal of Fluid Mechanics* **20**: 225-242.

Palacios-Vélex OL, Gandoy-Bernasconi W, Curvas-Renaud B. 1998. Geometric analysis of surface runoff and the computation order of unit elements in distributed hydrological modes. *Journal of Hydrology* **211**: 266-274.

Pietroniro A, Fortin V, Kouwen N, Neal C, Turcotte R, Davison B, Verseghy D, Soulis ED, Caldwell R, Evora N, Pellerin P. 2007. Development of the MESH modelling system for hydrological ensemble forecasting of the Laurentian Great Lakes at the regional scale. *Hydrology and Earth System Sciences* **11**: 1279-1294.

Pomeroy JW, Male DH. 1985. A physical model of blowing snow for agricultural land management. *Division of Hydrology Internal Report No. 85-7*. Division of Hydrology, University of Saskatchewan, Saskatoon, SK. 35 p.

Pomeroy JW, Male DH. 1986. Physical modelling of blowing snow for agricultural production. In *H Steppuhn and W Nicholaichuk (eds.), Proceedings, Snow Management for Agriculture Symposium, Great Plains Agricultural Council Publication No. 120*. Water Studies Institute: Saskatoon, SK. 73-108 p.

Pomeroy JW. 1988. Wind transport of snow. Ph.D. Thesis, Division of Hydrology, University of Saskatchewan, Saskatoon, SK. 226 p.

Pomeroy JW. 1989. A process-based model of snow drifting. Annals of Glaciology **13**: 237-240.

Pomeroy JW, Gray DM. 1990. Saltation of snow. *Water Resources Research* **26**: 1583-1594.

Pomeroy JW. 1991. Transport and sublimation of snow in wind-scoured alpine terrain. In *H Bergman, H Lang, W Frey, D Issler, B Salm (eds.), Snow, Hydrology and Forests in Alpine Areas. International Association of Hydrological Sciences Publication No. 205*. IAHS Press : Wallingford, UK. 131-140.

Pomeroy JW, Male DH. 1992. Steady-state suspension of snow. *Journal of Hydrology* **136**: 275-301.

Pomeroy JW, Gray DM, Landine PG. 1991. Modelling the transport and sublimation of blowing snow on the prairies. *Proceedings of the 48th Eastern Snow Conference*: 175-188.

Pomeroy JW, Gray DM, Landine PG. 1993. The Prairie Blowing Snow Model: characteristics, validation and operation. *Journal of Hydrology* **144**: 165-192.

Pomeroy JW, Schmidt RA. 1993. The use of fractal geometry in modelling intercepted accumulation and sublimation. *Proceedings of the 50th Eastern Snow Conference* **50**: 1-10.

Pomeroy JW, Gray DM. 1995. Snowcover Accumulation, Relocation and Management. *National Hydrological Research Institute Science Report No. 7*. Environment Canada, Saskatoon, SK. 144 p.

Pomeroy JW, Dion K. 1996. Winter radiation extinction and reflection in a boreal pine canopy: measurements and modelling. *Hydrological Processes* **10**: 1591-1608.

Pomeroy JW, Marsh P, Gray DM. 1997. Application of a distributed blowing snow model to the Arctic. *Hydrological Processes* **11**: 1451-1464.

Pomeroy JW, Parviainen J, Hedstrom N, Gray DM. 1998. Coupled modelling of forest snow interception and sublimation. *Hydrological Processes* **12**: 2317-2337.

Pomeroy JW, Hedstrom N, Parviainen J. 1999. The snow mass balance of Wolf Creek: effects of snow, sublimation and redistribution. In *JW Pomeroy and R Granger (eds.), Wolf Creek Research Basin: Hydrology, Ecology, Environment*. Environment Canada, Saskatoon, SK. 15-30.

Pomeroy JW, Li L. 2000. Prairie and arctic areal snow cover mass balance using a blowing snow model. *Journal of Geophysical Research-Atmospheres* **105**: 26619-26634.

Pomeroy JW, Toth B, Granger RJ, Hedstrom NR, Essery RLH. 2003. Variation in surface energetic during snowmelt in a subarctic mountain catchment. *Journal of Hydrometeorology* **4**: 702-719.

Pomeroy JW, Bewley DS, Essery RLH, Hedstrom NR, Link T, Granger RJ, Sicart JE, Ellis CR, Janowicz JR. 2006. Shrub tundra snowmelt. *Hydrological Processes* **20**: 923-941.

Pomeroy JW, Gray DM, Brown T, Hedstrom NR, Quinton W, Granger RJ, Carey SK. 2007. The cold regions hydrological model: a platform for basing process representation and model structure on physical evidence. *Hydrological Processes* **21**: 2650-2667.

Pomeroy JW, Marks DM, Link T, Ellis C, Hardy J, Rowlands A, Granger R. 2009. The impact of coniferous forest temperature on incoming longwave radiation to melting snow. *Hydrological Processes* **23**: 2513-2525.

Prairie Provinces Water Board. 2003. The 1969 Agreement on Master Apportionment. Environment Canada. Web. 10 April 2010. < http://www.library.cornell.edu/resrch/citmanage/mla#web_page>.

Prasad R, Tarboton DG, Liston GE, Luce CH, Seyfried MS. 2001. Testing a blowing snow model against distributed snow measurements at Upper Sheep Creek, Idaho, University States of America. *Water Resources Research* **37**: 1341-1350.

Purves RS, Barton JS, Mackaness WA, Sugden DE. 1998. The development of a rule-based spatial model of wind transport and deposition of snow. *Annals of Glaciology* **26:** 197-202.

Quick MC, Pipes A. 1977. UBC watershed model. *Hydrological Sciences Bulletin* **221**: 153-161.

Radok U. 1968. Deposition and erosion of snow by the wind. U.S. Army Cold Regions Research and Engineering Laboratory, Hanover, NH, Research Report 230. 23 p.

Raupach MR, Gillette DA, Leys JF. 1993. The effect of roughness elements on wind erosion threshold. *Journal of Geophysical Research* **98**: 3023-3029.

Refsgaard JC. 2001. Toward a formal approach to calibration and validation of models using spatial data. In *R Grayson and G Blöschl (eds.), Spatial Patterns in Catchment Hydrology – Observations and Modelling*. Cambridge University Press: Cambridge, UK. 329-354.

Rutter N, Essery R, Pomeroy J, and 48 co-authors. 2009. Evaluation of forest snow process models (SnowMIP2). *Journal of Geophysical Research* **114**: D06111.

Ryan BC. 1977. A mathematical model for diagnosis and prediction of surface winds in mountainous terrain. *Journal of Applied Meteorology* **16**: 571-584.

Savenije HHG. 2009. The art of hydrology. *Hydrology and Earth System Sciences* **13**: 157-161.

Schmidt RA. 1972. Sublimation of wind-transported snow – a model. United States Department of Agriculture, Forest Service Research Paper RM-90. Rocky Mountain Forest and Range Research Station, Fort Collins, CO. 24 p.

Schmidt RA. 1986. Transport rate of drifting snow and the mean wind speed profile. *Boundary Layer Meteorology* **34**: 213-241.

Shao Y, Li A. 1999. Numerical modelling of saltation in the atmospheric surface layer. *Boundary Layer Meteorology* **91**:

Shiotani M, Arai H. 1953. A short note on the snow storm. *Proceedings of the Second Japanese National Congress for Applied Mechanics*. 217-218.

Shook K, Gray DM. 1997. Snowmelt resulting from advection. *Hydrological Processes* **11**: 1725-1736.

Slater G, Schlosser CA, Desborough CE, Pitman AJ, Henderson- Sellers A, Robock A , Ya K, Vinnikov , Speranskaya NA, Mitchell K, Boone A, Braden H, Chen F, Cox P, de Rosnay P, Dickinson RE, Dai Y-J, Duan Q, Entin J, Etchevers P, Gedney N, Gusev Y M, Habets F, Kim J, Koren V, Kowalczyk E, Nasonova ON, Noilhan J, Shaake J, Shmakin AB, Smirnova T, Verseghy D, Wetzel P, Xue Y, Yang Z-L, Zeng Q. 2001. The Representation of snow in land-surface schemes ; results from PILPS 2(d). *Journal of Hydrometeorology* **2**: 7-25.

Smith RE, Goodrich DR, Woolhiser DA, Unkrich CL. 1995. KINEROS – A KINematic Runoff EROSion Mode. In *VP Singh (ed.), Computer Models of Watershed Hydrology*. Water Resources Publications: Highlands Ranch, CO. 697-732 p.

Soulis ED, Snelgrove KR, Seglenieks F, Verseghy DL. 2000. Towards closing the vertical water balance in Canadian atmospheric models: coupling of the land surface scheme CLASS with the distributed hydrological model WATFLOOD. *Atmosphere-Ocean* **38**: 251-269.

Stähli M, Papritz A, Waldner P, Forster F. 2001. Time-space linear regression of the snow cover in a pre-Alpine semi-forested catchment. *Annals of Glaciology* **32**: 125-129.

Stevenson DR. 1967. Geological and groundwater investigations in the Marmot Creek experimental basin of southwestern Alberta, Canada. M.Sc. Thesis, University of Alberta, Edmonton, AB.

Stewart IT, Cayan DR, Dettinger MD. 2004. Changes in snowmelt runoff timing in western North America under a 'business-as-usual' climate change scenario. *Climatic Change* **62**: 212-232.

Tabler RD. 1975. Predicting profiles of snow drifts in topographic catchments. *Proceedings of the 43rd Western Snow Conference* **43**: 87-97.

Takeuchi M. 1980. Vertical profile and horizontal increase of drift-snow transport. *Journal of Glaciology* **26**: 481-492.

Thyer M, Kuczera G, Bates BC. 1999. Probabilistic optimization for conceptual rainfall-runoff models: a comparison of the shuffled complex evolution and simulated annealing algorithms. *Water Resources Research* **35**: 767-773.

Tolson BA, Shoemaker CA. 2007. Dynamically dimensioned search algorithm for computationally efficient watershed model calibration. *Water Resources Research* **43**: W01413.

Thorpe AD, Mason BJ. 1966. The evaporation of ice spheres and ice crystals. *British Journal of Applied Physics* **17**: 541-548.

Utnes T, Eidsvik KJ. 1996. Turbulent flows over mountainous terrain modelled by the Reynolds equations. *Boundary-Layer Meteorology* **79**: 393-416.

Verseghy DL. 1991. CLASS – A Canadian land surface scheme for GCMs, I. Soil model. *International Journal of Climatology* **11**: 111-133.

Verseghy DL, McFarlane NA, Lazare M. 1993. CLASS – A Canadian land surface scheme for GCMs, II. Vegetation model and coupled runs. *International Journal of Climatology* **13**: 347-370.

Verseghy D. 2008. CLASS – The Canadian Land Surface Scheme (Version 3.4), Technical Documentation (Version 1.1). Climate Research Division, Science and Technology Branch, Environment Canada. 180 p.

Vertessy RA, Hatton TJ, O`Shaughnessy PJ, Jayasuriya MDA. 1993. Predicting water yield from a mountain ash forest catchment using a terrain analysis-based catchment model. *Journal of Hydrology* **150**: 665-700.

Vivoni ER, Ivanov VY, Bras RL, Entekhabi D. 2004. Generation of triangulated irregular networks based on hydrologic similarity. *Journal of Hydrologic Engineering* **9**: 288-302.

Walmsley JL, Taylor PA, Salmon JR. 1989. Simple guidelines for estimating wind speed variations due to small-scale topographic features – an update. *Climatological Bulletin* **23**: 3-14.

Wang QJ. 1991. The genetic algorithm and its application to calibrating rainfall-runoff models. *Water Resources Research* **27**: 2467-2471.

Webb BW, Hannah DM, Moore RD, Brown LE, Nobilis F. 2008. Recent advances in stream and river temperature research. *Hydrological Processes* **22**: 902-918.

Weng W, Taylor PA, Walmsley JL. 2000. Guidelines for airflow over complex terrain: model developments. *Journal of Wind Engineering* **86**: 169-186.

Winstral A, Elder K, Davis RE. 2002. Spatial snow modeling of wind-redistributed snow using terrain-based parameters. *Journal of Hydrometeorology* **3**: 524-538.

Winstral A, Marks D. 2002. Simulating wind fields and snow redistribution using terrain-based parameters to model snow accumulation and melt over a semi-arid mountain catchment. *Hydrological Processes* **16**: 3585-3603.

Winstral A, Marks D, Gurney R. 2008. An efficient method for distributing wind speeds over heterogeneous terrain. *Hydrological Processes* **23**: 2526-2535.

Woo MK, Marsh P. 1978. Analysis of error in determination of snow storage for small high arctic basins. *Journal of Applied Meteorology* **17**: 1537-1541.

Wood N. 2000. Wind flow over complex terrain: a historical perspective and the prospect for large-eddy modelling. *Boundary-Layer Meteorology* **96**: 11-32.

Wyatt VE, Nickling WG. 1997. Drag and shear stress partitioning in sparse desert creosote communities. *Canadian Journal of Earth Sciences* **34**: 1486-1498.

Zhang H, Henderson-Sellers A, Pitman AJ, McGregor JL, Desborough CE, Katzfey JJ. 2001. Limited-area model sensitivity to the complexity of representation of the land surface energy balance. *Journal of Climate* **14**: 3965-3986.

APPENDIX A: FIELD WORK PERFORMED BY THE M.SC. CANDIDATE

Date	Location	Tasks
17-18 November 2007	Marmot Creek	Snow surveys; data downloads
21-22 January 2008	Marmot Creek	Snow surveys; data downloads
12-15 February 2008	Wolf Creek	Snow surveys; shrub measurements
4 February 2008	Marmot Creek	Snow surveys; data downloads
1-2 March 2008	Marmot Creek	Snow surveys; data downloads
26-28 March 2008	Marmot Creek	Snow surveys; data downloads
16-17 April 2008	Marmot Creek	Snow surveys; data downloads
22-23 April 2008	Marmot Creek	Snow surveys; data downloads
29 April 2008	Marmot Creek	Snow surveys; data downloads
11-20 May 2008	Marmot Creek	Snow surveys; data downloads
3 July 2008	Marmot Creek	Fisera Ridge shrub survey
29 January 2009	Marmot Creek	Snow surveys; data downloads
28 February-1 March 2009	Marmot Creek	Snow surveys; data downloads
16-18 April 2009	Marmot Creek	Snow surveys; data downloads

APPENDIX B: CLASS AND MESH PARAMETER DEFINITIONS

The following parameter descriptions and recommended parameter values are compiled from the documents "Description of CLASS I/O using the RUNCLASS driver and CLASS version 3.4 for single-column testing against field data (1 grid cell, 1 mosaic tile)" by Diana Verseghy, Environment Canada (accessed: March 2009) and ``CLASS – The Canadian Land Surface Scheme (Version 3.4) Technical Documentation (Version 1.1)`` by Diana Verseghy, May 2008.

Vegetation parameters

ALIC: Average near-IR albedo of vegetation category when fully-leafed [ ]
ALVC: Average visible albedo of vegetation category when fully-leafed [ ]
CMAS: Annual maximum canopy mass for vegetation category [kg m^{-2}]
FCAN: Annual maximum fractional coverage of modelled area [ ]
LNZO: Natural logarithm of maximum vegetation roughness length [ ]
PAMN: Annual minimum plant area index of vegetation category [ ]
PAMX: Annual maximum plant area index of vegetation category [ ]
ROOT: Annual maximum rooting depth of vegetation category [m]

Stomatal resistance parameters

PSGA: Soil moisture suction coefficient (used in stomatal resistance formula) [ ]
PSGB: Soil moisture suction coefficient (used in stomatal resistance formula) [ ]
QA50: Reference value of incoming shortwave radiation (used in stomatal resistance formula) [W m^{-2}]
RSMN: Minimum stomatal resistance of vegetation category [s m^{-1}]
VPDA: Vapour pressure deficit coefficient (used in stomatal resistance formula) [ ]
VPDB: Vapour pressure deficit coefficient (used in stomatal resistance formula) [ ]

Soil parameters

CLAY: Percentage clay content
DELZ: Soil layer thickness [m]
ORGM: Percentage organic matter content
SAND: Percentage sand content
ZBOT: Depth of bottom of soil profile [m]

Other surface parameters

ZSNL: Limiting snow depth below which snow coverage < 100% [m]
ZPLG: Maximum water ponding depth for snow-free subareas [m]
ZPLS: Maximum water ponding depth for snow-covered subareas [m]
DRN: Soil drainage index
SDEP: Soil column permeable depth [m]

Vegetation type (as recognized by Canadian GCM)	***ALIC***	***ALVC***	***exp (LNZO)***	***PAMX***	***PAMN***	***CMAS***	***ROOT***
Evergreen needleleaf forest	0.03	0.19	1.5	2.0	1.6	25.0	1.0
Evergreen broadleaf shrub	0.03	0.19	0.05	2.0	2.0	2.0	0.2
Deciduous shrub	0.05	0.29	0.15	4.0	0.5	8.0	1.0
Thorn shrub	0.06	0.32	0.15	3.0	3.0	8.0	5.0
Short grass and forbs	0.06	0.34	0.02	3.0	3.0	1.5	1.2
Long grass	0.05	0.31	0.08	4.0	4.0	3.0	1.2

Vegetation type	***RSMN***	***QA50***	***VPDA***	***VPDB***	***PSGA***	***PSGB***
Needleleaf trees	200.0	30.0	0.65	1.05	100.0	5.0
Grass	100.0	30.0	0.50	1.00	100.0	5.0

APPENDIX C: MESH INITIALIZATION FILES FOR FISERA RIDGE POINT SIMULATIONS

```
  Fisera Ridge Point - MESH
  M. Macdonald
  Centre for Hydrology
     50.95    115.17     10.00      2.00     50.00   -1.0    1    2    1
   0.250   0.000   0.000   0.250   0.000   0.307   0.000   0.000   0.902
  -3.002   0.000   0.000  -3.642   0.000   0.188   0.000   0.000   0.584
   0.025   0.000   0.000   0.044   0.000   0.500   0.000   0.000   1.500
   0.188   0.000   0.000   0.202   0.000   1.000   0.000   0.000   1.200
 200.000   0.000   0.000 100.000          30.000   0.000   0.000  30.000
   0.650   0.000   0.000   0.500           1.050   0.000   0.000   1.000
 100.000   0.000   0.000 100.000           5.000   0.000   0.000   5.000
   1.000   4.100   1.000  1.0000
  0.1000   0.300  10.000 1.00000       1
     60.00     60.00     60.00
      9.00     10.00     10.00
      1.00      0.00      0.00
      2.58      2.70      3.10      2.20     -0.10      0.00
     0.340     0.240     0.140     0.000     0.000     0.000     0.000
    0.0000    0.0000      0.00     0.900   274.300     0.000
       288       142       288       142         0         0
      2008      2009      2008      2009         0         0
         0         0       288      2008
123456789*123456789*123456789*123456789*123456789*123456789*123456789*123
```

```
1.2.1MM: MESH Parameters, Hydrology Input File
##### Option Flags #####
----#
    2 # Number of option flags
  0.0 #1
  0.0 #2
##### Channel River Roughness Factors (WF_R2) #####
-----#-----#-----#-----#-----#
 0.040 0.000 0.000 0.000 0.000
##### GRU-Independent Hydrologic Parameters #####
-------#
       2 # Number of GRU independent hydrologic parameters
     0.0 #1
     0.0 #2
##### GRU-Dependent Hydrologic Parameters #####
-------#
       1 #Number of GRUs (must match number in mesh_parameters_class.ini file)
       3 #Number of GRU dependent hydrologic parameters
---------#---------#---------#---------#---------#
      0.02
      0.01
      0.01
```

```
 Fisera Ridge Point - MESH-PBSM
 M. Macdonald
 Centre for Hydrology
    50.95    115.17     10.00      2.00     50.00   -1.0    1    2    1
  0.250   0.000   0.000   0.250   0.000   0.426   0.000   0.000   0.965
 -2.492   0.000   0.000  -3.871   0.000   0.149   0.000   0.000   0.235
  0.094   0.000   0.000   0.070   0.000   0.500   0.000   0.000   1.500
  0.232   0.000   0.000   0.284   0.000   1.000   0.000   0.000   1.200
200.000   0.000   0.000 100.000          30.000   0.000   0.000  30.000
  0.650   0.000   0.000   0.500           1.050   0.000   0.000   1.000
100.000   0.000   0.000 100.000           5.000   0.000   0.000   5.000
  1.000   4.100   1.000  1.0000
 0.1000   0.300  10.000 1.00000       1
    60.00     60.00     60.00
     9.00     10.00     10.00
     1.00      0.00      0.00
     2.58      2.70      3.10      2.20     -0.10      0.00
    0.340     0.240     0.140     0.000     0.000     0.000     0.000
   0.0000    0.0000      0.00     0.900   274.300     0.000
  300.0
   0.10   1.048
  0.088   0.000
    0.0
      295        99       295        99         0         0
     2007      2008      2007      2008         0         0
        5         0       295      2007
123456789*123456789*123456789*123456789*123456789*123456789*123456789*123
```

```
1.2.1MM: MESH Parameters, Hydrology Input File
##### Option Flags #####
----#
    2 # Number of option flags
  0.0 #1
  0.0 #2
##### Channel River Roughness Factors (WF_R2) #####
-----#-----#-----#-----#-----#
 0.040 0.000 0.000 0.000 0.000
##### GRU-Independent Hydrologic Parameters #####
-------#
       2 # Number of GRU independent hydrologic parameters
     0.0 #1
     0.0 #2
##### GRU-Dependent Hydrologic Parameters #####
-------#
       1 #Number of GRUs (must match number in mesh_parameters_class.ini file)
       3 #Number of GRU dependent hydrologic parameters
---------#---------#---------#---------#---------#
      0.17
      0.01
      0.01
```

APPENDIX D: MESH INITIALIZATION FILES FOR FISERA RIDGE DISTRIBUTED SIMULATIONS

```
 Fisera HRUs - MESH
 M. MacDonald
 Centre for Hydrology
    50.95    115.17     10.00      2.00     50.00   -1.0    1    2    5
  0.100   0.000   0.000   0.400   0.000   0.359   0.000   0.000   0.497
 -3.668   0.000   0.000  -4.568   0.000   0.191   0.000   0.000   0.312
  0.028   0.000   0.000   0.047   0.000   8.000   0.000   0.000   2.000
  0.161   0.000   0.000   0.285   0.000   1.000   0.000   0.000   1.200
200.000   0.000   0.000 100.000          30.000   0.000   0.000  30.000
  0.650   0.000   0.000   0.500           1.050   0.000   0.000   1.000
100.000   0.000   0.000 100.000           5.000   0.000   0.000   5.000
  1.000   4.100   1.000  1.0000
 0.1000   0.300  10.000 1.00000       1
    60.00     60.00     60.00
     9.00     10.00     10.00
     1.00      0.00      0.00
     2.58      2.70      3.10      2.20     -0.10      0.00
    0.340     0.240     0.140     0.000     0.000     0.000     0.000
   0.0000    0.0000      0.00     0.900   274.300     0.000
  0.300   0.000   0.000   0.400   0.000   0.403   0.000   0.000   0.908
 -3.687   0.000   0.000  -3.916   0.000   0.200   0.000   0.000   0.553
  0.036   0.000   0.000   0.021   0.000   8.000   0.000   0.000   2.000
  0.158   0.000   0.000   0.201   0.000   1.000   0.000   0.000   1.200
200.000   0.000   0.000 100.000          30.000   0.000   0.000  30.000
  0.650   0.000   0.000   0.500           1.050   0.000   0.000   1.000
100.000   0.000   0.000 100.000           5.000   0.000   0.000   5.000
  1.000   4.100   1.000  1.0000
 0.1000   0.300  10.000 1.00000       2
    60.00     60.00     60.00
     9.00     10.00     10.00
     1.00      0.00      0.00
     2.58      2.70      3.10      2.20     -0.10      0.00
    0.340     0.240     0.140     0.000     0.000     0.000     0.000
   0.0000    0.0000      0.00     0.900   274.300     0.000
  0.600   0.000   0.000   0.400   0.000   0.374   0.000   0.000   0.538
 -0.273   0.000   0.000  -3.294   0.000   0.107   0.000   0.000   0.303
  0.044   0.000   0.000   0.039   0.000   8.000   0.000   0.000   2.000
  0.285   0.000   0.000   0.234   0.000   1.000   0.000   0.000   1.200
200.000   0.000   0.000 100.000          30.000   0.000   0.000  30.000
  0.650   0.000   0.000   0.500           1.050   0.000   0.000   1.000
100.000   0.000   0.000 100.000           5.000   0.000   0.000   5.000
  1.000   4.100   1.000  1.0000
 0.1000   0.300  10.000 1.00000       3
    60.00     60.00     60.00
     9.00     10.00     10.00
     1.00      0.00      0.00
     2.58      2.70      3.10      2.20     -0.10      0.00
    0.340     0.240     0.140     0.000     0.000     0.000     0.000
   0.0000    0.0000      0.00     0.900   274.300     0.000
  0.600   0.000   0.000   0.400   0.000   0.324   0.000   0.000   0.575
  0.136   0.000   0.000  -3.298   0.000   0.200   0.000   0.000   0.502
  0.054   0.000   0.000   0.069   0.000   8.000   0.000   0.000   2.000
  0.293   0.000   0.000   0.397   0.000   1.000   0.000   0.000   1.200
200.000   0.000   0.000 100.000          30.000   0.000   0.000  30.000
  0.650   0.000   0.000   0.500           1.050   0.000   0.000   1.000
100.000   0.000   0.000 100.000           5.000   0.000   0.000   5.000
  1.000   4.100   1.000  1.0000
 0.1000   0.300  10.000 1.00000       4
    60.00     60.00     60.00
     9.00     10.00     10.00
     1.00      0.00      0.00
     2.58      2.70      3.10      2.20     -0.10      0.00
    0.340     0.240     0.140     0.000     0.000     0.000     0.000
   0.0000    0.0000      0.00     0.900   274.300     0.000
  0.900   0.000   0.000   0.100   0.000   0.879   0.000   0.000   1.094
  0.100   0.000   0.000  -3.389   0.000   0.791   0.000   0.000   0.597
  0.048   0.000   0.000   0.045   0.000  25.000   0.000   0.000   2.000
  0.192   0.000   0.000   0.310   0.000   1.000   0.000   0.000   1.200
```

```
 200.000   0.000   0.000 100.000          30.000   0.000   0.000  30.000
   0.650   0.000   0.000   0.500           1.050   0.000   0.000   1.000
 100.000   0.000   0.000 100.000           5.000   0.000   0.000   5.000
   1.000   4.100   1.000  1.0000
  0.1000   0.300  10.000 1.00000       5
     60.00     60.00     60.00
      9.00     10.00     10.00
      1.00      0.00      0.00
      2.58      2.70      3.10      2.20     -0.10      0.00
     0.340     0.240     0.140     0.000     0.000     0.000     0.000
    0.0000    0.0000      0.00     0.900   274.300     0.000
       293       121       293       121         0         0
      2007      2008      2007      2008         0         0
         1         0       293      2007
123456789*123456789*123456789*123456789*123456789*123456789*123456789*123
```

```
1.2.1MM: MESH Parameters, Hydrology Input File
##### Option Flags #####
----#
    2 # Number of option flags
  0.0 #1
  0.0 #2
##### Channel River Roughness Factors (WF_R2) #####
-----#-----#-----#-----#-----#
 0.040 0.000 0.000 0.000 0.000
##### GRU-Independent Hydrologic Parameters #####
-------#
       2 # Number of GRU independent hydrologic parameters
     0.0 #1
     0.0 #2
##### GRU-Dependent Hydrologic Parameters #####
-------#
       5 #Number of GRUs (must match number in mesh_parameters_class.ini file)
       3 #Number of GRU dependent hydrologic parameters
---------#---------#---------#---------#---------#
      0.02      0.02      1.00      0.99      0.37
      0.01      0.01      0.01      0.01      0.01
      0.01      0.01      0.01      0.01      0.01
```

```
 Fisera HRUs - MESH-PBSM
 M. MacDonald
 Centre for Hydrology
    50.95    115.17     10.00      2.00     50.00   -1.0    1    2    5
  0.100   0.000   0.000   0.400   0.000   0.297   0.000   0.000   0.202
 -3.339   0.000   0.000  -4.250   0.000   0.058   0.000   0.000   0.145
  0.077   0.000   0.000   0.047   0.000   8.000   0.000   0.000   2.000
  0.183   0.000   0.000   0.382   0.000   1.000   0.000   0.000   1.200
200.000   0.000   0.000 100.000          30.000   0.000   0.000  30.000
  0.650   0.000   0.000   0.500           1.050   0.000   0.000   1.000
100.000   0.000   0.000 100.000           5.000   0.000   0.000   5.000
  1.000   4.100   1.000  1.0000
 0.1000   0.300  10.000 1.00000       1
    60.00     60.00     60.00
     9.00     10.00     10.00
     1.00      0.00      0.00
     2.58      2.70      3.10      2.20     -0.10      0.00
    0.340     0.240     0.140     0.000     0.000     0.000     0.000
   0.0000    0.0000      0.00     0.900   274.300     0.000
  300.0
   0.68    0.110
  0.103   0.000
    0.0
  0.300   0.000   0.000   0.400   0.000   0.171   0.000   0.000   0.284
 -2.949   0.000   0.000  -5.144   0.000   0.128   0.000   0.000   0.205
  0.025   0.000   0.000   0.045   0.000   8.000   0.000   0.000   2.000
  0.207   0.000   0.000   0.205   0.000   1.000   0.000   0.000   1.200
200.000   0.000   0.000 100.000          30.000   0.000   0.000  30.000
  0.650   0.000   0.000   0.500           1.050   0.000   0.000   1.000
100.000   0.000   0.000 100.000           5.000   0.000   0.000   5.000
  1.000   4.100   1.000  1.0000
 0.1000   0.300  10.000 1.00000       2
    60.00     60.00     60.00
     9.00     10.00     10.00
     1.00      0.00      0.00
     2.58      2.70      3.10      2.20     -0.10      0.00
    0.340     0.240     0.140     0.000     0.000     0.000     0.000
   0.0000    0.0000      0.00     0.900   274.300     0.000
  300.0
   0.57    0.193
  0.216   0.250
    0.0
  0.600   0.000   0.000   0.400   0.000   0.477   0.000   0.000   1.457
 -0.425   0.000   0.000  -3.004   0.000   0.101   0.000   0.000   0.486
  0.069   0.000   0.000   0.077   0.000   8.000   0.000   0.000   2.000
  0.265   0.000   0.000   0.382   0.000   1.000   0.000   0.000   1.200
200.000   0.000   0.000 100.000          30.000   0.000   0.000  30.000
  0.650   0.000   0.000   0.500           1.050   0.000   0.000   1.000
100.000   0.000   0.000 100.000           5.000   0.000   0.000   5.000
  1.000   4.100   1.000  1.0000
 0.1000   0.300  10.000 1.00000       3
    60.00     60.00     60.00
     9.00     10.00     10.00
     1.00      0.00      0.00
     2.58      2.70      3.10      2.20     -0.10      0.00
    0.340     0.240     0.140     0.000     0.000     0.000     0.000
   0.0000    0.0000      0.00     0.900   274.300     0.000
  300.0
   0.73    0.307
  0.894   0.250
    0.0
  0.600   0.000   0.000   0.400   0.000   0.478   0.000   0.000   0.601
  0.277   0.000   0.000  -2.634   0.000   0.200   0.000   0.000   0.554
  0.100   0.000   0.000   0.054   0.000   8.000   0.000   0.000   2.000
  0.297   0.000   0.000   0.303   0.000   1.000   0.000   0.000   1.200
200.000   0.000   0.000 100.000          30.000   0.000   0.000  30.000
  0.650   0.000   0.000   0.500           1.050   0.000   0.000   1.000
100.000   0.000   0.000 100.000           5.000   0.000   0.000   5.000
```

```
  1.000   4.100   1.000  1.0000
 0.1000   0.300  10.000 1.00000       4
    60.00     60.00     60.00
     9.00     10.00     10.00
     1.00      0.00      0.00
     2.58      2.70      3.10      2.20     -0.10      0.00
    0.340     0.240     0.140     0.000     0.000     0.000     0.000
   0.0000    0.0000      0.00     0.900   274.300     0.000
  300.0
   0.48    0.695
  1.174    0.250
    0.0
  0.900   0.000   0.000   0.100   0.000   0.910   0.000   0.000   2.898
  0.688   0.000   0.000  -4.486   0.000   0.758   0.000   0.000   0.806
  0.035   0.000   0.000   0.041   0.000  25.000   0.000   0.000   2.000
  0.243   0.000   0.000   0.382   0.000   1.000   0.000   0.000   1.200
200.000   0.000   0.000 100.000          30.000   0.000   0.000  30.000
  0.650   0.000   0.000   0.500           1.050   0.000   0.000   1.000
100.000   0.000   0.000 100.000           5.000   0.000   0.000   5.000
  1.000   4.100   1.000  1.0000
 0.1000   0.300  10.000 1.00000       5
    60.00     60.00     60.00
     9.00     10.00     10.00
     1.00      0.00      0.00
     2.58      2.70      3.10      2.20     -0.10      0.00
    0.340     0.240     0.140     0.000     0.000     0.000     0.000
   0.0000    0.0000      0.00     0.900   274.300     0.000
  300.0
   0.50    2.000
  2.300   0.250
    0.0
      268       142       268       142         0         0
     2008      2009      2008      2009         0         0
        1         0       268      2008
123456789*123456789*123456789*123456789*123456789*123456789*123456789*123
```

```
1.2.1MM: MESH Parameters, Hydrology Input File
##### Option Flags #####
----#
    2 # Number of option flags
  0.0 #1
  0.0 #2
##### Channel River Roughness Factors (WF_R2) #####
-----#-----#-----#-----#-----#
 0.040 0.000 0.000 0.000 0.000
##### GRU-Independent Hydrologic Parameters #####
-------#
       2 # Number of GRU independent hydrologic parameters
     0.0 #1
     0.0 #2
##### GRU-Dependent Hydrologic Parameters #####
-------#
       5 #Number of GRUs (must match number in mesh_parameters_class.ini file)
       3 #Number of GRU dependent hydrologic parameters
---------#---------#---------#---------#---------#
      0.93      0.52      0.25      0.99      0.20
      0.01      0.01      0.01      0.01      0.01
      0.01      0.01      0.01      0.01      0.01
```

APPENDIX E: MESH INITIALIZATION FILES FOR GRANGER BASIN DISTRIBUTED SIMULATIONS

```
Granger Basin - MESH
M. MacDonald
Centre for Hydrology
   60.52    135.12     10.00      2.10     50.00   -1.0    1    2    5
 0.350   0.000   0.000   0.650   0.000   0.141   0.000   0.000   1.080
-3.329   0.000   0.000  -5.234   0.000   0.463   0.000   0.000   0.146
 0.035   0.000   0.000   0.181   0.000   2.981   0.000   0.000   0.157
 0.540   0.000   0.000   0.438   0.000   0.500   0.000   0.000   1.200
 175.0     0.0     0.0    91.6            40.6     0.0     0.0    27.3
  1.13     0.0     0.0    1.47            0.61     0.0     0.0    0.70
  96.8     0.0     0.0   130.0            2.08     0.0     0.0    6.01
 0.817   4.100   1.000  1.0000
0.0050   0.920  10.000 0.00001       1
   20.00     20.00     20.00
   10.00     10.00     10.00
    1.00      0.00      0.00
    6.20      7.00      9.00      8.20      0.00      6.20
   0.100     0.080     0.060     0.200     0.200     0.200     0.010
  0.0000    0.0000      0.00     0.000     0.000     0.000
 0.800   0.000   0.000   0.200   0.000   0.368   0.000   0.000   1.512
-3.140   0.000   0.000  -3.547   0.000   0.284   0.000   0.000   1.013
 0.216   0.000   0.000   0.219   0.000   6.969   0.000   0.000   0.064
 0.358   0.000   0.000   0.398   0.000   0.500   0.000   0.000   1.200
 145.1     0.0     0.0   251.5            58.3     0.0     0.0    46.1
  1.19     0.0     0.0    1.31            0.61     0.0     0.0    0.61
  81.6     0.0     0.0   146.7            2.57     0.0     0.0    4.92
 0.817   4.100   1.000  1.0000
0.0050   0.920  10.000 0.00001       2
   -2.00     75.00     20.00
   18.00     10.00     10.00
    1.00      0.00      0.00
    8.30      9.00     10.00     10.30      0.00      8.30
   0.100     0.080     0.060     0.200     0.170     0.130     0.010
  0.0000    0.0000      0.00     0.000     0.000     0.000
 0.780   0.000   0.000   0.220   0.000   0.369   0.000   0.000   2.118
-3.735   0.000   0.000  -4.333   0.000   0.263   0.000   0.000   1.947
 0.198   0.000   0.000   0.097   0.000   9.178   0.000   0.000   0.171
 0.682   0.000   0.000   0.290   0.000   1.000   0.000   0.000   1.200
  51.9     0.0     0.0   140.5            21.1     0.0     0.0    37.6
  1.08     0.0     0.0    0.87            0.93     0.0     0.0    0.23
  93.5     0.0     0.0   135.6            1.09     0.0     0.0    1.15
 0.615   4.100   1.000  1.0000
0.0470   0.400  10.000 0.00000       3
   -2.00     -2.00     55.00
   10.00     10.00     10.00
    1.00      1.00      0.00
    8.00      8.90      9.90     10.30      0.00      8.00
   0.100     0.080     0.060     0.200     0.170     0.130     0.010
  0.0000    0.0000      0.00     0.000     0.000     0.000
 0.740   0.000   0.000   0.260   0.000   0.354   0.000   0.000   2.864
-1.616   0.000   0.000  -4.672   0.000   0.245   0.000   0.000   0.445
 0.246   0.000   0.000   0.159   0.000   8.808   0.000   0.000   0.122
 0.692   0.000   0.000   0.468   0.000   1.000   0.000   0.000   1.200
 115.8     0.0     0.0   214.9            38.4     0.0     0.0    35.3
  1.28     0.0     0.0    0.63            0.78     0.0     0.0    0.89
  87.7     0.0     0.0   141.1            1.23     0.0     0.0    5.09
 0.615   4.100   1.000  1.0000
0.0470   0.400  10.000 0.00000       4
   -2.00     75.00     20.00
   18.00     10.00     10.00
    1.00      0.00      0.00
    9.90     11.00     12.00     11.60      0.00      9.90
   0.100     0.080     0.060     0.100     0.090     0.060     0.000
  0.0000    0.0000      0.00     0.000     0.000     0.000
 0.710   0.000   0.000   0.290   0.000   0.353   0.000   0.000   2.140
-1.739   0.000   0.000  -4.195   0.000   0.204   0.000   0.000   1.997
 0.130   0.000   0.000   0.127   0.000   8.037   0.000   0.000   0.144
 0.696   0.000   0.000   0.551   0.000   2.000   0.000   0.000   1.200
```

```
   104.9     0.0     0.0   268.4            47.2     0.0     0.0    49.9
    0.32     0.0     0.0    1.42            1.21     0.0     0.0    0.46
    71.8     0.0     0.0    76.3            4.30     0.0     0.0    2.18
   0.615   4.100   1.000  1.0000
  0.0470   0.400  10.000 0.00000       5
    -2.00     75.00     20.00
    18.00     10.00     10.00
     1.00      0.00      0.00
    12.90     14.00     14.50     14.90      0.00     12.90
    0.100     0.080     0.060     0.100     0.090     0.060     0.000
   0.0000    0.0000      0.00     0.000     0.000     0.000
      274       137       274       137         0         0
     2003      2004      2003      2004         0         0
        1         0       274      2003
123456789*123456789*123456789*123456789*123456789*123456789*123456789*123
```

```
1.2.1MM: MESH Parameters, Hydrology Input File
##### Option Flags #####
----#
    2 # Number of option flags
  0.0 #1
  0.0 #2
##### Channel River Roughness Factors (WF_R2) #####
-----#-----#-----#-----#-----#
 0.170 0.170 0.170 0.170 0.170
##### GRU-Independent Hydrologic Parameters #####
-------#
       2 # Number of GRU independent hydrologic parameters
     0.0 #1
     0.0 #2
##### GRU-Dependent Hydrologic Parameters #####
-------#
       5 #Number of GRUs (must match number in mesh_parameters_class.ini file)
       3 #Number of GRU dependent hydrologic parameters
---------#---------#---------#---------#---------#
      0.69      0.96      0.40      0.28      0.78
      0.08      0.08      0.08      0.08      0.08
      0.18      0.18      0.18      0.18      0.18
```

```
Granger Basin - MESH-PBSM
M. MacDonald
Centre for Hydrology
   60.52    135.12     10.00      2.10     50.00   -1.0    1    2    5
 0.350   0.000   0.000   0.650   0.000   0.408   0.000   0.000   1.694
-3.812   0.000   0.000  -4.971   0.000   0.226   0.000   0.000   0.227
 0.110   0.000   0.000   0.022   0.000   4.825   0.000   0.000   0.331
 0.364   0.000   0.000   0.383   0.000   0.500   0.000   0.000   1.200
 175.0     0.0     0.0    91.6            40.6     0.0     0.0    27.3
  1.13     0.0     0.0    1.47            0.61     0.0     0.0    0.70
  96.8     0.0     0.0   130.0            2.08     0.0     0.0    6.01
 0.817   4.100   1.000  1.0000
0.0050   0.920  10.000 0.00001       1
   20.00     20.00     20.00
   10.00     10.00     10.00
    1.00      0.00      0.00
    6.20      7.00      9.00      8.20      0.00      6.20
   0.100     0.080     0.060     0.200     0.200     0.200     0.010
  0.0000    0.0000      0.00     0.000     0.000     0.000
 674.8
  0.15   0.149
 0.104   1.000   0.600
   0.0
 0.800   0.000   0.000   0.200   0.000   0.374   0.000   0.000   1.392
-2.702   0.000   0.000  -3.677   0.000   0.301   0.000   0.000   0.597
 0.142   0.000   0.000   0.200   0.000   4.653   0.000   0.000   0.281
 0.463   0.000   0.000   0.274   0.000   0.500   0.000   0.000   1.200
 145.1     0.0     0.0   251.5            58.3     0.0     0.0    46.1
  1.19     0.0     0.0    1.31            0.61     0.0     0.0    0.61
  81.6     0.0     0.0   146.7            2.57     0.0     0.0    4.92
 0.817   4.100   1.000  1.0000
0.0050   0.920  10.000 0.00001       2
   -2.00     75.00     20.00
   18.00     10.00     10.00
    1.00      0.00      0.00
    8.30      9.00     10.00     10.30      0.00      8.30
   0.100     0.080     0.060     0.200     0.170     0.130     0.010
  0.0000    0.0000      0.00     0.000     0.000     0.000
 332.7
  0.62    0.493
 0.394   0.000
   0.0
 0.780   0.000   0.000   0.220   0.000   0.422   0.000   0.000   1.014
-2.317   0.000   0.000  -4.525   0.000   0.218   0.000   0.000   0.513
 0.089   0.000   0.000   0.146   0.000   9.943   0.000   0.000   0.246
 0.346   0.000   0.000   0.301   0.000   1.000   0.000   0.000   1.200
  51.9     0.0     0.0   140.5            21.1     0.0     0.0    37.6
  1.08     0.0     0.0    0.87            0.93     0.0     0.0    0.23
  93.5     0.0     0.0   135.6            1.09     0.0     0.0    1.15
 0.615   4.100   1.000  1.0000
0.0470   0.400  10.000 0.00000       3
   -2.00     -2.00     55.00
   10.00     10.00     10.00
    1.00      1.00      0.00
    8.00      8.90      9.90     10.30      0.00      8.00
   0.100     0.080     0.060     0.200     0.170     0.130     0.010
  0.0000    0.0000      0.00     0.000     0.000     0.000
 300.0
  1.00    0.800
 0.726   0.280
   0.0
 0.740   0.000   0.000   0.260   0.000   0.436   0.000   0.000   2.185
-1.675   0.000   0.000  -4.696   0.000   0.252   0.000   0.000   0.557
 0.227   0.000   0.000   0.094   0.000   6.351   0.000   0.000   0.090
 0.691   0.000   0.000   0.564   0.000   1.000   0.000   0.000   1.200
 115.8     0.0     0.0   214.9            38.4     0.0     0.0    35.3
  1.28     0.0     0.0    0.63            0.78     0.0     0.0    0.89
  87.7     0.0     0.0   141.1            1.23     0.0     0.0    5.09
```

```
  0.615   4.100   1.000  1.0000
 0.0470   0.400  10.000 0.00000       4
    -2.00     75.00     20.00
    18.00     10.00     10.00
     1.00      0.00      0.00
     9.90     11.00     12.00     11.60      0.00      9.90
    0.100     0.080     0.060     0.100     0.090     0.060     0.000
   0.0000    0.0000      0.00     0.000     0.000     0.000
  319.0
   1.00    0.800
  0.715   0.160
    0.0
  0.710   0.000   0.000   0.290   0.000   0.662   0.000   0.000   3.161
 -1.324   0.000   0.000  -4.423   0.000   0.252   0.000   0.000   1.374
  0.218   0.000   0.000   0.193   0.000  10.373   0.000   0.000   0.121
  0.686   0.000   0.000   0.590   0.000   2.000   0.000   0.000   1.200
  104.9     0.0     0.0   268.4            47.2     0.0     0.0    49.9
   0.32     0.0     0.0    1.42            1.21     0.0     0.0    0.46
   71.8     0.0     0.0    76.3            4.30     0.0     0.0    2.18
  0.615   4.100   1.000  1.0000
 0.0470   0.400  10.000 0.00000       5
    -2.00     75.00     20.00
    18.00     10.00     10.00
     1.00      0.00      0.00
    12.90     14.00     14.50     14.90      0.00     12.90
    0.100     0.080     0.060     0.100     0.090     0.060     0.000
   0.0000    0.0000      0.00     0.000     0.000     0.000
  300.0
   1.00    0.800
  0.721   0.060
    0.0
     274       137       274       137         0         0
    2003      2004      2003      2004         0         0
       1         0       274      2003
123456789*123456789*123456789*123456789*123456789*123456789*123456789*123
```

```
1.2.1MM: MESH Parameters, Hydrology Input File
##### Option Flags #####
----#
    2 # Number of option flags
  0.0 #1
  0.0 #2
##### Channel River Roughness Factors (WF_R2) #####
-----#-----#-----#-----#-----#
 0.170 0.170 0.170 0.170 0.170
##### GRU-Independent Hydrologic Parameters #####
-------#
       2 # Number of GRU independent hydrologic parameters
     0.0 #1
     0.0 #2
##### GRU-Dependent Hydrologic Parameters #####
-------#
       5 #Number of GRUs (must match number in mesh_parameters_class.ini file)
       3 #Number of GRU dependent hydrologic parameters
---------#---------#---------#---------#---------#
      0.03      0.95      0.29      0.19      0.33
      0.08      0.08      0.08      0.08      0.08
      0.18      0.18      0.18      0.18      0.18
```